PB90-231275

Development of Infrared Methods for Characterization of Inorganic Sulfur Species Related to Injection Desulfurization Processes

Duke Univ., Durham, NC

Prepared for:

Environmental Protection Agency, Research Triangle Park, NC

May 90

U.S. Department of Commerce
National Technical Information Service
NTIS

United States
Environmental Protection
Agency

EPA-600/7-90-012

May 1990

EPA

Research and Development

PB90-231275

DEVELOPMENT OF INFRARED METHODS FOR CHARACTERIZATION OF INORGANIC SULFUR SPECIES RELATED TO INJECTION DESULFURIZATION PROCESSES

Prepared for

Office of Environmental Engineering
and Technology Demonstration

Prepared by

Air and Energy Engineering Research
Laboratory
Research Triangle Park NC 27711

REPRODUCED BY
U.S. DEPARTMENT OF COMMERCE
NATIONAL TECHNICAL
INFORMATION SERVICE
SPRINGFIELD, VA 22161

RESEARCH REPORTING SERIES

Research reports of the Office of Research and Development, U.S. Environmental Protection Agency, have been grouped into nine series. These nine broad categories were established to facilitate further development and application of environmental technology. Elimination of traditional grouping was consciously planned to foster technology transfer and a maximum interface in related fields. The nine series are:

1. Environmental Health Effects Research
2. Environmental Protection Technology
3. Ecological Research
4. Environmental Monitoring
5. Socioeconomic Environmental Studies
6. Scientific and Technical Assessment Reports (STAR)
7. Interagency Energy-Environment Research and Development
8. "Special" Reports
9. Miscellaneous Reports

This report has been assigned to the INTERAGENCY ENERGY-ENVIRONMENT RESEARCH AND DEVELOPMENT series. Reports in this series result from the effort funded under the 17-agency Federal Energy/Environment Research and Development Program. These studies relate to EPA's mission to protect the public health and welfare from adverse effects of pollutants associated with energy systems. The goal of the Program is to assure the rapid development of domestic energy supplies in an environmentally-compatible manner by providing the necessary environmental data and control technology. Investigations include analyses of the transport of energy-related pollutants and their health and ecological effects; assessments of, and development of, control technologies for energy systems; and integrated assessments of a wide range of energy-related environmental issues.

EPA REVIEW NOTICE

This report has been reviewed by the participating Federal Agencies, and approved for publication. Approval does not signify that the contents necessarily reflect the views and policies of the Government, nor does mention of trade names or commercial products constitute endorsement or recommendation for use.

This document is available to the public through the National Technical Information Service, Springfield, Virginia 22161.

EPA-600/7-90-012
May 1990

DEVELOPMENT OF INFRARED METHODS FOR CHARACTERIZATION OF INORGANIC SULFUR SPECIES RELATED TO INJECTION DESULFURIZATION PROCESSES

by

Meg Martin Thompson and Richard A. Palmer

Department of Chemistry

Duke University

Durham, NC 27706

Final Report

on

EPA Cooperative Agreement

EPA Assistance No. CR813023-02-0

EPA Project Officer

Frank E. Briden

Air and Energy Engineering Research Laboratory

Research Triangle Park, NC 27711

Prepared for:

US Environmental Protection Agency

Office of Research and Development

Washington, DC 20460

TECHNICAL REPORT DATA (Please read Instructions on the reverse before completing)		
1. REPORT NO. EPA-600/7-90-012	2.	3. RECIPIENT'S ACCESSION NO. PB90 231275/AS
4. TITLE AND SUBTITLE Development of Infrared Methods for Characterization of Inorganic Sulfur Species Related to Injection Desulfurization Processes		5. REPORT DATE May 1990 6. PERFORMING ORGANIZATION CODE
7. AUTHOR(S) Meg Martin Thompson and Richard A. Palmer		8. PERFORMING ORGANIZATION REPORT NO.
9. PERFORMING ORGANIZATION NAME AND ADDRESS Duke University Department of Chemistry Durham, North Carolina 27706		10. PROGRAM ELEMENT NO. 11. CONTRACT/GRANT NO. CR813023-02-0
12. SPONSORING AGENCY NAME AND ADDRESS EPA, Office of Research and Development Air and Energy Engineering Research Laboratory Research Triangle Park, NC 27711		13. TYPE OF REPORT AND PERIOD COVERED Final report; 12/85 - 6/88 14. SPONSORING AGENCY CODE EPA/600/13

15. SUPPLEMENTARY NOTES AEERL project officer is Frank E. Briden, Mail Drop 4, 919/541-7808.

16. ABSTRACT The report gives results of using photoacoutsic (PA) and diffuse reflectance (DR) detection methods in Fourier transform infrared spectroscopy (FTIRS) to evaluate the reactions of particulate CaO, CaCO3, and Ca(OH)2 samples with SO2 at temperatures of 25-900 C. The work involved three types of studies: post-exposure FTIR-PAS (25-900 C), in situ FTIR-DRS (25-700 C), and in situ FTIR-PAS (25-400 C). Post-exposure FTIR-PAS experiments involved obtaining spectral measurements of particulate CaO, CaCO3, and Ca(OH)2 samples after they had been exposed to 1.5% SO2 in He as a function of exposure time, temperature, and gas composition. These data indicate that: the initial product formed is CaSO3; at temperatures above 500 C, CaSO3 is converted to CaSO4; the formation of CaSO4 is not as extensive for exposures of 900 C as it is at 750 C; in the presence of O2, the production of CaS2O3 is reduced; and the extent of SO2 capture by the reactants decreases in the order Ca(OH)2 > CaCO3 > CaO. In situ FTIR-DRS experiments confirmed post-exposure FTIR-PAS results. FTIR-DRS also indicated that the formation of S2O3(--) depends on the concentration of CaO, CaCO3, or Ca(OH)2 in the NaCl diluent. Two SO3(--) species and an intermediate monodentate SO4(--) species were also detected and identified.

17. KEY WORDS AND DOCUMENT ANALYSIS

a. DESCRIPTORS	b. IDENTIFIERS/OPEN ENDED TERMS	c. COSATI Field/Group
Pollution Particles Infrared Spectroscopy Inorganic Compounds Sulfur Dioxide Calcium Oxides Desulfurization Calcium Carbonates Injection Calcium Hydroxides	Pollution Control Stationary Sources Particulate	13B 14B 07B 07A, 07D 14G

18. DISTRIBUTION STATEMENT	19. SECURITY CLASS (This Report)	21. NO. OF PAGES
Release to Public	Unclassified	
	20. SECURITY CLASS (This page) Unclassified	22. PRICE

EPA Form 2220-1 (9-73)

ABSTRACT

Photoacoustic (PA) and diffuse reflectance (DR) detection methods in Fourier transform infrared spectroscopy were used to evaluate the reactions of particulate CaO, $CaCO_3$ and $Ca(OH)_2$ samples with SO_2 at temperatures ranging from 25 to 900°C. More specifically, this work involved three types of studies: 1) post-exposure FTIR-PAS (25-900°C); 2) in situ FTIR-DRS (25-700°C); and 3) in situ FTIR-PAS (25-400°C). The emphasis of this work was on determining the utility of FTIR-PA and FTIR-DR techniques for understanding the mechanisms by which SO_2 is captured by particulate samples of CaO, $Ca(OH)_2$ and $CaCO_3$.

Post-exposure FTIR-PAS experiments involved obtaining spectral measurements of particulate CaO, $CaCO_3$ and $Ca(OH)_2$ samples after they had been exposed to 1.5% SO_2 in He as a function of exposure time, temperature and gas composition. These data indicate that: 1) the initial product formed is $CaSO_3$; 2) at temperatures above 500°C $CaSO_3$ is converted to $CaSO_4$, predominantly through the reaction of $CaSO_3$ with SO_2; 3) additional $CaSO_4$ production, as well as the production of CaS_2O_3, occurs via $CaSO_3$ disproportionation; 4) the formation of $CaSO_4$ is not as extensive for exposures of 900°C as it is at 750°C; 5) in the presence of O_2 the production of CaS_2O_3 is reduced; 6) the products form as a thin layer on the surface of the 50 to 100 μm particles; and 7) the extent of SO_2 capture by the reactants decreases in the following order: $Ca(OH)_2 > CaCO_3 > CaO$.

In situ FTIR-DRS experiments confirmed post-exposure FTIR-PAS results. In addition, the inherent sensitivity and in situ capabilities of FTIR-DRS enabled the detection and identification of: 1) two different $SO_3^=$ species and 2) an intermediate monodentate $SO_4^=$ species. FTIR-DRS also indicated that the formation of $S_2O_3^=$ is dependent upon the concentration of CaO, $CaCO_3$ or $Ca(OH)_2$ in the NaCl diluent.

In order to be able to perform in situ high temperature FTIR-PAS measurements the development of a photoacoustic cell with elevated temperature and atmosphere control was necessary. The design of the cell is described. The interaction of 1.5% SO_2 with $Ca(OH)_2$, $CaCO_3$ and Na_2CO_3 as a function of time and temperature of exposure was monitored. Preliminary data, depicting the presence of physisorbed SO_2 on the $CaCO_3$ surface at 360°C, demonstrated the sensitivity of in situ FTIR-PA detection methods for both gas and solid phase reaction intermediates.

CONTENTS

	page
Abstract	ii
List of Figures	v
List of Tables	ix
Quality Assurance/Quality Control Statement	x
1. INTRODUCTION	1
SURVEY OF ANALYTICAL METHODS USED TO STUDY THE REACTIONS OF SO_2 WITH SOLID SORBENTS	2
INFRARED SPECTROSCOPY	6
PHOTOTHERMAL SPECTROSCOPY (PHOTOTHERMAL DETECTION)	6
DIFFUSE REFLECTANCE SPECTROSCOPY	11
SCOPE OF WORK AND OF THIS REPORT	13
2. CONCLUSIONS	16
AN ASSESSMENT OF FTIR-DRS AND FTIR-PAS APPLICABILITY TO THIS STUDY	16
MECHANISM	17
CAPACITIES OF SORBENTS FOR SO_2	19
DEPTH PROFILING	21
3. RECOMMENDATIONS	23
4. EXPERIMENTAL	25
CHEMICALS	25
INSTRUMENTATION	26
SAMPLE-GAS EXPOSURE PROCEDURES	29
WET CHEMICAL ANALYSIS	47
5. RESULTS AND DISCUSSION	49
INTRODUCTION	49
POST-EXPOSURE FTIR PHOTOACOUSTIC STUDIES	49

	page
IN SITU FTIR DIFFUSE REFLECTANCE STUDIES	65
IN SITU PHOTOACOUSTIC SPECTROSCOPY	104
6. REFERENCES	124

LIST OF FIGURES

		page
Figure 1.	Characteristic vibrational frequencies of representative inorganic sulfur-oxygen species.	7
Figure 2.	Characteristic vibrational frequencies of adsorbed SO_2 as a function of bonding mode.	8
Figure 3.	Schematic representation of the generation of the PA signal in a PA cell.	10
Figure 4.	Schematic illustration of proposed mechanisms for the reaction of SO_2 with CaO, $CaCO_3$ and $Ca(OH)_2$.	18
Figure 5.	Peak areas for sulfate formed from the reaction of replicate samples of CaO, $CaCO_3$ and $Ca(OH)_2$ with SO_2 in He at 750°C as a function of time.	20
Figure 6.	Schematics of particles of CaO, $CaCO_3$ and $Ca(OH)_2$ after exposure to SO_2 at elevated temperatures depicting the optical absorption (l_a) and thermal diffusion length (u) within the sample.	22
Figure 7.	Cross-sectional front view of the Harrick heatable vacuum chamber for FTIR-DRS.	28
Figure 8.	Schematic diagram of gas-exposure apparatus.	30
Figure 9.	FTIR-DR spectra of a single NaCl sample at 25°C, heated to 750°C and cooled to 25°C.	34
Figure 10.	FTIR-DR spectra of $CaCO_3$ (S/R) as a function of the number of scans.	35
Figure 11.	Cross-sectional view of the HT-PA cell.	37
Figure 12.	Schematic diagram of the HT-PA cell sample cup.	39
Figure 13.	Top view of HT-PA cell.	40

page

Figure 14. 100% lines for FTIR-PA spectra of carbon black with and without gas flow through the sample chamber of the HT-PA cell. 41

Figure 15. Schematic diagram of the HT-PA microphone holder. 43

Figure 16. Schematic diagram of the HT-PA cooling jacket. 45

Figure 17. Cross-sectional view of HT-PA cell assembled with Spectra-Tech optics. 46

Figure 18. FTIR-PAS of $Ca(OH)_2$ exposed to 1.5% SO_2 in He at 25°C as a function of time. 55

Figure 19. Peak areas of sulfite and hydroxyl bands for $Ca(OH)_2$ exposed to 1.5% SO_2 in He as a function of time. 56

Figure 20. FTIR-PAS of $Ca(OH)_2$ exposed to 1.5% SO_2 in He for 30 min as a function of temperature. 58

Figure 21. FTIR-PAS of $Ca(OH)_2$ exposed to 1.5% SO_2 in He at 750°C as a function of time. 61

Figure 22. FTIR-PA signal intensities for sulfite, thiosulfate and sulfate formed from the reaction of $Ca(OH)_2$ with 1.5% SO_2 in He at 750°C as a function of time. 62

Figure 23. FTIR-PAS of $Ca(OH)_2$ exposed to 1.5% SO_2 in He at 750 and 900°C; and 1.5% SO_2 in He/O_2 at 750 and 900°C. 64

Figure 24. *In situ* FTIR-DR spectra plotted in Kubelka-Munk (K-M) units of CaO exposed to SO_2 as a function of temperature. 71

Figure 25. Plots of $SO_3^=$ and $SO_4^=$ peak intensity for the exposure of CaO to SO_2 as a function of temperature. 72

Figure 26. *In situ* FTIR-DR spectra of $Ca(OH)_2$ as a function of temperature. 75

page

Figure 27. In situ FTIR-DR spectra for the exposure of $Ca(OH)_2$ to SO_2 at 25 and 200°C as a function of time. 77

Figure 28. In situ FTIR-DR spectra for the exposure of $Ca(OH)_2$ to SO_2 at 300 and 400°C as a function of time. 78

Figure 29. Plots of $SO_3^=$ and OH^- peak intensity (K-M units) for the exposure of $Ca(OH)_2$ to SO_2 at 25°C as a function of time. 80

Figure 30. Plots of $SO_3^=$ and OH^- peak intensity (K-M units) for the exposure of $Ca(OH)_2$ to SO_2 at 200°C and 300°C as a function of time. 81

Figure 31. In situ FTIR-DR spectra and OH^- peak intensity data for $Ca(OH)_2$ exposed to SO_2 at 300°C as a function of time. 83

Figure 32. Plots of $SO_3^=$ peak intensity (K-M units) for the exposure $Ca(OH)_2$ exposed to SO_2 at 400°C as a function of time. 84

Figure 33. Plots of $SO_3^=$ peak intensity for exposures of $Ca(OH)_2$ to SO_2 at 25, 200, 300 and 400°C as a function of time. 86

Figure 34. In situ FTIR-DR spectra of $Ca(OH)_2$ exposed to SO_2 as a function of temperature up to 468°C. 87

Figure 35. In situ FTIR-DR spectra of $Ca(OH)_2$ exposed to SO_2 for temperatures of 507 to 696°C; and cooled to 25°C under N_2. 88

Figure 36. In situ FTIR-DR spectra of $Ca(OH)_2$ exposed to SO_2 at 700°C and cooled to 25°C under N_2. 92

Figure 37. Plots of $SO_3^=$ and $SO_4^=$ peak intensity (K-M units) for $Ca(OH)_2$ exposed to SO_2 as a function of temperature of exposure. 93

page

Figure 38. In situ FTIR-DR spectra and peak intensity data plotted in Kubelka-Munk units for $CaCO_3$ under N_2 as a function of temperature. 96

Figure 39. In situ FTIR-DR spectra of $CaCO_3$ exposed to SO_2 at 400°C as a function of time. 97

Figure 40. Plots of $SO_3^=$ and $CO_3^=$ peak intensity (K-M units) for the exposure of $CaCO_3$ to SO_2 at 400°C as a function of time. 99

Figure 41. In situ FTIR-DR spectra of $CaCO_3$ exposed to SO_2 as a function of temperature. 100

Figure 42. Plots of $SO_3^=$ and $SO_4^=$ peak intensity for the exposure of $CaCO_3$ to SO_2 as a function of temperature. 103

Figure 43. In situ FTIR-PA spectra of Na_2CO_3 exposed to 1.5% SO_2 in N_2 and purged of the excess SO_2 gas. 105

Figure 44. In situ FTIR-PA spectra of Na_2CO_3 exposed to 1.5% SO_2 in N_2 at 25°C as a function of time. 107

Figure 45. In situ FTIR-PA spectra of the sample of Na_2CO_3 after exposure to SO_2 as a function of temperature under N_2. 110

Figure 46. In situ FTIR-PA spectra of Na_2CO_3 exposed to SO_2 as a function of temperature and time. 112

Figure 47. In situ FTIR-PA spectra of $Ca(OH)_2$ exposed to SO_2 at 25°C as a function of time. 114

Figure 48. Peak areas for $SO_3^=$ (950 cm^{-1}) and OH^- (3641 cm^{-1}) for $Ca(OH)_2$ to SO_2 as a function of time. 115

Figure 49. In situ FTIR-PA spectra of $Ca(OH)_2$ exposed to SO_2 as a function of temperature. 117

page

Figure 50. FTIR-PA spectra (25°C) of a single sample of $Ca(OH)_2$ exposed to SO_2 at 25, 100, 200, 300 and 400°C. 119

Figure 51. *In situ* FTIR-PA spectra of $CaCO_3$ exposed to SO_2 at 25°C as a function of time. 121

Figure 52. *In situ* FTIR-PA spectra of $CaCO_3$ exposed to SO_2 as a function of temperature and time. 123

LIST OF TABLES

page

Table 1. BET multipoint analysis of CaO, $CaCO_3$ and $Ca(OH)_2$. 25

Table 2. Summary of post-exposure FTIR-PAS sample types and exposure conditions. 51

Table 3. Summary of photothermal modulation frequency studies. 52

Table 4. Correlation tables for $SO_3^=$ and $SO_4^=$ species. 67

Table 5. FTIR band summary for sulfur-oxygen species. 68

Table 6. Sulfur-oxygen species for the exposure of 2% $Ca(OH)_2$ in NaCl to 1.5% SO_2 in N_2 up to temperatures of 468°C. 89

QUALITY ASSURANCE/QUALITY CONTROL STATEMENT

QA/QC requirements are applicable to this project. However, the data contained in this report are NOT supported by QA/QC documentation as required by U.S. EPA Quality Assurance policy.

SECTION 1

INTRODUCTION

Current methods designed to control and reduce the amount of sulfur dioxide emitted into the atmosphere from coal-fired power plants and factories rely upon the reaction between SO_2 and alkaline earth compounds and are called flue gas desulfurization (FGD) processes. Of these methods, dry desulfurization processes, using fine particulate limestone, have emerged as the preferred technology for future SO_2 emission control due to the reduced quantities of solid waste generated (as compared to wet methods), the (relative) ease of their installation into existing power plants and their high effectiveness (up to 90% removal of SO_2).[1] Briefly stated, dry desulfurization processes include two methods: 1) the dry limestone injection process, in which particulate limestone is injected into the smoke stack directly above the coal furnace and 2) the limestone injection with multistage burners process, known widely as LIMB, in which limestone is injected directly into the furnace. Although dry sorbent processes for the removal of SO_2 have been under development for several years, no commercial testing of these systems has occurred,[1] and questions still exist concerning the chemical mechanisms of the reactions between the sorbent and gas.

The development of a reliable <u>in situ</u> spectroscopic technique for studying heterogeneous reactions, such as those occurring in FGD systems, is the key to understanding the surface mechanisms which control these reactions. This report covers the development and application of Fourier transform infrared spectrometry with photoacoustic and diffuse reflectance detection for this purpose. The specific reactions chosen for study are those of SO_2 with CaO, $CaCO_3$ and $Ca(OH)_2$. The conditions of the

→ con't on pg 2

investigations were chosen, not with the intent to mimic actual smokestack conditions or to approximate any particular scrubbing methodology, but to provide a well characterized and controlled test of the spectroanalytical method as applied to relevant particulate samples. The project evaluates the feasibility of using these infrared spectroscopic techniques to monitor reactions between limestone and related materials with SO_2 at various temperatures so as to aid in obtaining a clear understanding of the chemical mechanisms by which SO_2 is captured.

SURVEY OF ANALYTICAL METHODS USED TO STUDY THE REACTIONS OF SO_2 WITH SOLID SORBENTS

The list of analytical methods previously used to examine the solid-gas reaction between alkaline earth compounds and SO_2 can be divided into six categories: 1) electron probe spectroscopy,[2,3] 2) thermogravimetric analysis[4-6] (TGA), 3) dissociation-pressure methods,[3,7-11] 4) physical surface characterization techniques such as the Brunauer, Emmett and Teller method (BET),[2,12,13] 5) wet chemical analyses[6,14] and 6) infrared transmission spectroscopy.[15,16]

Electron probe spectroscopy

High energy, or electron probe, spectroscopies involve the bombardment of a sample surface with electrons or ions, and then subsequent detection of scattered particles or emergent radiation from the surface. The energy of scattered particles or of the emergent radiation is characteristic of a given atom; and hence, a measurement of the energy spectrum of the particles or radiation identifies the surface atoms.[17] Often accompanying these techniques is scanning electron microscopy (SEM), which enables a study of surface morphology.

Experimentally, the conditions for accumulating results with these

techniques are optimal when the sample surface is smooth. This reduces the applicability of these techniques for examining solid-gas reactions involving particulate samples, such as those employed in the flue gas desulfurization processes. For example, a scanning Auger microanalysis of representative FGD samples was unsuccessful because the high surface area and feathery nature of the material effected the energy of the Auger electrons.[13] Secondly, and perhaps more importantly, electron probe spectroscopies require measurements of the sample to be made while the sample is in a vacuum. This necessarily precludes any in situ investigation of the reaction between gaseous SO_2 and particulate samples of CaO, $CaCO_3$ and $Ca(OH)_2$ and, of course, eliminates the possibility of detecting any unstable intermediate reaction products.

Thermogravimetric analysis

Thermogravimetric analysis (TGA) monitors changes in the weight of a sample as a function of temperature or as a function of time at a given temperature while the sample is in a controlled atmosphere. In fairly simple and predictable analyses, such as the determination of calcination temperatures of known samples, this technique is quite useful. For example, this technique successfully detects the weight changes for samples of $CaCO_3$ and $Ca(OH)_2$ upon calcination or the emission of gaseous CO_2 and H_2O, respectively.[4,13] However, for complex and uncharacterized reactions in which the sample is reacting with a gas to form an unidentified product or products, weight changes in the sample are difficult to interpret. Therefore, to interpret TGA results, wet chemical analyses of the sample at the completion of a TGA run are required. The inability of this technique to identify products during the reaction greatly reduces any possibility of detecting intermediate species. Furthermore, this technique does not

detect any changes in the sample that do not cause a weight change (such as a disproportionation reaction in which the bonding character of the sample changes but not the weight).

Dissociation-pressure method

The dissociation-pressure method has been predominantly used by Van Houte and Delmon[3,7-11] in the investigation of the reaction between SO_2 and alkaline earth compounds. For these experiments a sample is enclosed in a reactor which enables the control of the sample temperature and atmospheric environment. Upon addition of a known pressure of SO_2 to the reactor chamber (also at a known temperature) the reaction progress between the solid and gas is monitored using a manometer. Using the pressure changes of the gas in the reactor chamber and the ideal gas laws, the amount of SO_2 captured by the solid sorbent is determined. From this information the reaction products are inferred.

Surface area analysis

Several researchers have reported strong correlations between the surface area of solid sorbents and the reactivity of the sorbents towards SO_2. To characterize the effect of particulate sorbent surface area, nitrogen adsorption-desorption isotherms, or BET measurements,[18] have been made on samples of CaO, $CaCO_3$ and $Ca(OH)_2$ before and after exposure to SO_2 under various conditions. This analysis proved informative in these controlled experiments, in which the sample composition was known. Unfortunately, in a realistic situation, the surface area of samples would be difficult to relate to SO_2 capture since sorbent samples in coal-furnace systems contain many impurities which drastically alter their surface areas. For example, small amounts of carbon contamination in the sample

from ash produced in the furnace result in large increases in measured surface area of the bulk material.[13]

Wet chemical analyses

Although wet chemical methods have often been employed to support instrumental evaluations of reaction systems, these methods are often time consuming and impractical for the analysis of multi-component samples. For wet chemical analyses it is necessary to develop several procedures for the identification of all components in a reaction product. Since each constituent has to be measured by a different analytical method, in many cases each determination requires a separate replicate sample. Sample preparation is often extensive and elaborate, and analysis typically requires 6 hr from sample collection to final results.

Infrared transmission spectroscopy

Although the literature contains numerous reports describing the use of transmission spectroscopy to study gas-solid reactions, these studies have usually involved sample preparations which destroyed the integrity of the original sample. Neat samples, although desirable, almost always yield transmission spectra with saturated, nondiagnostic bands. Sample dilutions, intended to reduce spectral saturation, such as potassium bromide pellets,[19,20] hydro- or fluoro-carbon mulls[20] and solutions,[21] all interact with the sample to some extent and absorb radiation at their own characteristic frequencies as well. In fact, even just applying high pressure to the sample to form a pellet may result in undesirable changes in the sample; Blitz and colleagues found that pressing pellets of Cab-O-Sil modified trimethoxymethylsilane resulted in rapid unwanted hydrolysis of the silane.[22]

INFRARED SPECTROSCOPY

Infrared spectroscopy involves detection and measurement of the internal vibrational modes of molecules and as such is almost universally applicable to the study of molecular structure and bonding.[23,24] Despite the limitations of sample preparation and signal saturation previously described above, infrared spectroscopy, when coupled with effective detection accessories, can provide a wealth of information about solid-gas reactions. The study of solid-gas reactions involves the characterization of the solid sorbent surface and then subsequent identification of any reaction intermediates and/or products formed or adsorbed to this surface. The success of infrared spectroscopy in determining this information and hence in resolving reaction mechanisms can be ascribed to the fact that it is one of the few analytical methods that allows direct examination of adsorbed molecules on solid surfaces under a wide range of experimental conditions such as those of temperature and pressure. In the examination of the reaction of SO_2 with alkali sorbents vibrational spectroscopy can be used to differentiate between closely related sulfur-oxygen species (Figure 1), and in favorable cases can even detect differences in modes of surface bonding of absorbed species (Figure 2). The abilities of IR spectroscopy to examine solid-gas reactions are greatly enhanced through Fourier transform instrumentation (FTIR).[27-33]

PHOTOTHERMAL SPECTROSCOPY (PHOTOTHERMAL DETECTION)

Generation of the photothermal signal

Photothermal spectroscopy is based upon the generation of heat as the result of radiation absorption. In its simplest form, photothermal spectroscopy of condensed media involves placing a solid sample and microphone in a sealed gas-filled cell behind a transparent window (Figure

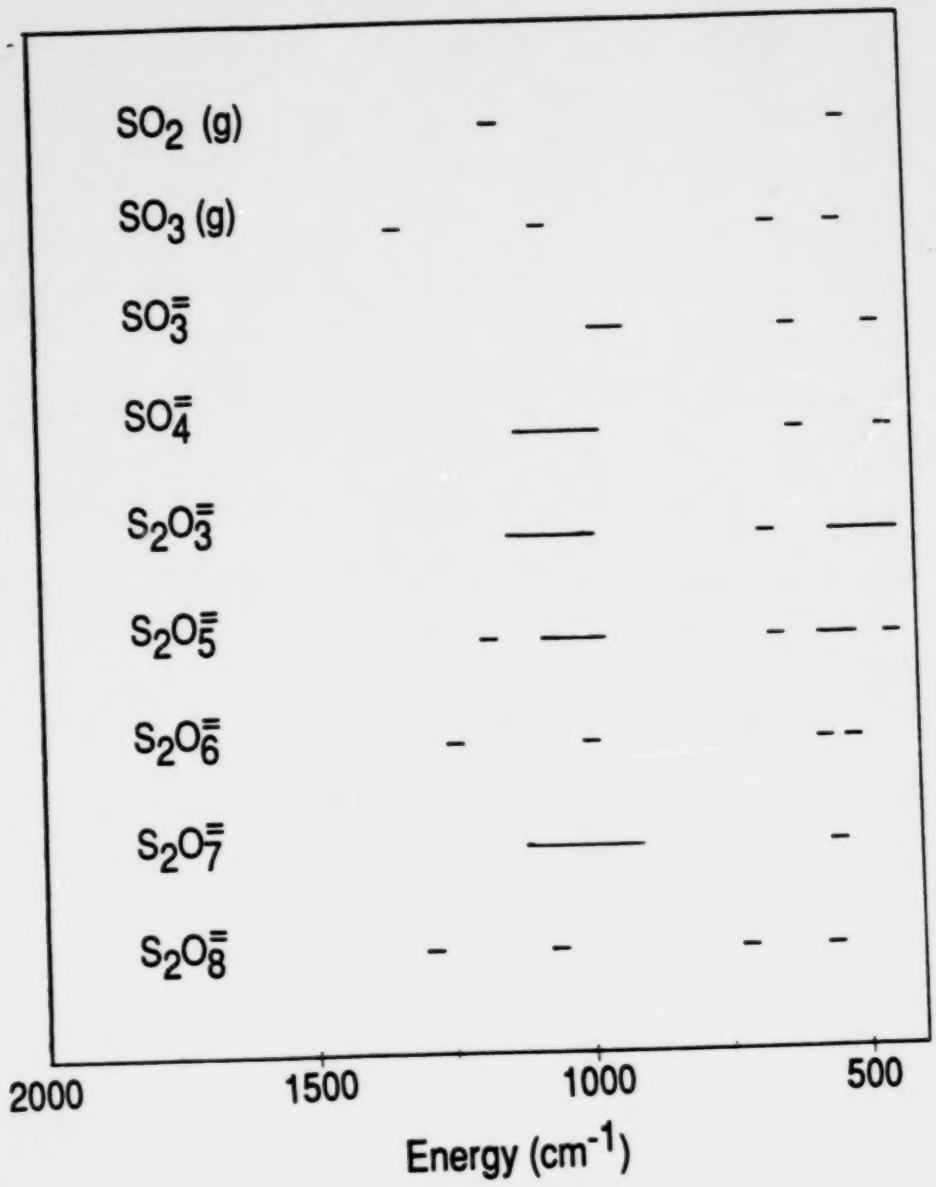

Figure 1. Characteristic vibrational frequencies of representative inorganic sulfur-oxygen species.[25]

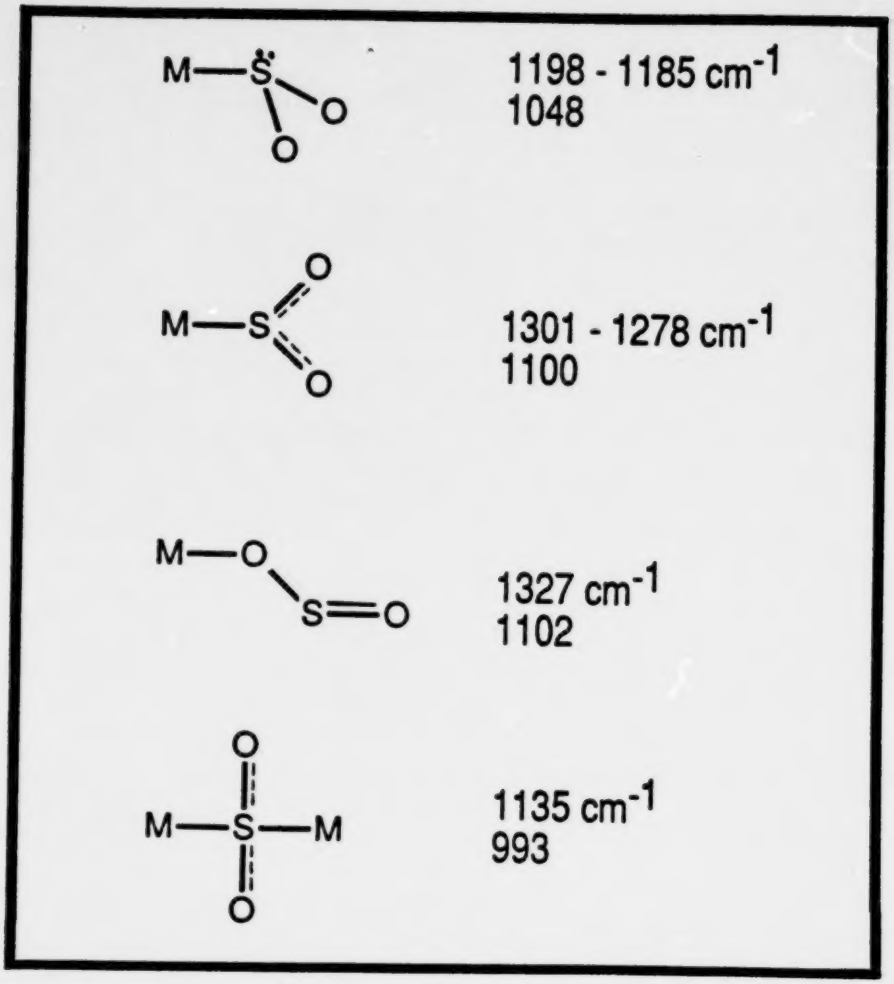

Figure 2. Characteristic vibrational frequencies of adsorbed SO_2 as a function of bonding mode.[26]

3). Modulated light is then shown upon the sample. The intensity modulation of the incident light can be synchronous or, as in the work reported here, the result of a scanning interferometer. Some of this light is absorbed by the sample and converted via nonradiative decay processes to thermal energy or heat. A fraction of this thermal energy diffuses to the sample surface and subsequently warms a thin layer of gas adjacent to the sample surface. This results in a periodic expansion of the thin layer of gas at the sample-gas interface. Since the sample is enclosed in a small, sealed cell, the periodic expansion of the gas produces pressure fluctuations which are then detected by a sensitive microphone also enclosed in the cell. This method of "listening to light" is commonly known as photoacoustic spectroscopy (PAS).[27]

As a detection method in FTIR, photoacoustic spectroscopy is particularly suitable for the study of heterogeneous reactions. The depth profiling capabilities of PAS allow a distinction between surface and near surface absorption. Furthermore, PAS typically requires no sample preparation and is therefore a thoroughly non-destructive technique. PAS shows little sensitivity to particle size or shape and is relatively insensitive to saturation effects. Thus it can be used on strongly absorbing samples without need to reduce the particle size or disperse the sample in a non-absorbing matrix. This also enables FTIR-PAS to be used for samples on the surface of strongly absorbing substrates or in mixtures with other absorbers. In addition, since only the light absorbed by the sample contributes to the PA signal, the method can also be used on strongly specularly reflecting samples (although the signal strength is lower than for powdered and other non-specularly reflective samples). The combination of photoacoustic detection with Fourier transform infrared spectroscopy is commonly referred to as FTIR-PAS.

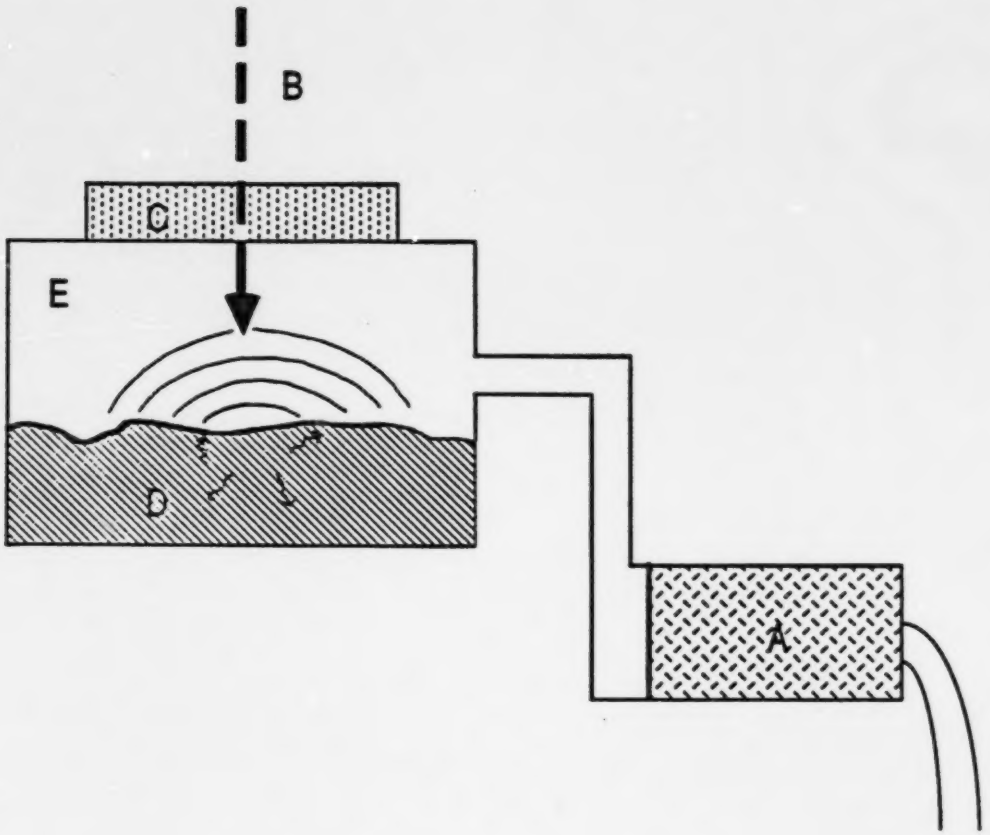

Figure 3. Schematic representation of the generation of the PA signal: (A) microphone; (B) modulated incident radiation; (C) window; (D) sample; (E) coupling gas.

DIFFUSE REFLECTANCE SPECTROSCOPY

Measuring the diffuse reflectance signal

Diffuse reflectance spectroscopy (DRS) is often regarded as the complementary technique to PAS for the investigation of powdered samples. In this technique, it is the incident light diffusely reflected from the surface of the sample that is detected.

The radiation reflected by a solid or matte surface can be regarded as a superposition of two distinct components. The first is due to specular reflection at the surface, for which the angles of incidence and reflectance are equal. This type of reflection is well characterized by Fresnel equations.[28] The second component of reflection originates from radiation penetrating the surface of the medium undergoing multiple scattering at the surfaces of individual particles and then returning to the surface by the scattering process to emerge as the diffuse reflection. During the reflection, refraction and scattering of light within the sample, some of the diffused radiation penetrates sample particles resulting in absorption by the sample.

For a typical Fourier transform infrared diffuse reflectance spectrum of a powder, the sample is placed in a shallow cup (1-3 mm deep) and irradiated with a focused beam from the interferometer. The incident radiation passes into the bulk of the sample, undergoes reflection, refraction, scattering and absorption by varying degrees before re-emerging at the sample surface. The light reflected in this manner is distributed in all directions of the surrounding hemisphere and is collected by an ellipsoidal mirror before being focused onto the detector.

A diffuse reflectance spectrum is derived by measuring the single beam reflectance spectrum of the sample and ratioing this to the single beam

spectrum of a nonabsorbing powder (such as KBr or NaCl in the infrared spectral region). The reflectance of a sample (relative to the standard reference) is defined as R_∞. Both the sample and reference materials must be held in a sample cup, which is sufficiently deep that an increase in its depth would cause no further change in signal. For "infinitely thick" samples, R_∞ is related to the scattering coefficient $\underline{s}$ and the molar absorption coefficient $\underline{k}$ by the Kubelka-Munk (K-M) function,[29-30] $f(R_\infty)$:

$$f(R_\infty) = (1-R_\infty)^2/2R_\infty = k/s \qquad (1)$$

Important assumptions of the K-M theory are that the sample is illuminated with diffuse radiation, the sample is infinitely thick, and no specular reflection is present. Experimentally these requirements are met by illuminating the sample with diffuse light, using samples 1 to 3 mm thick and collecting only the diffusely reflected component of light. Furthermore, Equation 1 predicts a linear relationship between the K-M function $f(R_\infty)$, and the absorption coefficient, $\underline{k}$, providing $\underline{s}$ remains constant. It has been found that a linear relationship between $\underline{k}$ and $f(R_\infty)$ is observed only when examining weakly absorbing samples of relatively small particle size. Deviations from linearity are attributed to an increase in the specular reflection from the sample in cases of strongly absorbing samples exhibiting large values of $\underline{k}$ and large particle size.[31] However, strong absorbers can be studied using diffuse reflectance when they are mixed with a powdered nonabsorbing sample of NaCl or KBr.

Implications of diffuse reflectance spectroscopy for this study

In the work reported here, diffuse reflectance spectroscopy is used to complement the results obtained via photoacoustic spectroscopy in the investigation of the reaction between SO_2 and CaO, $CaCO_3$ and $Ca(OH)_2$. Compared to the FTIR-PA signal, the FTIR-DR signal is more susceptible to

saturation, and thus this technique is limited to examining weakly absorbing samples. On the other hand, this tendency of the diffuse reflectance signal to saturate for strongly absorbing samples is directly related to the greater sensitivity of this technique relative to PAS. Saturation effects may be eliminated by mixing a portion of the strongly absorbing sample with a nonabsorbing powder such as KBr or NaCl. In this manner, the concentration, and hence absorbance, of the sample is reduced without encapsulating the sample in a nonabsorbing matrix. In fact, the area of contact of the adsorbent with a gas is much greater than if the sample were pressed into a transparent pellet. Consequently, diffusion of the gaseous reactants into, and effusion of the gaseous products from the sample is faster than it would be for pressed pellets. In some cell designs, such as the Harrick high temperature evacuable diffuse reflectance accessory,[32] the gas can be drawn through the sample so that equilibrium may be established in a matter of seconds throughout the sample. Once a strongly absorbing sample has been diluted so that spectral measurements are not saturated, quantitative determinations of absorbing species are possible by using the K-M analysis. DRS measurement times are frequently in the range of seconds, whereas PAS measurements usually require data collection times of several minutes. Finally, commercial manufacturers have recognized the applicability of DRS to investigate heterogeneous reactions, and consequently there are commercially available high temperature evacuable DR accessories.

SCOPE OF WORK AND OF THIS REPORT

Although numerous studies have focused on the understanding of mechanisms involved in heterogeneous reactions, such as the reactions between particulate samples of CaO, $CaCO_3$ and $Ca(OH)_2$ with SO_2 gas, a

complete picture of the mechanisms, intermediates, and limiting factors has not emerged. This is due to the complicated nature of the reaction, which is governed, not only by acid-base and oxidation-reduction chemistry, but also by factors such as particle size, pore clogging, product layer impermeability and sintering (at elevated temperatures). Consequently, in order to better understand these reactions, studies must be conducted such that there is minimal disturbance of the integrity of the particulate sample. Diffuse reflectance and particularly photoacoustic techniques enable the examination of particulate samples with minimal to no sample preparation. Coupled with FTIR spectroscopy, both DR and PA techniques enable the detection of molecular species on the surface of the particles and thereby provide unique information which may be used for determining reaction mechanisms in controlled atmospheres and at variable temperatures. Specifically, this project involved:

1). The determination of FTIR-DR and FTIR-PA signal saturation limits for samples simulating reaction products, such as $CaSO_4$ and $CaSO_3$.

2). Post-exposure FTIR-PA studies of the reactions between 1.5% SO_2 in He and particulate samples of a. CaO, b. $CaCO_3$ and c. $Ca(OH)_2$.

3). <u>In situ</u> FTIR-DR studies of the above reactions using a 1.5% SO_2 in N_2 reaction gas.

4). The development of a photoacoustic cell with temperature and atmosphere control and its application to <u>in situ</u> studies of the reactions of 1.5% SO_2 in N_2 with $CaCO_3$, $Ca(OH)_2$ and Na_2CO_3.

Parts 1, 2a and 2b have also been reported in the open literature.[33] This

report details particularly the work in parts 2c, 3 and 4. The conclusions and recommendations are based on the results of the combined studies. This report is abstracted from the Ph.D. dissertation of Meg Martin Thompson, Duke University, 1988.[34]

SECTION 2

CONCLUSIONS

These conclusions are based on the results presented here and in reference 33.

AN ASSESSMENT OF FTIR-DRS AND FTIR-PAS APPLICABILITY TO THIS STUDY

The general capabilities of photoacoustic and diffuse reflectance spectroscopies for examining the reaction of particulate samples of CaO, $CaCO_3$ and $Ca(OH)_2$ with SO_2 have been demonstrated. Together, these techniques were found to be very useful for characterizing the conversion of SO_2 to $SO_3^=$ and $SO_4^=$ on the surface of the particulate samples.

PAS was found to be more useful than DRS, since for PAS the samples could be examined without dilution into a nonabsorbing matrix (e.g. NaCl). This guaranteed that the reaction observed was undisturbed by the presence of a diluent. Results obtained in this study indicate that the diluent necessary for DR spectroscopy can effect the reaction observed.

Inherent difficulties of <u>in situ</u> FTIR-PAS for the investigation of solid-gas reactions at elevated temperatures are 1) the decrease in signal strength due to increase in sample temperature, as well as, 2) the sensitivity of this technique to ambient noise. In the work reported here, these factors limited the <u>in situ</u> spectral investigations to temperatures and gas flow rates not exceeding 400°C and 2 ml/min, respectively. On the other hand, DRS is not significantly effected by increases in sample temperature or ambient noise. If the samples studied had not been affected by the diluent, then, in fact, the superior S/N and sensitivity of DRS would have made it the method of choice.

MECHANISM

From the FTIR-PAS and FTIR-DRS data acquired using these techniques, it can be concluded that under the described conditions (relatively large particles, low flow rates, long exposure times and in the absence of O_2) the following reactions are important in the capture of SO_2 by CaO, $CaCO_3$ and $Ca(OH)_2$:

$$CaO(s) + SO_2(g) \xrightarrow{25^oC} CaSO_3(s) \quad (1)$$

$$CaCO_3(s) + SO_2(g) \xrightarrow{400^oC} CaSO_3(s) + CO_2(g) \quad (2)$$

$$Ca(OH)_2(s) + SO_2(g) \xrightarrow{25^oC} CaSO_3(s) + H_2O(g) \quad (3)$$

$$2CaSO_3(s) + SO_2(g) \xrightarrow{500^oC} 2CaSO_4(s) + S(g) \quad (4)$$

$$4CaSO_3(s) \xrightarrow{500^oC} 2CaSO_4(s) + CaS_2O_3(s) + CaO(s) \quad (5)$$

The ways in which the reactions may occur on the solid surface are schematically illustrated in Figure 4.[35] The initial reactions (reactions 1, 2, 3) occurring on each of the substrates, CaO, $CaCO_3$ and $Ca(OH)_2$, result in the formation of $CaSO_3$. The most likely mechanism for the conversion of SO_2 to $SO_3^=$ first involves the physical adsorption of the SO_2 gas on the sample surface; this process is then followed by the stabilization of SO_2 on the sample surface as an oxygen-bound sulfite ion. Finally, this initial oxygen-bound sulfite ion transforms to a pyramidal $SO_3^=$ ion. Continued SO_2 uptake then results in the buildup of more oxygen bound sulfite on the particle surface.

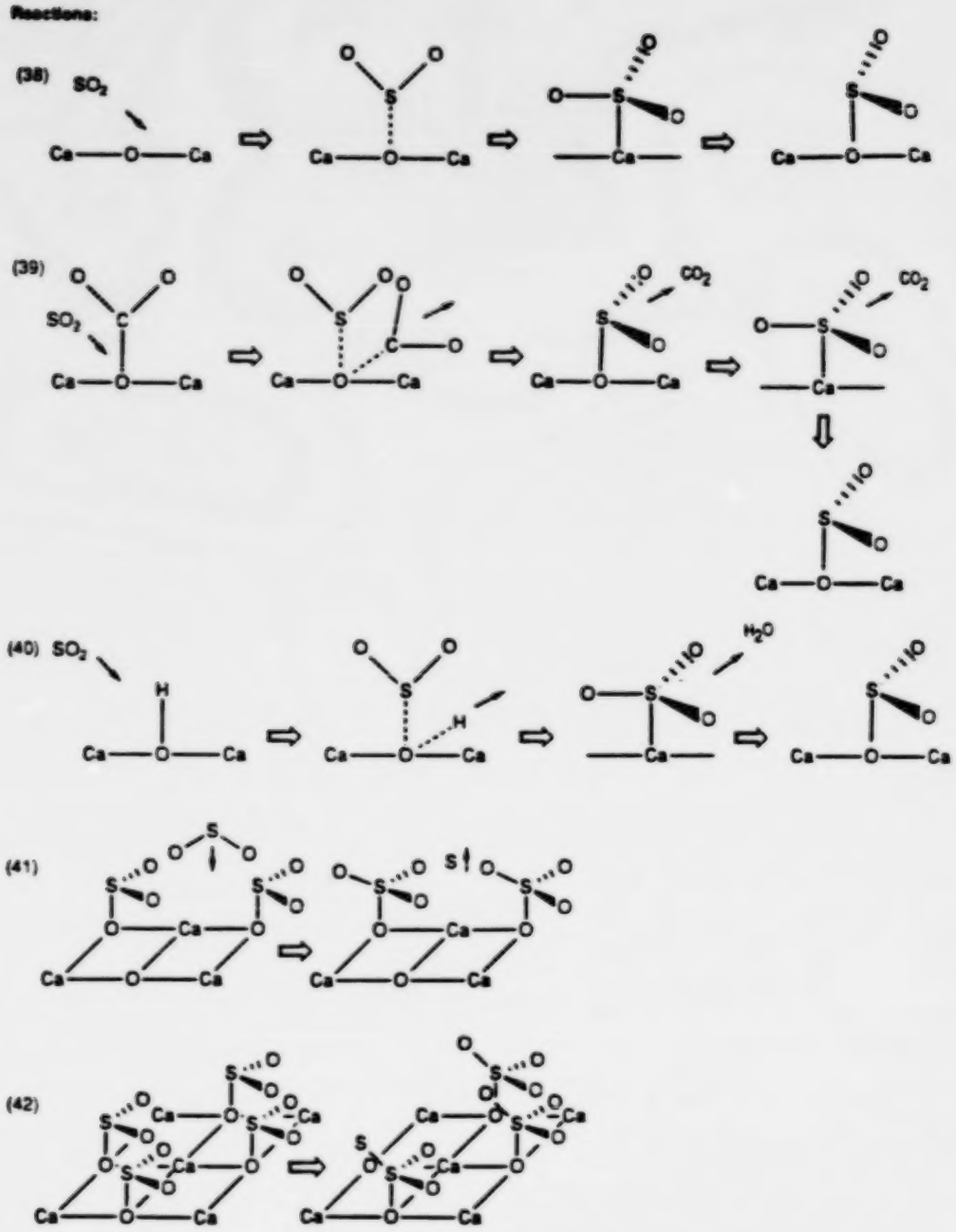

Figure 4. Schematic illustration of proposed Reactions (1, 2, 3, 4, and 5) of SO_2 with the surface of CaO, $CaCO_3$ and $Ca(OH)_2$.

The formation of $SO_4^=$ begins at 500°C and becomes dominant for all systems, (i.e. CaO, $CaCO_3$ and $Ca(OH)_2$) at temperatures of 600°C and above. The most likely sequence of chemical reaction steps in the conversion of SO_2 to $CaSO_4$ in the absence of O_2 is: first, the formation of $SO_3^=$ via reactions (1), (2) or (3) depending upon the reactive sorbent, followed by the disproportionation of the newly formed $CaSO_3$ to $CaSO_4$ via reactions (4) and (5).

Reaction (4) results in the formation of sulfur gas which can then react with "nascent" CaO to form CaS. The formation of CaS has been confirmed for exposed samples by wet chemical analysis. The disproportionation of $CaSO_3$ to sulfate and thiosulfate species as shown in reaction (5), has also been shown to be a route to $SO_4^=$ production in the absence of both O_2 and NaCl.

Another possible route to $SO_4^=$ production is the disproportionation of $SO_3^=$.

$$4CaSO_3(s) \text{ ---> } 3CaSO_4(s) + CaS(s) \qquad (6)$$

However, in the experiments reported here, it appears that this path is relatively unimportant.

In the presence of O_2, the mechanism for SO_2 to $SO_4^=$ conversion at 750°C is altered as indicated by the increases in $SO_4^=$ production for both $CaCO_3$ and $Ca(OH)_2$ exposures and the absence of $S_2O_3^=$ for all reaction. Although the CaO exposure did not exhibit an increase in $SO_4^=$ production, this is believed to be due to the production of an impervious product layer on the surface of these particles.

CAPACITIES OF SORBENTS FOR SO_2

The 679 cm^{-1} peak intensities for $SO_4^=$ formed on the surface of

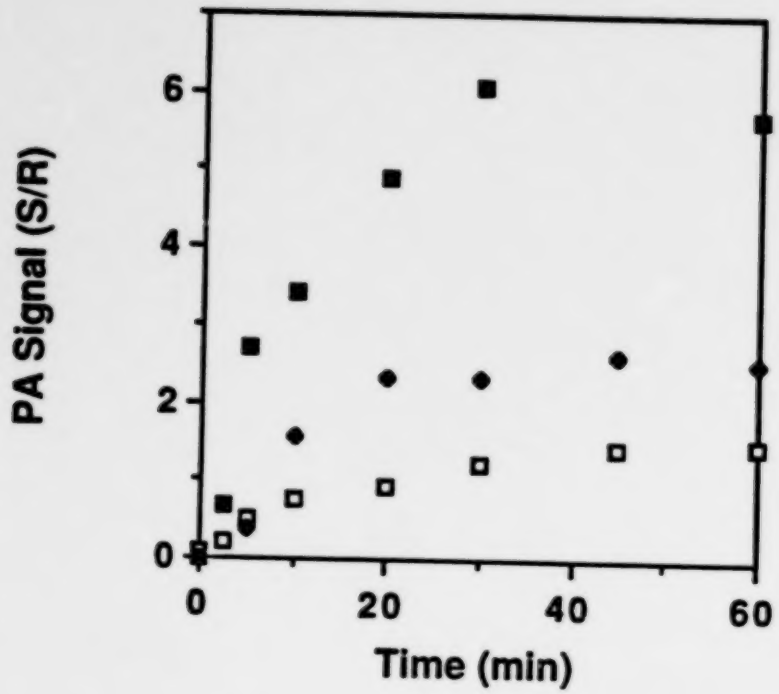

Figure 5. Peak areas for sulfate (679 cm^{-1}) formed from the reaction of replicate samples of CaO (□), $CaCO_3$ (◆) and $Ca(OH)_2$ (■) with SO_2 in He at 750°C as a function of time.

CaO, $CaCO_3$ and $Ca(OH)_2$ are plotted in Figure 5. These plots indicate that the extent of $SO_4^=$ formation on these 75 μm particles decreases in the order: $Ca(OH)_2 > CaCO_3 > CaO$. These data indicate that the initial product layer formed on the surface of $Ca(OH)_2$ is much more permeable to SO_2 than the layer formed on the CaO and $CaCO_3$ particles. This conclusion is consistent with the surface area properties reported for calcined samples of CaO, $CaCO_3$ and $Ca(OH)_2$, in which the surface areas of the calcined samples increase in the order: $CaO < CaCO_3 < Ca(OH)_2$.[35-37]

DEPTH PROFILING

Photoacoustic depth profiling experiments indicate that the products form in a reaction limiting layer on the surface of the particle. Based upon a Rosencwaig-Gersho analysis of the depth profiling data, the relationship between the product thickness, optical pathlength and thermal diffusion length was determined. Figure 6 summarizes these properties for $SO_4^=$ formed from the reaction of 75 μm particles of CaO, $CaCO_3$ and $Ca(OH)_2$ with SO_2 at elevated temperatures in which the $SO_4^=$ product layer thickness is estimated to be ca. <2.2 μm, 16 μm and >16μm, respectively.

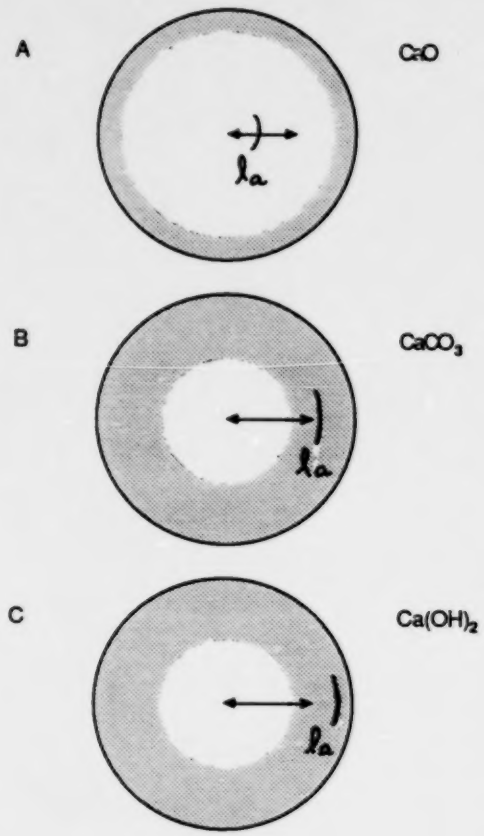

Figure 6. Schematics of particles of CaO (A), $CaCO_3$ (B) and $Ca(OH)_2$ (C) after exposure to SO_2 at elevated temperatures depicting the optical absorption (l_a) and thermal diffusion length range (<-->) within the sample.

SECTION 3

RECOMMENDATIONS

The work carried out so far in evaluating FTIR photoacoustic and diffuse reflectance spectral methods for characterizing the reactions of SO_2 with various alkali materials related to dry desulfurization processes has achieved a significant number of the original goals of the project, but the possibilities for additional work are considerable.

Extensive FTIR-PAS and -DRS studies have been carried out on the reaction of SO_2 with $CaCO_3$, CaO, $Ca(OH)_2$ and Na_2CO_3. PAS data have been measured in a "post-exposure" procedure for samples exposed to SO_2/He atmospheres at temperatures up to 900°C. In situ spectra measurements (i.e., during exposure to the reacting gas) have been made at temperatures up to 700°C for DRS and 400°C for PAS. For the in situ PAS studies, a high temperature PAS cell was constructed. Most of the work has been carried out using SO_2/He or SO_2/N_2 gas mixtures, but some studies involving addition of O_2 to the exposure gas were also completed. Only preliminary experiments involving promoters were accomplished.

In light of the results so far achieved, the following recommendations are made:

1. Continue to improve the high temperature PAS cell for in situ measurements in the temperature range up to 500°C.
2. Limit future work to the reaction of SO_2 with $CaCO_3$ and $Ca(OH)_2$.
3. Use DRS measurements as a compliment to the PAS data with due regard to the potential matrix effects of the diluent (NaCl, eg.).
4. Carry out systematic studies on the role of O_2 in influencing the reaction path.
5. Investigate the mechanism of various "promoters" of the SO_2

capture process, both those that have the potential for acting as oxidation catalysts and those that may act to increase the effective surface area of the particles.

SECTION 4

EXPERIMENTAL

CHEMICALS

Chemicals used in this investigation were: $CaCO_3$ (Fisher), Na_2CO_3 (Fisher), CaO (Aldrich Gold Label), $Ca(OH)_2$ (Baker), NaCl (Fisher) and carbon black (Norit A) (MCB). All these materials except the carbon black were ground and then sieved to achieve a 50-100 μm particle size range. For mixtures, the separately sieved components were mixed for five minutes in a Wig-L-Bug (Cresent Dental Mfg) without the grinding ball in order to achieve uniform mixing without significant decrease in particle size.

Samples of the pure sieved reactants were further characterized using the BET[18] method and a Quantasorb Surface Analyser (Quantachrome Corp.) to determine effective surface areas. Table 1 lists the surface area of these materials prior to reaction.

Table 1.

BET multipoint analysis of pure samples.

Sample	Surface area ($m^2/g \pm 10\%$)
CaO	4.99
$CaCO_3$	0.792
$Ca(OH)_2$	9.66

The exposure gas was 1.5% SO_2 in either He or N_2 (Matheson certified mixtures). The SO_2/He mixture was used only for the post-exposure studies. For sample cell purging either pure He or N_2 (National Welders) was used, depending on the diluent in the exposure mixture. IR transmission spectra

of these gases did not show any evidence of water.

INSTRUMENTATION

All spectra reported here were measured using an IBM Instruments Fourier transform infrared spectrometer (IBM/FTIR-95). This N_2-purged instrument incorporates a Genzel interferometer,[39-42] f/3.5 optics, a 7 W globar source and a germanium-on-KBr beam splitter for mid-infrared operation. The Genzel interferometer contains a double-sided moving mirror as opposed to the single-sided mirror used in the standard Michelson interferometer. This dictates that the Fourier frequency $\underline{f}$ is equal to four times the product of the mirror velocity and wavenumber.

FTIR-PA spectra were normally acquired with the IBM Instruments Photoacoustic Accessory (Model A6120890) using 8 cm^{-1} resolution and a mirror velocity of 0.059 cm/s (optical velocity, 0.235 cm/s). This produced Fourier (photothermal modulation) frequencies of 140 to 940 Hz over a range of 600 to 4000 cm^{-1}. Electronic high pass and low pass filters were set at 550 Hz and 6250 Hz, respectively. For depth profiling studies involving the dependence of the PA signal strength on modulation frequency, faster mirror velocities were also used. During depth profiling experiments no electronic filters were used. Standard spectra consisted of 512 co-added interferograms transformed using the Cooley-Tukey fast Fourier transform and Happ-Genzel apodization. All spectra were measured at ambient temperature (25°C). Sample spectra were normalized against the spectrum of Norit-A carbon black (MCB). By so normalizing the spectra to a blackbody absorber, band intensities are independent of source, beam splitter and PA cell variations.[43] All transformations and data manipulations, such as peak area determinations and Kubelka-Munk calculations were carried out on the Aspect 2000 computer associated with

the spectrometer, using standard IBM Instruments software.

FTIR-DR spectra were recorded using the IBM/FTIR-95 spectrometer accompanied by "praying mantis" optics (DRA-2CO) and an elevated temperature high vacuum diffuse reflectance accessory (HVC-DRP) both supplied by Harrick Scientific Corporation. The "praying mantis" optics intercept the transmission beam of the FTIR with a flat mirror and then with a second mirror, reflect the beam to a 6:1 off-axis ellipsoidal mirror that focuses the beam onto the horizontal sample stage. Light diffusely reflected from the sample stage is collected by a second 6:1 ellipsoidal mirror and is reflected to the LN_2-cooled MCT detector by two flat mirrors in the DRS accessory and three additional mirrors of the IBM Instruments FTIR-95.

The elevated temperature high vacuum diffuse reflectance accessory (Figure 7), consisting of a top cover and base plate, is easily placed between the two ellipsoid mirrors of the "praying mantis" assembly. The top cover of the cell is 2 3/4 in. high and contains two ZnSe windows and one glass viewing window. The ZnSe windows (15 mm d., 2 mm t.) (A), through which the IR radiation enters and exits the cell, are sealed in place by Kalrez@ (B) and Teflon@ (C) O-rings. These windows are positioned in the apparatus so as to allow only diffusely reflected light to be collected as signal. The viewing port (12 mm d., 2 mm t.), located between the ZnSe windows, is also held by Kalrez@ and Teflon@ O-rings. The windows were selected based upon the experimental wavelength range of operation and the resistance of the window material to the reactants and products examined. ZnSe was chosen particularly since it is resistant to water (a product of most $Ca(OH)_2$ reactions) and transparent from 550 to 4000 cm^{-1}. The transmission throughput for two ZnSe windows (refractive index 2.89) is

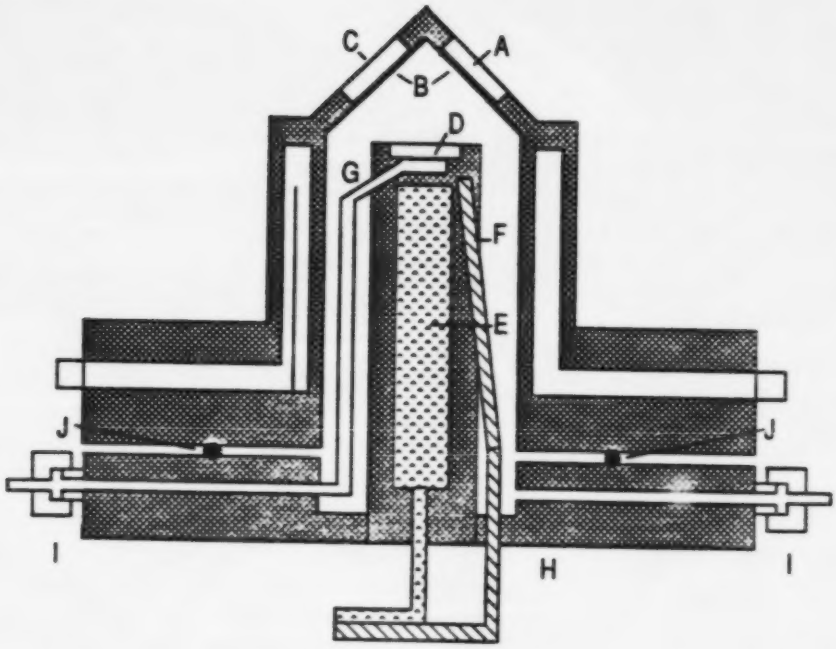

Figure 7. Schematic cross-sectional view of the Harrick heatable vacuum chamber for FTIR-DRS. (A) ZnSe window; (B) Kalrez@ O-ring (12 mm); (C) Teflon@ O-ring; (D) stainless steel screen; (E) 100 W cartridge heater; (F) type J thermocouple; (G) gas inlet port; (H) gas outlet port; (I) Cajun@ fittings; (J) Kalrez@ O-ring (50 mm).

50%. For samples with concentrations of absorbing species greater than 10%, better throughput was required for spectral measurements. In these instances, the ZnSe windows were replaced by KBr windows (refractive index 1.56) to enable more light to reach the detector and hence better spectra to be obtained. During short periods of use, the KBr windows were unaffected by water vapor emitted by the sample.

FTIR-DR spectra acquired using the Harrick Diffuse Reflectance Accessory were transforms of 512 co-added interferograms accumulated at 4 cm^{-1} resolution. Sample spectra (S) were referenced to the spectrum (R) of 50 to 100 um particle size NaCl. Spectral data manipulations involving Kubelka-Munk and peak area calculations were performed using standard IBM FTIR software.

SAMPLE-GAS EXPOSURE PROCEDURES

Post exposure photoacoustic spectroscopy of $Ca(OH)_2$

The equipment used for solid-gas exposures is illustrated in Figure 8. this is the same equipment used for the earlier post exposure experiments with $CaCO_3$, CaO and other materials. In a glove bag filled with dry He, samples of the powder to be exposed were placed on the quartz frit at the center of the 60 cm long quartz reaction tube (all quartz parts from GM Associates, Inc.). The reaction tube was composed of two sections which joined together just above the frit with a 19/38 quartz joint. This reaction tube containing the sample was sealed by Teflon® valves at either end and mounted vertically to the stainless steel gas delivery system. In order to ensure immediate delivery of the reactant gas, the stainless steel tubing was purged for 2 min with the 1.5 or 0.75% SO_2/He gas mixture prior to exposure. For exposures at elevated temperatures the reaction tube was positioned in the bore of a vertically mounted Lindberg tube furnace (Model

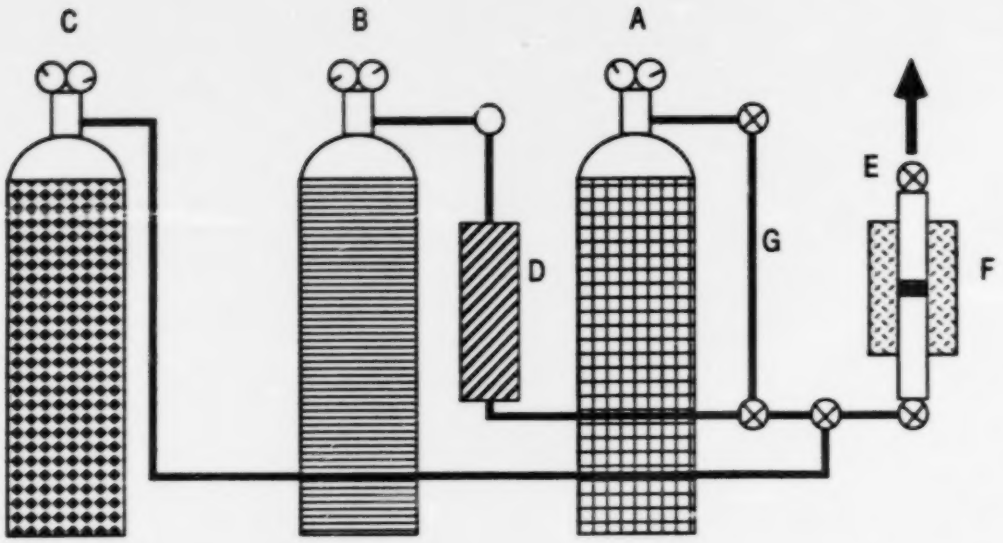

Figure 8. Schematic diagram of gas-exposure apparatus for post-exposure spectral measurements: (A) 1.5% SO_2 in He gas cylinder; (B) 100% He gas cylinder; (C) 100% O_2 gas cylinder; (D) Alltech gas dryer; (E) quartz reaction tube; (F) Lindberg tube furnace; (G) stainless steel tubing. Reprinted with permission from Appl. Spectros., 41, 120 (1987). Copyright Kansas State University.

55035). The furnace was heated to and equilibrated at the desired reaction temperature before the insertion of the reaction tube. After exposure of the sample for the desired amount of time the reaction tube was immediately flushed with He, and in the case of elevated temperature exposures, removed from the furnace and cooled to ambient temperature. The reaction tube was again sealed and transferred to the He filled glove bag. While in the glove bag the powdered sample was transferred from the reaction tube to the photothermal cell[44] (IBM Instruments Photoacoustic Accessory), which had been previously purged with He. The photoacoustic cell was then sealed and placed in the sample compartment of the FTIR spectrometer.

In situ diffuse reflectance spectroscopy

Materials--

Samples of $CaCO_3$, $Ca(OH)_2$ and CaO were prepared as described for post-exposure experiments (Section II. A. 1.). These samples were then diluted with 50 to 100 μm particle size NaCl to 2, 10 and 50% by weight mixtures. Samples were mixed as described above.

For FTIR-DRS experiments the sample is placed on top of a stainless steel screen (80 mesh, 1/4 in. d.; Alltech) (D) in a sample holder region at the top of the 1/2 in. diameter stainless steel sample stage mounted on the base plate. The base plate is designed so that the sample stage heating and temperature control devices are external to the vacuum system. The heater assembly consists of a 1 1/4 in. long, 100 W, 120 V heater (Hotwatt) (E) and an iron-constantan (type-J) thermocouple (F) embedded in the sample stage 1/8 of an inch from the sample. The bottom of the sample stage is constructed as a thin walled section of stainless steel to slow the transfer of heat from the sample stage to the rest of the base plate. The temperature of the sample is monitored and controlled via a PID

temperature programmer (Rika Kogyo Co., Ltd.; RKC Model REX-P100). Rates of sample temperature change for these experiments ranged from 3 to 5°C/min and were accurately (± 1% of the desired temperature) controlled by the PID temperature programmer.

Atmosphere control in the chamber is maintained through three ports, a gas inlet (G) and exit (H) port as well as a vacuum port. These ports are made from Cajun® fittings (I) welded to the base plate to ensure vacuum seals. The gas inlet port enters the DRS chamber through the sample post directly under the stainless steel screen on which the sample is placed. The position of this port ensures that the reactant gas passes through the powdered sample. Maximum gas flow rates used were 30 ml/min. The top cover and base plate of the heatable atmosphere chamber are clamped together in three spots. A Kalrez® O-ring (J) located between these two pieces ensures a vacuum seal between the two components.

In situ FTIR-DR spectra were recorded with the LN_2-cooled MCT photodetector of the IBM/FTIR-95 spectrometer because of its high sensitivity ($D^* = 36.7 \times 10^9$ $cmH^{1/2}/W$) and fast response time compared to the DTGS pyroelectric detector also supplied with the spectrometer. Sample spectra (S) were referenced to the spectrum (R) of 50 to 100 um particle size NaCl (Fisher Scientific). For experiments involving the detection of H_2O emitted by $Ca(OH)_2$, the NaCl was not ground and sieved until shortly before use. This is because alkali halides tend to adsorb water and organics from air. Although KBr has previously been recommended as the preferred reference material for FTIR-DRS;[45] NaCl was chosen for this work since it has a higher melting point than KBr ($mp_{NaCl} = 801°C$ vs. $mp_{KBr} = 734°C$). However, after heating a sample of NaCl under N_2 at 750°C a fine white film coating the inside of the window jacket was observed,

indicating that the sample did vaporize at this temperature. The spectrum of the sample before and after heating indicated that the sample was chemically unaffected by this process with the exception of the loss of some physisorbed water (Figure 9).

In situ experiments were monitored using loop functions available via the standard spectrometer software which enabled spectra to be recorded at exact intervals in time. To ensure that no interruption in the spectral recording cycle occurred, the correlation function for sequential interferograms was turned off. Spectra of a sample of $CaCO_3$ recorded using increasing numbers of scans indicate that, even after a single scan, the IR characteristics of the sample are distinguishable (Figure 10). For better signal-to-noise (S/N), 16 scans accumulated in 16 s were found to be optimal. However, a spectrum obtained every 16 s generated unreasonably large and unneeded amounts of data for experiments taking over a half hour in time. For these experiments, 512 scans were accumulated, requiring 186 s per spectrum.

For a typical in situ experiment, the sample was loaded onto the stainless steel screen of the sample stage and leveled in the holder by drawing the flat edge of a spatula over the top of the sample. The top cover of the high temperature DRS chamber was then secured over the sample stage, the gas lines were attached to the Cajun® fittings and the FTIR sample compartment was sealed. When no water vapor was evident in the spectrum of the sample (S/R) (after 3 to 4 hr), experimentation continued. It should be mentioned that the reference spectrum was generally acquired after purging the FTIR sample chamber overnight (ca. 12 hr) and that the P_2O_5 was kept in the FTIR sample compartment as a desiccant. One of three basic types of experiments was performed, (1) the sample was heated under an inert atmosphere of N_2, (2) the sample was heated to a determined

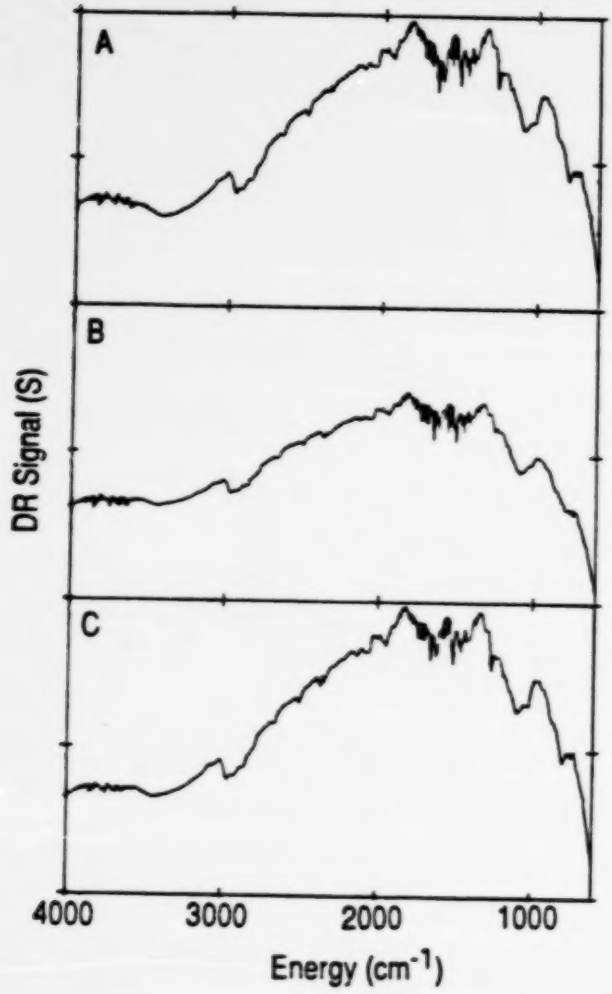

Figure 9. FTIR-DR spectra of NaCl (A) at 25°C; (B) heated to 750°C; and (C) cooled to 25°C under N_2. (The Y axis is scaled 1.000 to 1.022 for all spectra.)

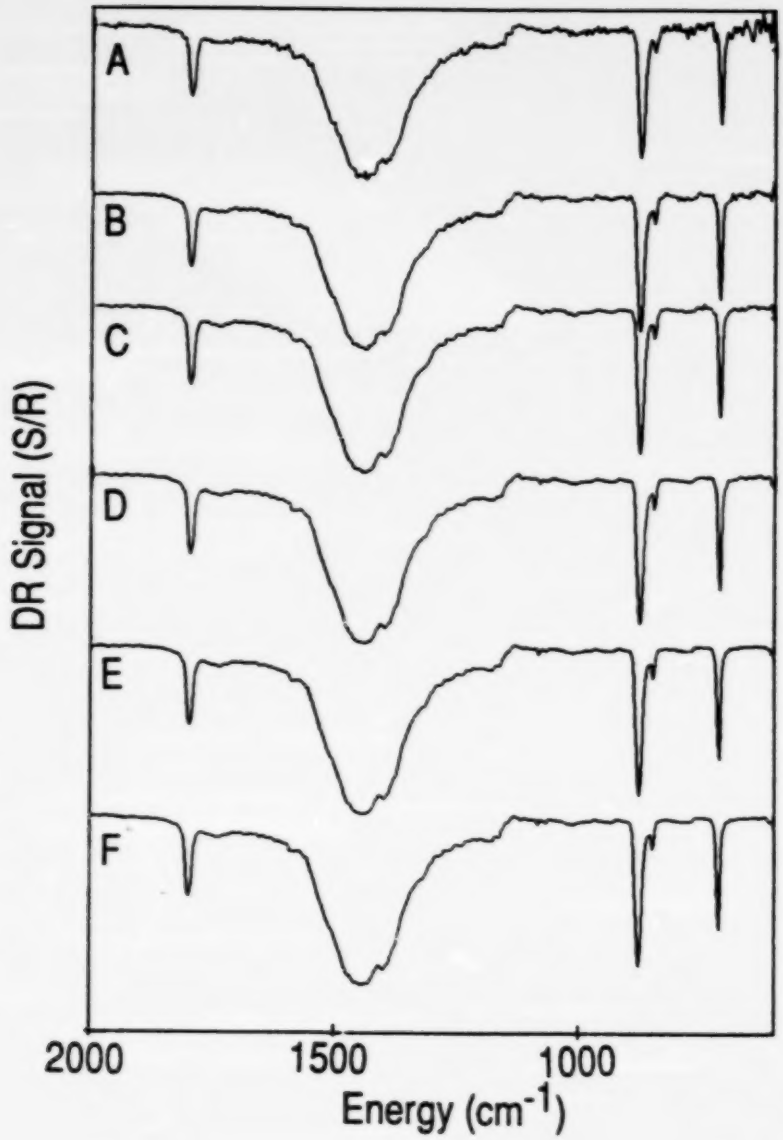

Figure 10. FTIR-DR spectra of $CaCO_3$ (S/R) as a function of the number of scans (A) 1; (B) 4; (C) 16; (D) 32; (E) 128; (F) 512.

temperature under N_2 and then exposed to a reactant gas mixture, or (3) the sample was simultaneously heated and exposed to the reactant gas mixture. Interferograms of the sample were accumulated at a nominal resolution of 4 cm^{-1} as each reaction occurred and then transformed as described above.

In situ photoacoustic spectroscopy

Materials--

Samples of $CaCO_3$, $Ca(OH)_2$ and CaO were prepared as described for post-exposure experiments. The gases used in these experiments were 1.5% SO_2 in N_2 and 100% N_2.

The high temperature photoacoustic (HT-PA) cell--

The high temperature photoacoustic (HT-PA) cell consists of four main parts: 1) window holder; 2) cell body; 3) microphone holder; and 4) cooling system. Figure 11 presents a schematic cross-sectional view of the cell.

The stainless steel window holder (1 1/2 in. ht.; 1 5/8 in. o.d.) is designed to hold two windows (32 mm d X 2 mm t.; 25 mm d X 2 mm t.) which may be quartz for UV-VIS or NaCl for IR experiments. The windows are held in place one inch apart with stainless steel threaded retainer rings that screw into the holder and wedge the window in between. The volume between the windows may be evacuated in order to provide added insulation[46] and thermal stability. The entire window holder screws down into the stainless steel body of the HT-PA cell such that the bottom window is 0.08 in. from the top of the sample. An optional window holder containing a single window can also be used and is adequate for temperatures up to 400°C. All seals were obtained using Teflon@ gaskets. For temperatures above 400°C, copper gaskets are required.

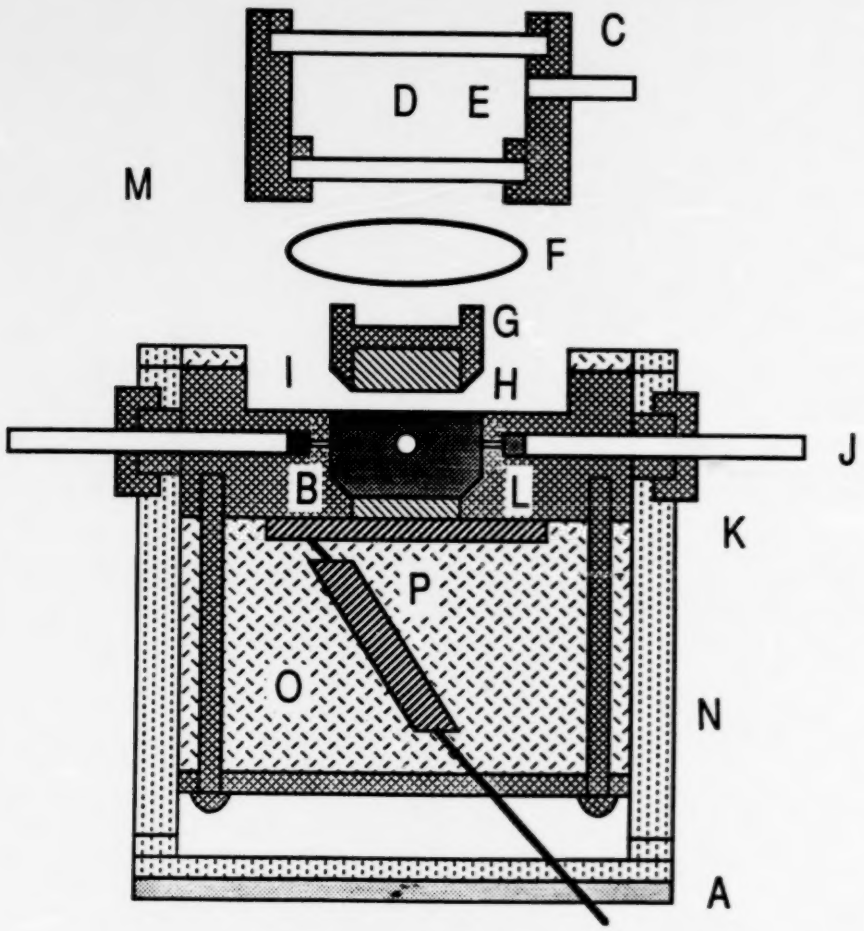

Figure 11. Schematic cross-sectional front view of the HT-PA cell: (A) foam; (B) copper plug; (C) window holder; (D) stainless steel rings; (E) window; (F) O-ring; (G) sample holder; (H) stainless steel cell body; (I) copper plug; (J) gas channels; (K) Swagelock fitting; (L) stainless steel frit; (M) microphone; (N) water jacket; (O) insulation; (P) coil heater with insulated wire adapter. Reprinted with permission from Anal. Chem., 60, 1027 (1988). Copyright American Chemical Society.

The cell body houses the sample chamber, gas and microphone channels and heater. A removable sample holder (Figure 12) with a copper plug at its base (1/2 in. d. X 1/4 in. t.) fits closely into the sample chamber and rests on another copper plug at the center of the HT-PA cell body. These copper plugs (1/4 in. d. X 1/8 in. t.) enhance the transfer of heat from the heater coil located directly below the sample holder to the sample. In addition, the base of the sample holder is made with slanted sides[46] to prevent jamming the holder in place due to expansion of the stainless steel during heating. The angles of the slanted side to the sample holder base encourage the holder to rise slightly when heated rather than to expand in place. Finally, four 1/8 in. square grooves at 90° intervals around the sides of the sample holder correspond to the positions of the gas inlet, gas outlet and microphone channels and a positioning pin.

The gas inlet and outlet channels (Figure 13, B, C) are made from 1/8 in. o.d. diameter tubing. The tubing is press fitted into holes in the cell body which are open to the sample chamber. At 1/16 of an inch from the sample chamber the holes in the cell body reduce to a 1/16 in. d.. The sample ends of the 1/8 in. stainless steel gas channel tubing fitted with 2 um stainless steel frits (Alltech) (E) seat against this 1/16 in. shoulder. As demonstrated by Royce et al.,[47-49] although the frits allow the gas to flow through the sample chamber, they do not destroy the acoustic integrity of the cell. Figure 14 demonstrates the S/N ratio for the spectrum of carbon black measured during gas flow conditions. The gas flow is controlled by a Rotamer manifold (Matheson) capable of mixing four separate gases. The tubing of the gas channels is further secured in place with stainless steel Swagelock@ fittings threaded into the body of the cell. The microphone channel, or acoustic coupling tube, (2.1 in. long) is

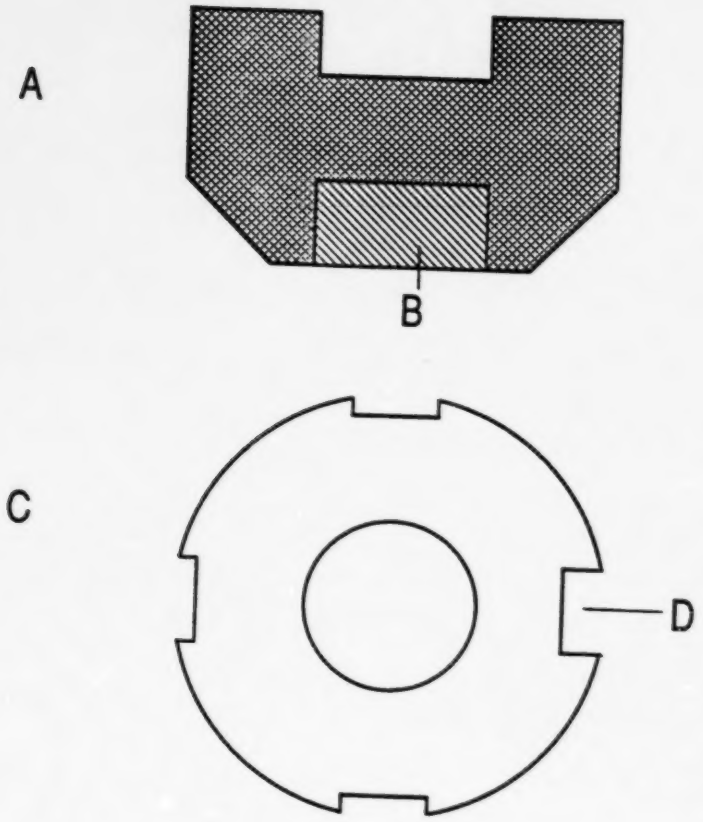

Figure 12. Schematic diagram of the HT-PA cell sample holder: (A) front cross-sectional view; (B) copper plug; (C) top view; (D) locator pin groove.

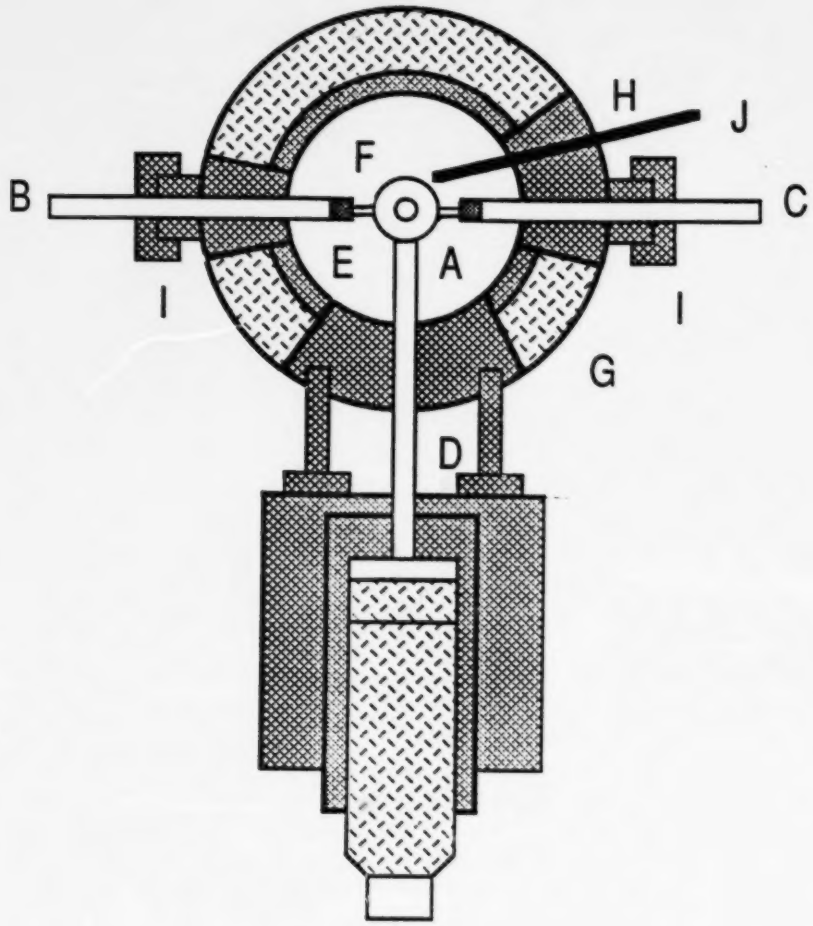

Figure 13. Schematic top view of HT-PA cell: (A) sample holder; (B) gas inlet channel; (C) gas outlet channel; (D) microphone channel; (E) 2 um stainless steel frit; (F) locator pin; (G) insulation; (H) stainless steel cell body; (I) Swagelock@ fittings; (J) J-type thermocouple.

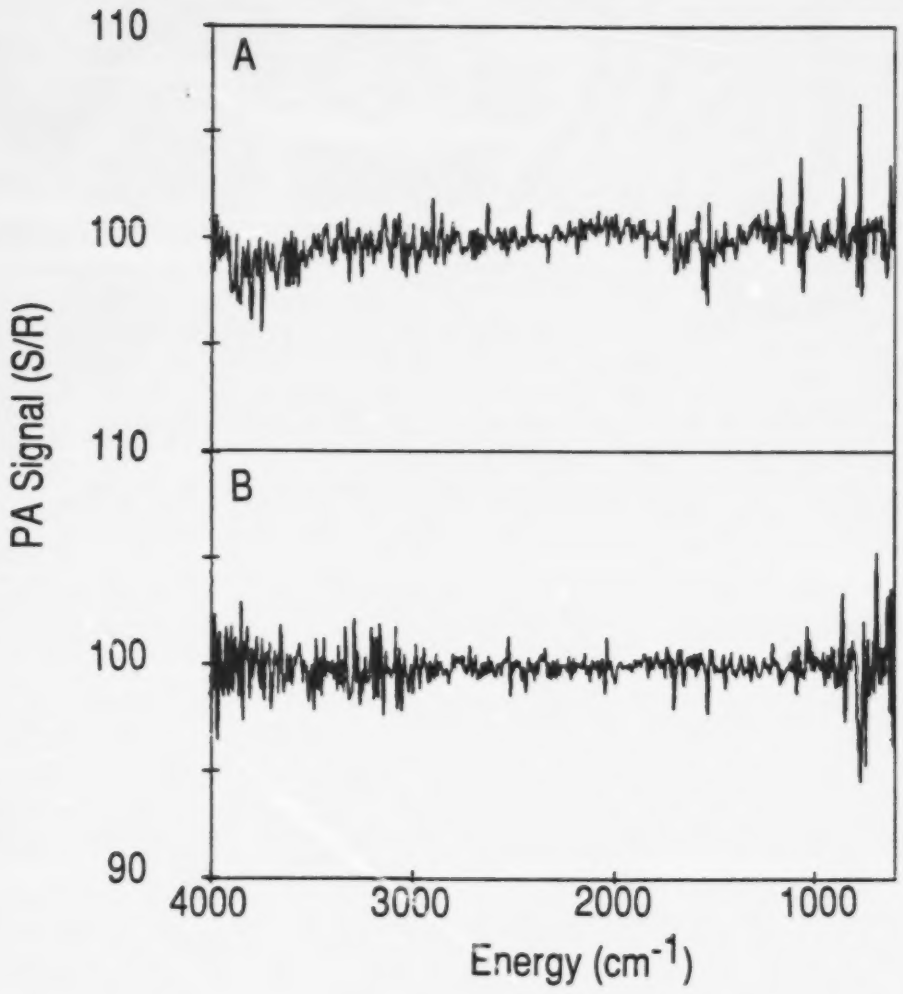

Figure 14. 100% lines for FTIR-PA spectra of carbon black (A) with no gas flow and (B) gas flow through the sample chamber of the HT-PA cell.

made of thin walled 1/16 in. stainless steel tubing (1 mm i.d.). The thin walled tubing limits the conduction of heat from the HT-PA sample region to the microphone chamber.

The microphone (Bruel and Kjaer 4165, Figure 15, A) is threaded into a stainless steel cylinder 3/4 in. o.d. which in turn is sealed with two O-rings into the cylindrical cavity of the stainless steel microphone chamber with the microphone normally flush against the end of the cavity, at the end of the acoustic coupling tube. The weight of the microphone chamber is borne by two stainless steel bolts which also serve to connect it to the cell body. The side of the microphone chamber exposed to the sample chamber is faced with 1/4 in. thick mylar insulation (Johns Manville).

The sample is heated by a 400 W bendable cartridge heater (0.062 in. o.d.; 31 in. long; ARi Industries, Inc.) coiled to a 2 in. diameter spiral. This heater is held against the bottom of the sample chamber (1/8 in. below the sample) by a 1 in. thick block of insulation (Moldatherm II, Lindberg). A 1/4 in. thick layer of this insulation is also placed around the cell body. Furthermore, a cylindrical ring of insulation (1/4 in. t.) is placed around the window holder and over the remaining stainless steel areas of the cell. The temperature of the sample is regulated with a PID temperature controller (Rika Kogyo Co.) and a type-J (iron-constantan) thermocouple (0.040 in. d.; Cole Parmer) which is positioned 1/8 of an inch from the sample holder edge. A triac circuit[50] is interfaced between the temperature controller and the heater to reduce the current flow into the temperature controller from the heater.

Although insulation at least 1/4 in. thick surrounds all stainless steel areas of the cell body, with the exception of the area directly over the sample, a cooling system is required to prevent the eventual heating of the spectrometer. A cylindrical aluminum cooling jacket surrounds the body

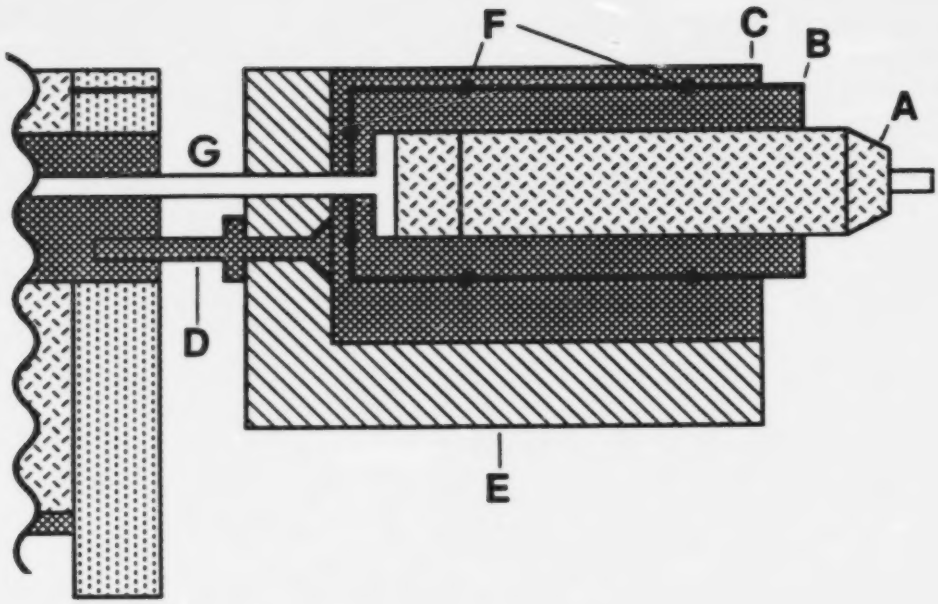

Figure 15. Schematic diagram of the HT-PA microphone holder: (A) microphone; (B) stainless steel cylinder; (C) rectangular stainless steel holder; (D) stainless steel bolt; (E) Mylar insulation; (F) O-ring; (G) sample-microphone connecting tube. Reprinted with permission from Anal. Chem., 60, 1027 (1988). Copyright American Chemical Society.

of the HT-PA cell (Figure 16). The cooling jacket is assembled from three pieces of aluminum: a 2 in. cylinder (2 3/4 in. i.d.; 4 3/4 in. o.d.) and two 1/4 in. thick aluminum rings that fit onto the top and bottom of the cylinder. Allowances are present in the water jacket for the microphone and gas inlet and outlet connectors (Figure 16). As shown in Figure 16F, holes 3/8 of an inch in diameter drilled through the center cylinder connected by milled paths on opposite ends of the cylinder create the channel through which the water flows. Flat rubber gaskets between each aluminum ring and the top and bottom of the water jacket seal the water in the jacket. Swagelock® fittings connected to the water channel serve as the inlet and outlet ports. A secondary water cooling system is required around the stainless steel tube connecting the sample and microphone chambers: A piece of 1/8 in. o.d. copper tubing is wrapped over the sample/microphone tube and is connected to the input port of the water jacket. Water flowing through the copper tubing reduces the conductive heat transferred by the sample/microphone connecting tube to the microphone. Consequently, the incoming or coolest water cools the microphone first, before removing heat from the outer layer of insulation around the cell.

In order to use the HT-PA cell with the IBM/FTIR-95 spectrometer, special transfer optics were required. These optics (supplied by Spectra-Tech) consist of one ellipsoidal and two flat mirrors which are mounted on an optical plate 5 1/2 in above the base of the sample chamber. The horizontal converging beam of the spectrometer is turned 90° downward and further focused to a 4 mm spot on the sample. The optical plate is mounted on hinges to permit its easy removal and hence access to the HT-PA cell (Figure 17).

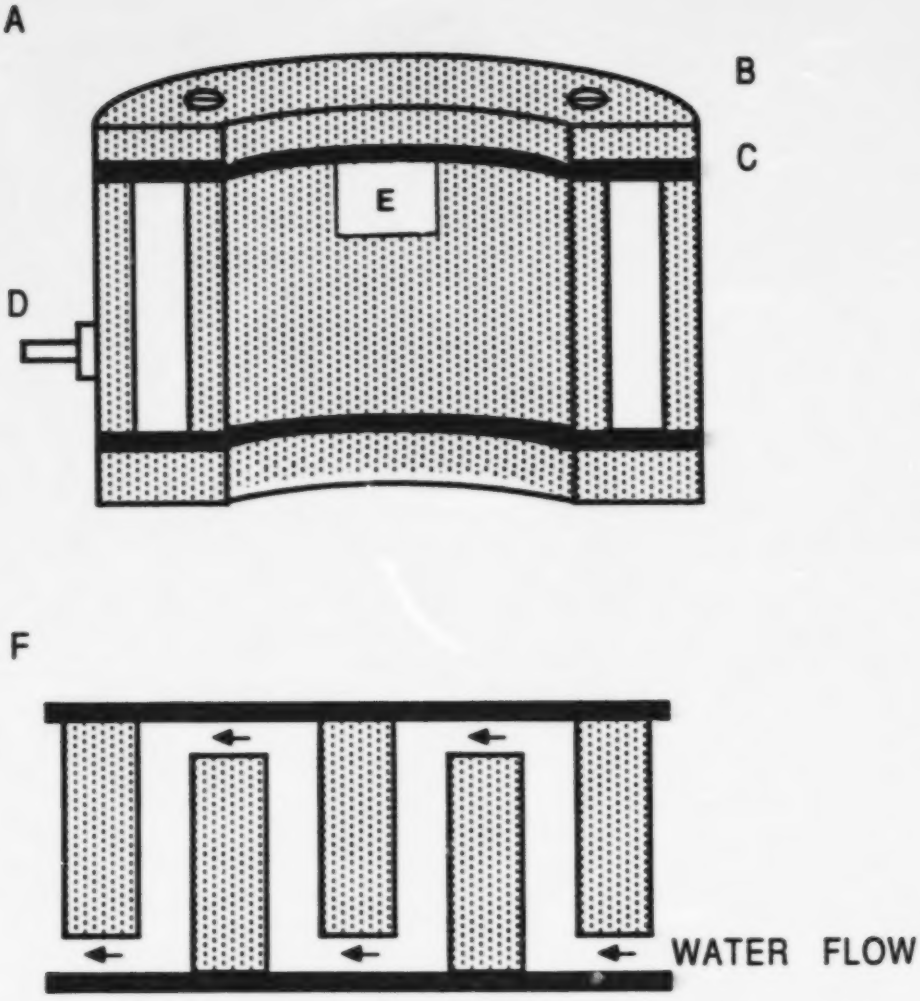

Figure 16. Schematic diagram of the HT-PA cell water jacket: (A) cross-sectional view; (B) 1/4 in. thick top; (C) rubber gasket; (D) Swagelock® fitting; (E) allowance for microphone fitting; (F) water channels.

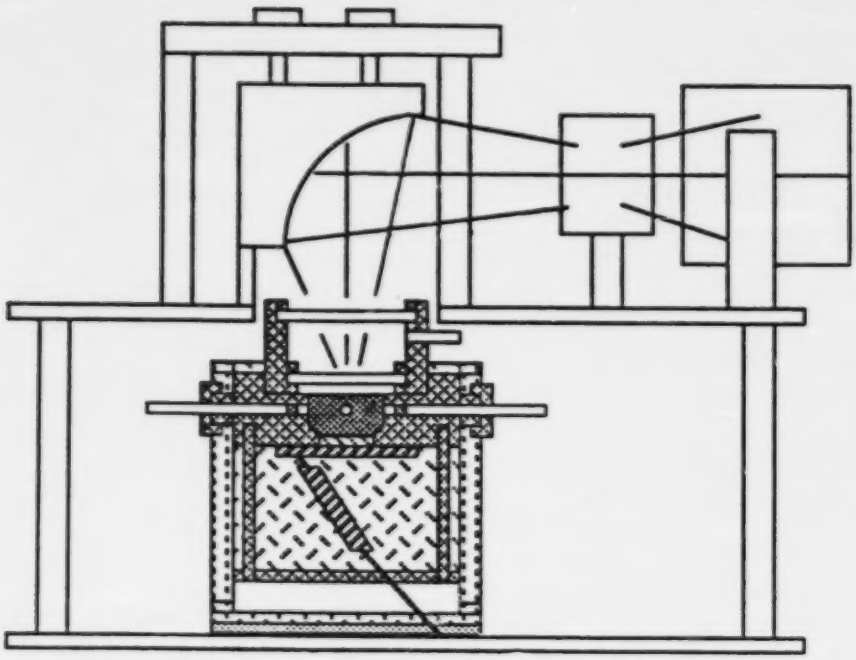

Figure 17. Schematic cross-sectional view of HT-PA cell assembled with Spectra-Tech optics.

Sample-gas exposure procedures--

For a typical, *in situ* FTIR-PA experiment, a sample is loaded into the HT-PA sample holder and leveled by drawing the flat edge of a spatula over the top of the sample. The sample holder is then placed into the sample chamber and the window holder is screwed in place. The optics plate is then mounted above the cell and the FTIR sample compartment closed. As in the *in situ* FTIR-DR experiments, exposure spectra were not recorded until the sample spectrum showed no evidence of water vapor (*ca.* 1 hr) indicating that the instrument and cell was completely purged. At this time the sample was either, (1) exposed to SO_2, (2) heated under N_2 or (3) heated and exposed to SO_2 gas simultaneously.

PA interferograms of the sample measured at 8 cm^{-1} resolution and at a mirror velocity of 0.059 cm/s were accumulated during the course of each reaction. Standard spectra were the result of either 128 or 512 co-added interferograms transformed as described above. Sample spectra were normalized against the spectrum of Norit-A carbon black. This procedure is particularly important in the case of the resonant PA cell since it is the only manner in which to normalize the enhancement of the PA signal at the cell resonance frequency.

WET CHEMICAL ANALYSIS

A colorimetric method involving barium chloranilate was used to quantify the amount of $CaSO_4$ in the reacted sample.[51] Materials used for this determination were barium chloranilate (Eastman Kodak Co.), a 0.05 M potassium acid phthalate (Fisher Scientific Co.) buffer solution, pH 4, potassium sulfate (Fisher Scientific Co.), 95% ethanol and a 20-50 mesh hydrogen-form ion exchange resin (Bio-Rad Laboratories, AG 50W-X8). Initially, four samples of K_2SO_4 (0.005 to 0.040 g of sulfate) and the

reacted samples to be analyzed were weighed and dissolved in water. It was often necessary to warm the solutions and add 1 M HCl for all the solid to dissolve. Each solution was adjusted to 10 ml and then passed through the ion exchange column (15 cm long X 1.5 cm i.d.) using 30 ml of distilled water to wash the sample into a 100 ml volumetric flask. To the effluent was added 50 ml of 95% ethanol and 10 ml of the buffer. The pH of the solution was measured with a Ag/AgCl pH combination electrode (Sargent Welch, S-30070-10) and a Beckman Zeromatic SS-3 pH meter. This solution was adjusted to pH 4 $\pm$ 0.1 using 1 M HCl or 1 M NH_4OH and diluted to 100.00 ml using distilled water. At this time 0.3 g of barium chloranilate was added to each solution and all solutions were stirred for 20 min. An aliquot from each flask was then centrifuged for 10 min to remove the excess barium chloranilate and precipitated barium sulfate. Finally, using a 1 cm quartz cell, the absorbance of the filtrate was measured on a Hewlett Packard 8451 Diode Array spectrometer. Using the absorbance value at 530 nm, a calibration curve of A_{530} versus sulfate concentration was obtained.

SECTION 5

RESULTS AND DISCUSSION

INTRODUCTION

The initial phases of this work have been reported previously.[33] These comprised primarily post-SO_2-exposure infrared photoacoustic spectra of replicate samples of $CaCO_3$ and CaO. In addition, some experiments with mixtures of $CaCO_3$ with Na_2CO_3 and Li_2CO_3 and spectra of other common components of flyash were reported. The additional experiments covered in this report represent a continuation of this previous work and include three types of experiment and measurement:

1. post SO_2-exposure FTIR-PA spectra of replicate samples of $Ca(OH)_2$
2. <u>in situ</u> FTIR diffuse reflectance studies of $Ca(CO_3)$, CaO and $Ca(OH)_2$ during their exposure to SO_2/N_2 at temperatures up to 750°C.
3. <u>in situ</u> FTIR-PAS studies of $CaCO_3$, Na_2CO_3 and $Ca(OH)_2$ during their exposure to SO_2/N_2 at temperatures up to 400°C.

POST-EXPOSURE FTIR PHOTOACOUSTIC STUDIES

Preliminary post-exposure experiments were performed in order to assess the qualitative and quantitative capabilities of FTIR-PAS as applied to the reaction of CaO, $CaCO_3$ and $Ca(OH)_2$ with 1.5% SO_2 in He. Since initial post-exposure experiments[33] were successful in characterizing the sulfur-oxygen species resulting from the above reactions, work was begun on the construction of a PA cell capable of <u>in situ</u> monitoring of elevated temperature solid gas reactions. Although the <u>in situ</u> PA cell was designed for operation at temperatures up to 750°C, this was not possible to achieve

due to the weakness of the PA signal above 400°C. Thus, post-exposure PA experiments (which allowed exposures at temperatures up to 900°C) played a vital role in examining these reactions.

Post-exposure FTIR experiments involved recording the photoacoustic spectra of replicate samples of particulate CaO, $CaCO_3$ and $Ca(OH)_2$ that had been exposed to SO_2 at temperatures ranging from 25 to 900°C (see Section 4 for experimental details). These experiments are summarized in Table 2 and those involving $Ca(OH)_2$ are described in detail below (see Figures 18-23).

In addition to the spectra as summarized in Table 2, peak heights of significant vibrational bands were measured as a function of photothermal modulation frequency (see Section 4 for experimental details). The plots of the log of the photothermal signal magnitude vs. the log of the modulation frequency yield straight lines, the slopes of which, for various absorption bands in selected samples, are given in Table 3.

CaO and $CaCO_3$

The results of post-exposure photoacoustic spectral measurements on CaO and $CaCO_3$ reported in Ref. 33 can be summarized as follows:

CaO--

1. At 25°C particulate (avg. diameter 75 um) CaO reacts with 0.75% SO_2/He (in the absence of O_2) to form $CaSO_3$. The reaction is limited by the formation of an impervious product layer < 2 um thick.

2. At 400°C and above the product $CaSO_3$ on the surface of the CaO particles is converted to $CaSO_4$. The conversion to $SO_4^=$ increases up to 750°C.

3. At 900°C the total capture of SO_2 is less than at 750°C owing apparently to the decomposition of $CaSO_3$ and $CaSO_4$.

Table 2.

Summary of Sample Types and Gas Exposure Conditions

Sample	Gas	Exposure Time (min)	Flow Rate (ml/min)	Exposure Temp. (C)	Figure(s)
A1. CaO	SO_2/He	0-90	6[a]	25	b
A2. CaO	SO_2/He	10	6[a]	25-900	b
A2. CaO	SO_2/He/O_2	5-10	6[a]	25-750	b
A2. CaO	SO_2/He	0-60	6[a]	750	b
A3. CaO	SO_2/He	10	6[a]	750, 25 and repeat	b
B1. $CaCO_3$	He	30	30	25-900	b
B2. $CaCO_3$	SO_2	30	30	350-900	b
B3. $CaCO_3$	SO_2	30	30	750	b
B4. $CaCO_3$	SO_2/O_2	30	30	750,900	b
C1. $Ca(OH)_2$	SO_2/He	0-60	30	25	18,19
C2. $Ca(OH)_2$	SO_2/He	30	30	25-900	20
C3. $Ca(OH)_2$	SO_2/He	0-60	30	750	21,22
C4. $Ca(OH)_2$	SO_2/O_2	30	30	750,900	23

[a]0.75% SO_2/He. [b]Ref. 33.

Table 3.

Summary of Photothermal Modulation Frequency Studies

Sample	Species	Band Max. (cm^{-1})	log Q vs. log f slope
100% Na_2SO_3	$SO_3^=$	988	-0.95
		656	-1.03
100% $CaSC_4.2H_2O$	$SO_4^=$	1153	-0.80
		660	-0.92
		610	-0.96
10% $CaSO_4.2H_2O$/KBr	$SO_4^=$	1153	-0.83
		660	-0.99
		610	-0.96
CaO exposed to SO_2 at 25°C for 10 min	$SO_3^=$	941	-1.04
CaO exposed to SO_2 at 750°C for 10 min	$SO_4^=$	1157	-1.09
		679	-1.00
		594	-1.14
$CaCO_3$ exposed to SO_2 at 750°C for 30 min	$SO_4^=$	1153	-1.05
		675	-1.15
		594	-1.18
	$S_2O_3^=$	980	-1.11
$Ca(OH)_2$ exposed to SO_2 at 750°C for 30 min	$SO_4^=$	1153	-0.99
		675	-1.05
		594	-1.10
	$S_2O_3^=$	979	-0.98

4. SO_2 is not detectably oxidized in the gas phase at temperatures up to 750°C (even with presence of O_2).

5. The extent and rate of capture of SO_2 and formation of $CaSO_4$ at temperatures up to 750°C is not appreciably affected by the presence of O_2.

6. The capture of SO_2 by CaO at 750°C is limited by formation of an impervious product layer of $CaSO_4$ < 3 um thick.

7. The major path for conversion of the initially formed $CaSO_3$ to $CaSO_4$ is:

$$2CaSO_3(s) + SO_2(g) \longrightarrow 2CaSO_4(s) + 1/2\ S_2(g),$$

even in the presence of O_2.

8. Above 750°C disproportionation reactions forming $S_2O_3^=$ and other polysulfates are detectable.

<u>$CaCO_3$</u>

1. $CaCO_3$ is not completely calcined even after heating at 900°C for 30 min but, even at temperatures as low as 750°C, is completely converted to $CaSO_4$ when exposed to 1.5% SO_2/He.

2. $CaCO_3$ reacts with SO_2 at 550°C to form initially $CaSO_3$ which is then converted at 750°C to $CaSO_4$ by further reaction with SO_2 in the absence of O_2.

3. Significant CaS_2O_3 is also produced at 750°C, but is a minor product for exposures at 900°C.

4. For these particulate samples, capture of SO_2 is limited (by the formation of an impervious product layer) to a mximum of 48% conversion of $CaCO_3$ to $CaSO_4$ (at 750°C). For nominal particle diameter of 75 μm this indicates a layer thickness of ~12 μm. This is supported by the PAS results.

5. Addition of 20% O_2 to the exposure gas mixture reduces the formation of $S_2O_3^=$ and causes a 20% increase in the conversion of $CaCO_3$ to $CaSO_4$ for exposures at 750°C.

$Ca(OH)_2$

Exposure of $Ca(OH)_2$ to SO_2 at 25°C

Figure 18 depicts the spectral data obtained for replicate 80 mg samples of $Ca(OH)_2$ exposed to 1.5% SO_2 in He for successively increasing periods of time at 25°C. A typical spectrum of $Ca(OH)_2$, as indicated by the peak at 3641 cm^{-1} characteristic of the O-H stretch,[52] is shown in Trace A of Figure 18. Trace A also shows the presence of residual amounts of carbonate in the $Ca(OH)_2$ sample as indicated by the broad band centered at ca. 1450 cm^{-1}. After the sample is exposed to SO_2 for one minute, a band centered at ca. 950 cm^{-1} is observed (Trace B, Figure 18). This band is assigned to $CaSO_3$. As replicate $Ca(OH)_2$ samples are exposed to increasing amounts of SO_2 at 25°C, the 950 cm^{-1} absorption band increases in intensity. Simultaneous with the increase in intensity of the $SO_3^=$ peak (Trace A, Figure 19) is a decrease in intensity of the OH^- band at 3641 cm^{-1} (Trace B, Figure 19).

These data indicate that the reaction occurring between SO_2 and $Ca(OH)_2$ is simply:

$$Ca(OH)_2(s) + SO_2(g) \text{ ---> } CaSO_3(s) + H_2O(g) \qquad (3)$$

The $SO_3^=$ band at 950 cm^{-1} ceases to increase in area after ca. 5 min of exposure (Trace A, Figure 19). This is interpreted as indicating the formation of an impervious product layer on the surface of the $Ca(OH)_2$ particles. The area of the $SO_3^=$ band formed during the reaction with

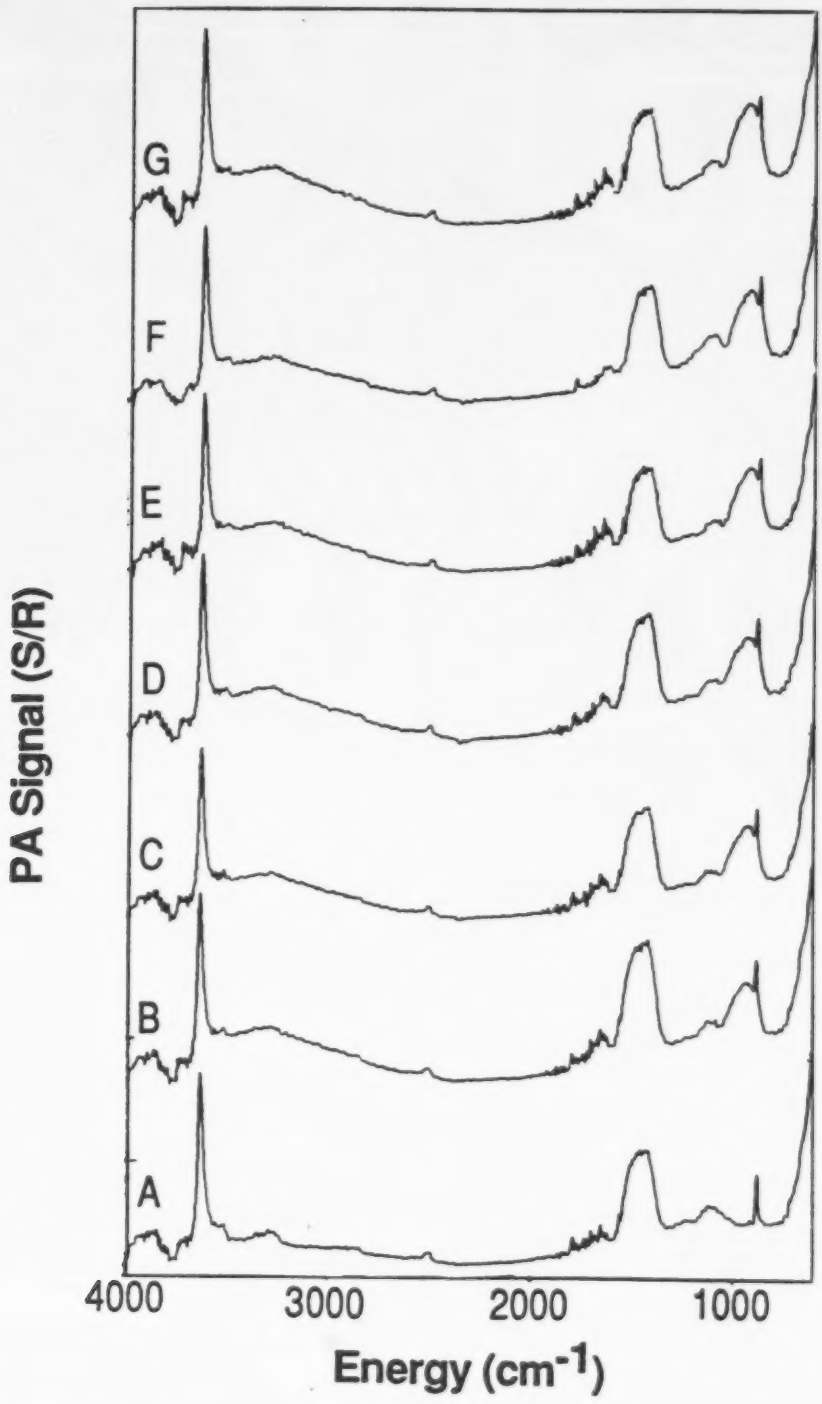

Figure 18. FTIR-PAS of $Ca(OH)_2$ (A) exposed to 1.5% SO_2 in He at 25°C for 2.5 min (B); 5 min (C); 10 min (D); 20 min (E); 30 min (F); 60 min (G).

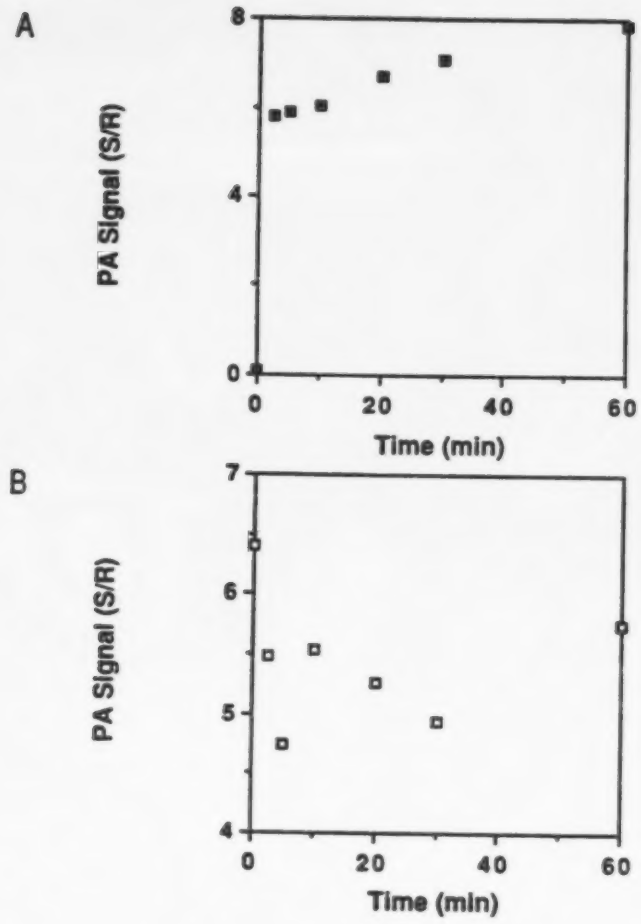

Figure 19. Peak areas of sulfite (A) and hydroxyl (B) bands for $Ca(OH)_2$ exposed to 1.5% SO_2 in He as a function of time.

$Ca(OH)_2$ is greater than that for the same band formed from the reaction of SO_2 with CaO.[33] This suggests that more $SO_3^=$ is formed on the surface of the $Ca(OH)_2$ particles than on particles of CaO. Consistent with these results are the surface area characteristics of the CaO and $Ca(OH)_2$ samples, which were determined to be 4.99 and 9.66 m^2/g, respectively. These surface area values indicate that the $Ca(OH)_2$ particles have ca. twice as much surface exposed to the SO_2 gas as the CaO particles and consequently have ca. two times as many reactive sites. However, the maximum amount of $SO_3^=$ formed on the $Ca(OH)_2$ surface was only 1.6 times greater than that formed on the CaO particle surface (determined from $SO_3^=$ peak areas). The less than expected production of sulfite on the $Ca(OH)_2$ particles is interpreted to indicate that some of the $Ca(OH)_2$ surface is located in pores of the particle which become plugged with the $SO_3^=$ product and consequently impermeable to SO_2 for further reaction with the particle core.

Exposure of $Ca(OH)_2$ to SO_2 as a function of temperature--

The data presented in Figure 20 were obtained from replicate samples of $Ca(OH)_2$ after exposure for 30 min to the 1.5% SO_2 in He gas mixture as a function of temperature. As shown earlier, the reaction of SO_2 with $Ca(OH)_2$ results in the production of $CaSO_3$ at 25°C (Trace B, Figure 18; Trace B, Figure 20). The production of $CaSO_3$ increases with temperature up to 570°C, as indicated by the growth of the sulfite bands centered at 950 cm^{-1}. Beginning at temperatures of 375°C the spectra also show the presence of bands at 1200, 679, 613 and 594 cm^{-1}. These bands increase in intensity for each successive temperature and are collectively assigned to the bidentate sulfate species. For exposures at temperatures of 570°C and higher, peaks at 1003, 984 and 656 cm^{-1} are observed which are

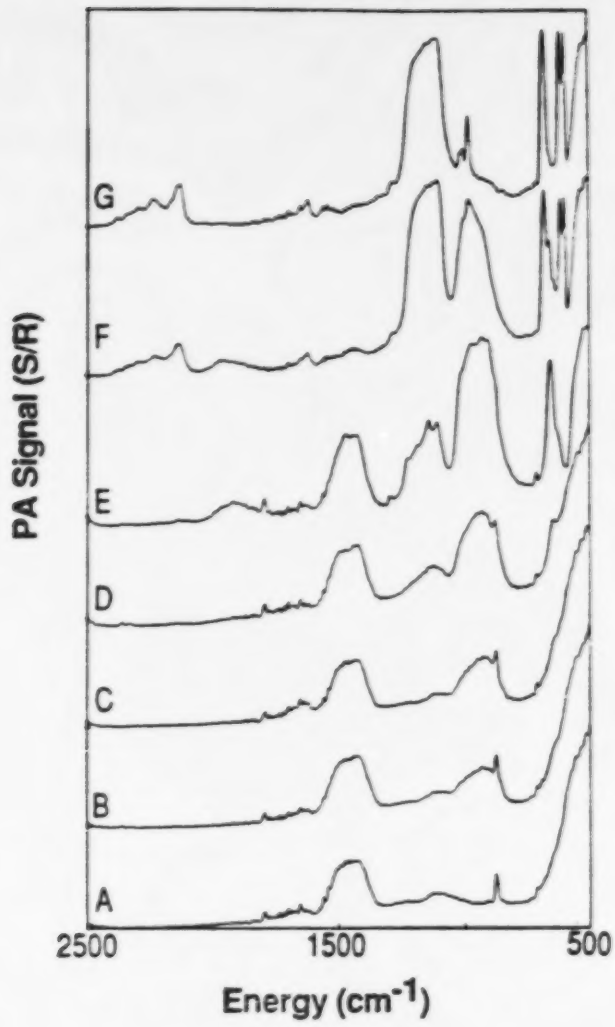

Figure 20. FTIR-PAS of $Ca(OH)_2$ (A) exposed to 1.5% SO_2 in He for 30 min at 25°C (B); 200°C (C); 375°C (D); 570°C (E); 750°C (F); 900°C (G).

characteristic of the thiosulfate species. The intensity of the $S_2O_3^=$ peaks increases for exposures up to 750°C, while the 900°C exposure shows a decrease in the intensity of these bands and simultaneous increase in the intensities of sulfate bands.

The above date are interpreted as follows:

1). The reaction of SO_2 with $Ca(OH)_2$ at room temperature results in the production of $CaSO_3$. The production of $CaSO_3$ is enhanced for this reaction with increasing temperature up to ca. 570°C.

2). The capture of SO_2 as $CaSO_4$ by $Ca(OH)_2$ is first evident for exposures at ca. 375°C. Increased production of $CaSO_4$ occurs at higher temperatures of exposure up to 900°C.

3). The formation of CaS_2O_3 resulting from the reaction of SO_2 with $Ca(OH)_2$ is first observed for exposures at ca. 375°C. The amount of CaS_2O_3 produced increases with increasing temperatures up to 750°C. However, at 900°C the production of CaS_2O_3 is negligible. The fact that the amount of $CaSO_4$ produced during the 900°C exposure increases while the amount of CaS_2O_3 decreases suggests that, at 900°C the CaS_2O_3 reacts with residual CaO:

$$CaS_2O_3(s) + CaO(s) \text{ ---> } CaSO_4 + CaS. \qquad (7)$$

The production of sulfide has been verified qualitatively by wet chemistry.

Exposure of $Ca(OH)_2$ to SO_2 at 750°C as a function of time--

The FTIR-PA spectra for the exposure of replicate 80 mg samples of $Ca(OH)_2$ (Trace A, Figure 21) to SO_2 at 750°C for successively longer times show the production of $SO_3^=$, $SO_4^=$ and $S_2O_3^=$. The initial exposure of $Ca(OH)_2$ to SO_2 at 750°C for 2.5 min resulted in the production of $SO_3^=$ and $SO_4^=$ as indicated by the peaks at 1200 and 950 cm^{-1} (Trace B, Figure 21).

Increases in the time of exposure resulted in increased production of both $SO_3^=$ and $SO_4^=$ for up to 30 min of exposure. The third product of the reaction, $S_2O_3^=$, is first observed after exposure of the sample for 5 min to SO_2. The production of $S_2O_3^=$ also increases with the time of exposure up to 30 min. A summary of the production of each species with time is depicted by plots of peak intensity at 2137 cm^{-1} for $SO_4^=$, 941 cm^{-1} for $SO_3^=$ and 984 cm^{-1} for $S_2O_3^=$ (Figure 22). These plots also indicate that the formation of $CaSO_4$ and CaS_2O_3 effectively ceases after ca. 30 min of exposure.

The 2137 cm^{-1} peak is the first overtone of the $SO_4^=$ ν_3 band[53] and is not saturated even for 100% concentrations of $SO_4^=$. The similarity between this peak's intensity with time of exposure and the 679 cm-1 peak's intensity with time of exposure indicates that the 679 cm^{-1} band is also not saturated for these exposures. Using a calibration curve generated from wet chemical determinations for $SO_4^=$ in exposed samples, the magnitude of the 679 cm^{-1} band after 30 min of exposure indicates approximately an 80% conversion of the $Ca(OH)_2$ particle to $CaSO_4$. For the 80% conversion of $Ca(OH)_2$ to $CaSO_4$, the product layer on the surface of the 75 μm particle (estimated to be 26 μm) is assumed to be optically opaque and thermally thick. Depth profiling experiments exhibit an f^{-1} dependence for the PA signal for $SO_4^=$ species for the optical modulation frequencies of 0.235 to 0.941 cm/s, which probe the sample from depths of 35 to 16 μm. Unlike the case of $CaCO_3$, the depth profile spectra of the sulfate bands on $Ca(OH)_2$ show no change in bandshape with increasing modulation frequency. This indicates that the optical absorption depth must be closer to the surface of the particle than 16 μm, which is very likely, given the high concentration of $CaSO_4$ present in the sample. Since the optical absorption depth is so close to the surface of the particle, the sample remains thermally thick even at high modulation frequencies.

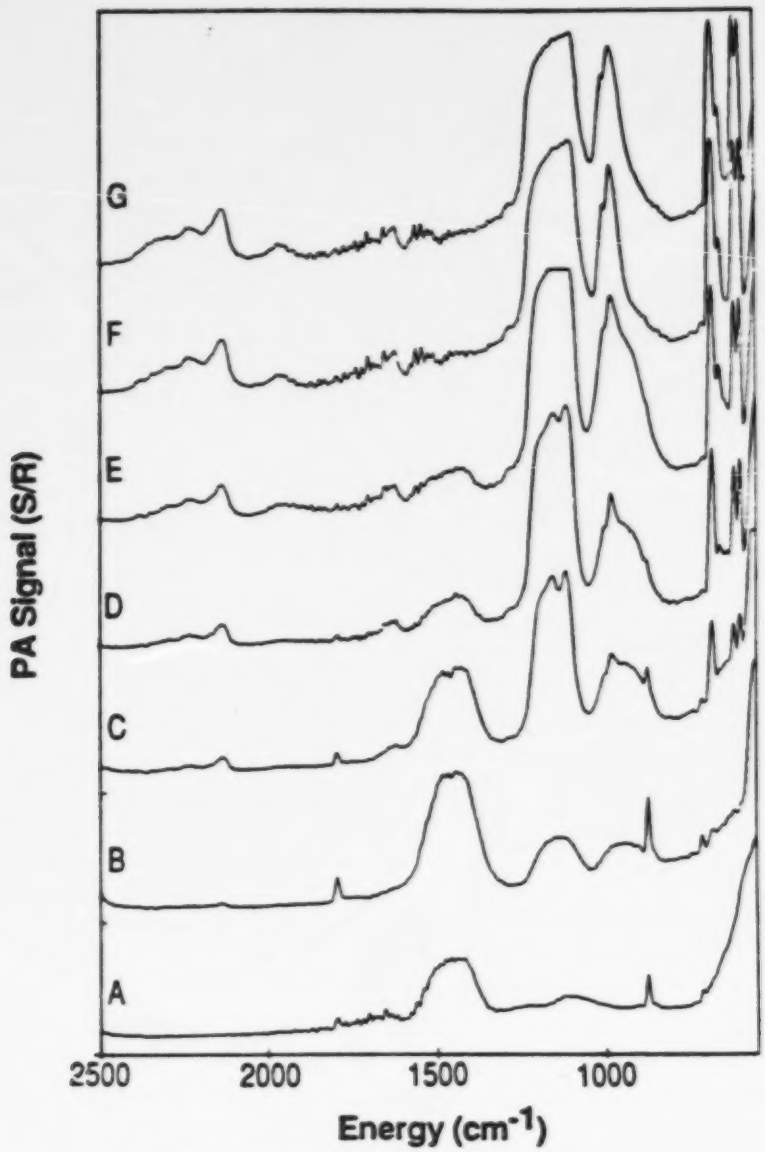

Figure 21. FTIR-PAS of $Ca(OH)_2$ (A) exposed to 1.5% SO_2 in He at 750°C for 2.5 min (B); 5 min (C); 10 min (D); 20 min (E); 30 min (F); 60 min (G).

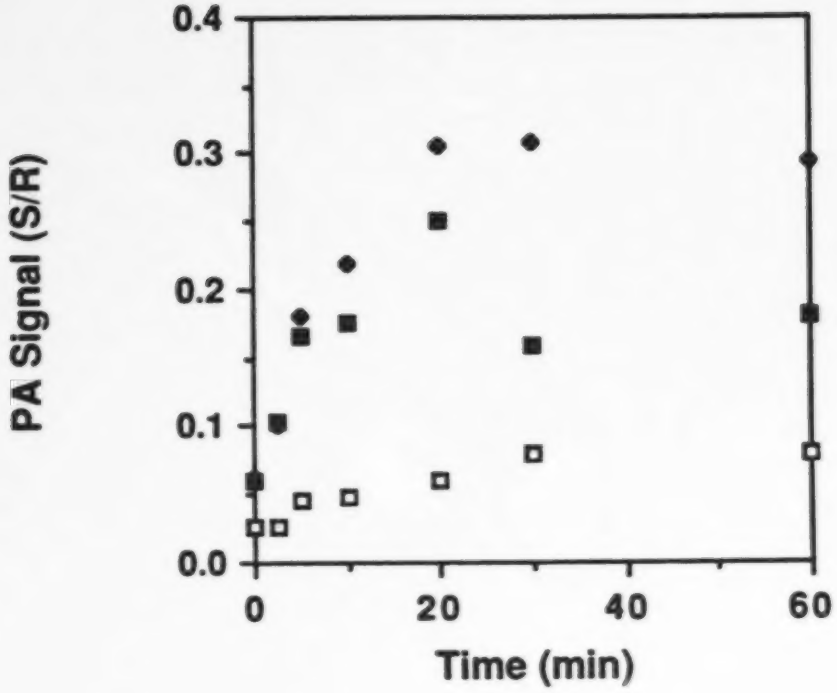

Figure 22. Peak intensities for sulfate (□); sulfite (■); and thiosulfate (◆).

Exposure of $Ca(OH)_2$ to SO_2 and $SO_2 + O_2$ at 750 and 900°C--

Replicate 80 mg samples of $Ca(OH)_2$ were exposed to the undiluted 1.5% SO_2 in He gas mixture and a diluted 5:1 1.5% SO_2 in He:O_2 gas mixture (Figure 23). All exposures were limited to 30 min and a gas flow rate of 30 ml/min. As shown in Trace A of Figure 23 exposure of $Ca(OH)_2$ to SO_2 at 750°C produces $CaSO_4$ and CaS_2O_3, as indicated by the bands at 1150, 679, 613 and 594 and 984 and 656 cm^{-1}. The 900°C exposure of $Ca(OH)_2$ to SO_2 results in the production of less CaS_2O_3 and $CaSO_4$ (Trace C) than at 750°C. The addition of O_2 to the SO_2 gas for exposures at 750 and 900°C also results in a reduction of CaS_2O_3 production. The reaction of $Ca(OH)_2$ with SO_2 in the presence of O_2 at 900°C indicates greater $SO_4^=$ production as opposed to the exposure in the absence of O_2. As in the case of the $CaCO_3$ SO_2/O_2 exposures, these data again suggest that O_2 reacts with $CaSO_3$ to form $CaSO_4$ and thereby hinders the decomposition and reaction of $CaSO_3$ to form CaS_2O_3.

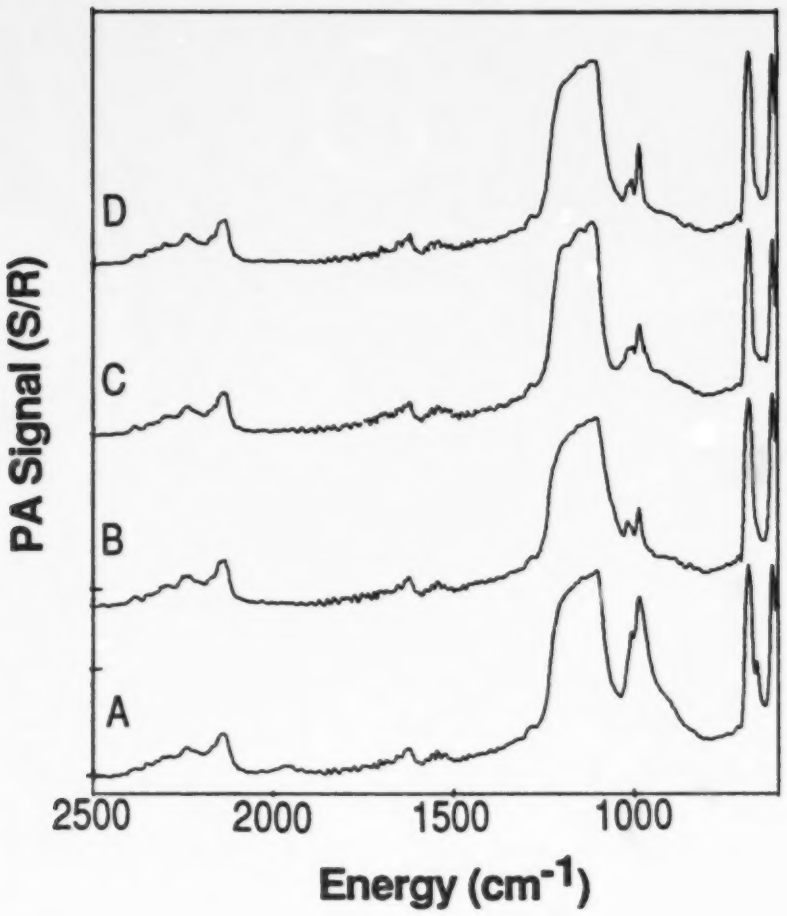

Figure 23. FTIR-PAS of $Ca(OH)_2$ exposed to 1.5% SO_2 in He at 750 and 900°C (A,C) and 1.5% SO_2 in He/O_2 at 750 and 900°C (B,D).

IN SITU FTIR DIFFUSE REFLECTANCE STUDIES

Many researchers studying powdered samples have coupled the abilities of photoacoustic spectroscopy with its most directly competitive technique, diffuse reflectance spectroscopy (DRS). For the work reported in this study, the application of DRS to evaluate the reaction of SO_2 with CaO, $CaCO_3$ and $Ca(OH)_2$ was particularly attractive due to the sensitivity of DR spectroscopy to low concentrations of absorbing species, the speed with which data may be recorded, the minimal sample preparation required and the ease with which the experiment is conducted.

Several characteristics of the DR experiments reported in this investigation which are important to consider when interpreting the data are:

1). The sorbent sample is dispersed in a non-absorbing matrix of NaCl at concentrations ranging from 2 to 50% by weight reactant to diluent.

2). The reaction is monitored as it occurs with time and/or temperature for a single reactant sample. This differs from the post-exposure PA studies in which the reaction is monitored from a series of replicate samples.

3). The DR spectra are measured while the 1.5% SO_2 in N_2 gas is flowing through the sample.

4). The DR signal is adversely affected by increases in the sample temperature. This is due to 1) the thermal expansion of the sample post which moves the sample from the optimum position at the focus of the optics[54] and 2) the thermal emission from the sample and sample post. Thermal emissions from the sample adversely affect the DR signal because the elevated temperature DR spectra represent measurements of the modulated sample absorptions as well as the unmodulated infrared signal radiated from the hot sample post.[55] As the temperature of the sample is increased, the

intensity of the unmodulated radiation from the sample post can exceed the intensity of the (modulated) diffusely reflected signal and result in saturating the detector response.

FTIR-DR data for the reaction of 1.5% SO_2 in N_2 with CaO, $Ca(OH)_2$ and $CaCO_3$ are depicted in Figures 24 through 42. Spectral features in these data are attributable to sulfur-oxygen species forming on the surface of the reactive particles. Although the band patterns are complex, with the use of symmetry arguments, described by the correlation tables in Table 4, the bands can be resolved into six groups, which are listed in Table 5.

Table 4.

Correlation Tables for $SO_3^=$ and $SO_4^=$ species.

$SO_4^=$.

Point Group	ν_1	ν_2	ν_3	ν_4
T_d	$A_1(R)$	$E(R)$	$F_2(I,R)$	$F_2(I,R)$
C_{3v}	$A_1(I,R)$	$E(R)$	$A_1(I,R)+$ $E(I,R)$	$A_1(I,R)+$ $E(I,R)$
C_{2v}	A_1	$A_1(I,R)+$ $A_2(R)$	$A_1(I,R)+$ $B_1(I,R)+$ $B_2(I,R)$	$A_1(I,R)+$ $B_1(I,R)+$ $B_2(I,R)$
$SO_4^{=a}$ (T_d)	983	450	1105	611

$SO_3^=$.

Point Group	v1	v2	v3	v4
C_{3v}	$A_1(I,R)$	$A_1(I,R)$	$E(I,R)$	$E(I,R)$
C_s	$A_1(I,R)$	$A_1(I,R)$	$A_1(I,R)+$ $A_2(I,R)$	$A_1(I,R)+$ $A_2(I,R)$
$SO_3^{=b}$ (C_{3v})	1010	633	933	469

I and R represent infrared and raman active bands.
[a] Landolt-Bornstein, Physikalisch-Chemische Tabellen, 2 Teil 1951.
[b] K. Nakamoto, Infrared Spectra of Inorganic Coordination Compounds, 4th Ed. (John-Wiley and Sons, Inc: New York 1963) p. 257.

Table 5.

FTIR Band Summary for Sulfur-Oxygen Species.[25]

Species	Energy (cm^{-1})	Assignment	References
SO_2.			
gaseous SO_2	1350	ν_3	25
	1150	ν_1	
$SO_3^=$.			
monodentate surface sulfito complex exhibiting C_s symmetry	1014	ν_1	58,60
	976	ν_3	
	940		
	676	ν_2	
	609		
monodentate surface sulfito complex exhibiting C_{3v} symmetry	950	$\nu_1 + \nu_3$	56,57,58,60
	633	ν_2	
$SO_4^=$.			
monodentate surface sulfato complex exhibiting C_{3v} symmetry	1163	ν_1	53
	1118		
surface sulfate exhibiting T_d symmetry	1150	ν_1	59
	970	ν_2	
	624	ν_4	
bidentate surface sulfato complex exhibiting C_{2v} symmetry	1205	ν_1	53
	1155		
	1114		
	997	ν_2	
	675	ν_4	
	613		
	594		

CaO

Exposure of CaO to SO_2 as a function of temperature--

Depicted in Figure 24 are the Kubelka-Munk treated DR spectra of a 2% by weight sample of as-received CaO in NaCl exposed to 1.5% SO_2 in N_2 (3 ml/min) as a function of temperature and time. For this experiment, the sample temperature was raised at a rate of 5°C/min to 500°C and then 3°C/min to 630°C. Spectra accumulated for the exposure of CaO to SO_2 at temperatures of 500°C and less, are depicted in Block A of Figure 24, while higher temperatures of exposure are shown in Block B.

The mid-IR spectrum of CaO is featureless. When the CaO sample is exposed to 1.5% SO_2 in N_2 the growth of bands at 940 and 632 cm^{-1} (A, Figure 24) is observed. After approximately 60 min of exposure the spectrum of the sample at 300°C exhibits, in addition to the bands at 940 and 632 cm^{-1}, a sharp peak at 1014 cm^{-1}. All three peaks increase in intensity during the exposure up to temperatures of 500°C. The peaks at 1014, 940 and 632 cm^{-1} are assigned to two different sulfite species. The initial sulfite species, represented by the peaks at 940 and 632 cm^{-1} is attributed to pyramidal sulfite. As the reaction progresses, a second sulfite species is observed which is indicated by the 1014 cm^{-1} band. The presence of this peak is indicative of a sulfite species bound to the CaO surface via an oxygen atom.[15]

At temperatures above 500°C, simultaneous with a decrease in sulfite band intensity, is the appearance of new bands at 1163 and 1118 cm^{-1}, as well as two bands on either side of the 632 cm^{-1} sulfite peak (B, Figure 24). With increasing temperature and time of exposure, the bands at 1163 and 1118 cm^{-1} increase and eventually coalesce into a single broad band at ca. 1150 cm^{-1}. In addition, two other bands at 970 and 624 cm^{-1} are observed.

CaO

Exposure of CaO to SO_2 as a function of temperature--

Depicted in Figure 24 are the Kubelka-Munk treated DR spectra of a 2% by weight sample of as-received CaO in NaCl exposed to 1.5% SO_2 in N_2 (3 ml/min) as a function of temperature and time. For this experiment, the sample temperature was raised at a rate of 5°C/min to 500°C and then 3°C/min to 630°C. Spectra accumulated for the exposure of CaO to SO_2 at temperatures of 500°C and less, are depicted in Block A of Figure 24, while higher temperatures of exposure are shown in Block B.

The mid-IR spectrum of CaO is featureless. When the CaO sample is exposed to 1.5% SO_2 in N_2 the growth of bands at 940 and 632 cm^{-1} (A, Figure 24) is observed. After approximately 60 min of exposure the spectrum of the sample at 300°C exhibits, in addition to the bands at 940 and 632 cm^{-1}, a sharp peak at 1014 cm^{-1}. All three peaks increase in intensity during the exposure up to temperatures of 500°C. The peaks at 1014, 940 and 632 cm^{-1} are assigned to two different sulfite species. The initial sulfite species, represented by the peaks at 940 and 632 cm^{-1} is attributed to pyramidal sulfite. As the reaction progresses, a second sulfite species is observed which is indicated by the 1014 cm^{-1} band. The presence of this peak is indicative of a sulfite species bound to the CaO surface via an oxygen atom.[15]

At temperatures above 500°C, simultaneous with a decrease in sulfite band intensity, is the appearance of new bands at 1163 and 1118 cm^{-1}, as well as two bands on either side of the 632 cm^{-1} sulfite peak (B, Figure 24). With increasing temperature and time of exposure, the bands at 1163 and 1118 cm^{-1} increase and eventually coalesce into a single broad band at ca. 1150 cm^{-1}. In addition, two other bands at 970 and 624 cm^{-1} are observed.

The peaks at 1163, 1118, 1150, 970, 624 cm^{-1} and on either side of the 632 cm^{-1} peak are characteristic of sulfate. The free sulfate ion belongs to the high-symmetry point group, T_d, in which the v_3 and v_4 vibrational modes are infrared active (Table 4).[53] The symmetry of the free ion is lowered by complex formation. For example, monodentate coordination of the $SO_4^=$ ion results in C_{3v} symmetry, while bidentate coordination results in C_{2v} symmetry. For monodentate coordination, the forbidden T_d v_1 vibrational mode becomes IR active and the triply degenerate v_3 and v_4 vibrational modes each split into two modes. Based upon the symmetry rules, the initial bands observed at 1163 and 1118 cm^{-1} and on either side of the 632 cm^{-1} band are assigned to the v_3 and v_4 vibrational modes of a monodentate $SO_4^=$ species. The IR active v_1 vibrational mode of this species which usually appears at ca. 970 cm^{-1} is apparently masked by the intense $SO_3^=$ absorption at 940 cm^{-1}. The spectrum of the sample acquired at ca. 630°C, depicts peaks at 1150, 970 and 624 cm^{-1}. This spectrum, in which the v_3 (1150 cm^{-1}) and v_4 (624 cm^{-1}) vibrational bands are not split, the v_2 band is not observed and the v_1 band (970 cm^{-1}) is very weak, indicates that the symmetry of the $SO_4^=$ ion is approximately T_d. A similar assignment has been made for the spectrum of $[Co(NH_3)_6]_2(SO_4)_3.5H_2O$ by Nakamoto et al.[60]

Sulfite (940 cm^{-1}) and sulfate (1153 cm^{-1}) production as a function of time and temperature of the reaction are clearly identified via plots of Kubleka-Munk treated DR peak intensities vs. temperature (The time can be monitored via the temperature axis also since the temperature was raised at a fixed rate, see above; Figure 25). For exposures at temperatures below 200°C, Figure 25 illustrates small increases in the $SO_3^=$ peak intensity with temperature (and time) indicating the slow production of $SO_3^=$. However,

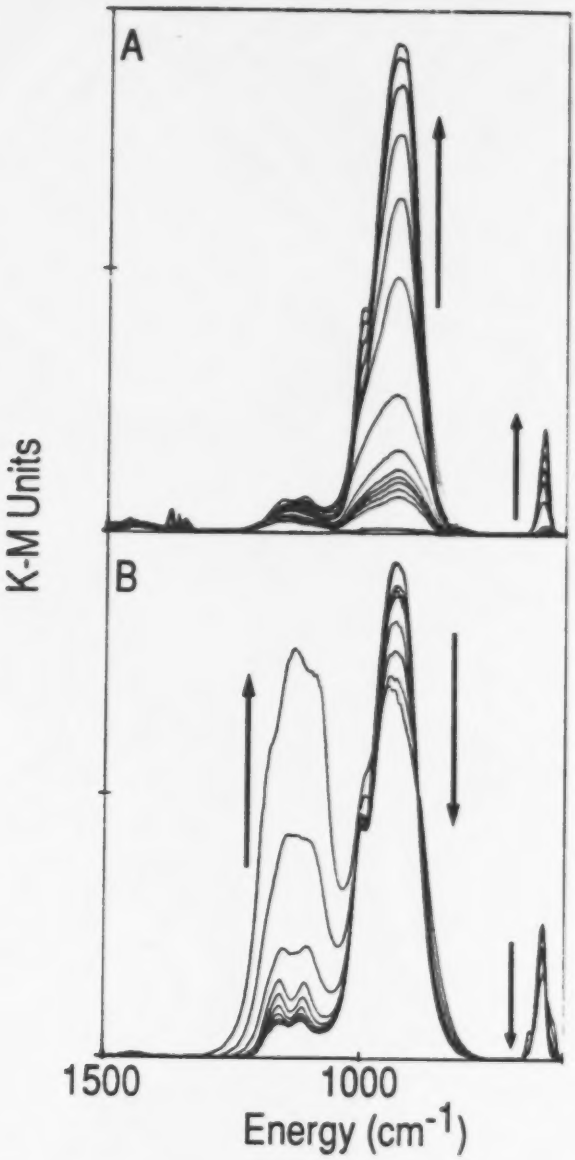

Figure 24. FTIR-DR spectra plotted in Kubelka-Munk (K-M) units of a 2% by weight CaO in NaCl sample exposed to 1.5% SO_2 in N_2 as a function of temperature. (A) $T < 500^{o}C$; (B) $500^{o}C < T \leq 630^{o}C$. The arrows represent the changes in the bands with increasing temperature.

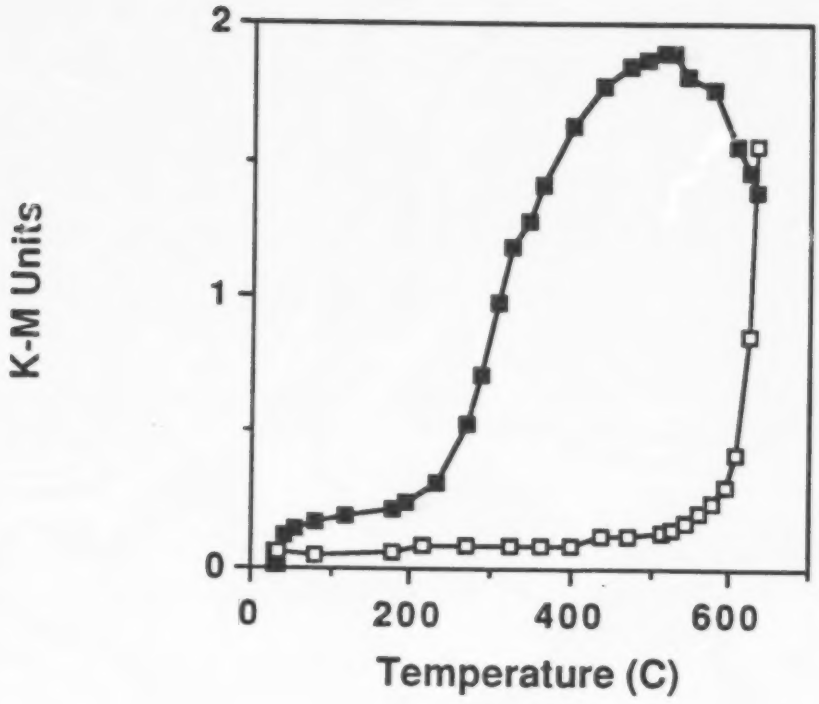

Figure 25. Plots of $SO_3^=$ (■) and $SO_4^=$ (□) peak intensity for a 2% by weight CaO in NaCl sample exposed to 1.5% SO_2 in N_2 as a function of temperature.

above 200°C, a dramatic increase in intensity of the 940 cm^{-1} band indicates an increase in sulfite production. For temperatures between ca. 400 and 500°C the rate of $SO_3^=$ production decreases.

On the other hand, between temperatures of 25 and 500°C, the plot indicates that virtually no $SO_4^=$ is produced. However, at temperatures above 500°C there is a large increase in $SO_4^=$ peak intensity, indicating the production of $SO_4^=$. Simultaneous with the increase in $SO_4^=$ peak intensity is a significant decrease in $SO_3^=$ intensity. Collectively, the DR data for the reaction of CaO with SO_2 indicate:

1). Below 500°C, the primary reaction is:

$$CaO(s) + SO_2(g) \text{ ---> } CaSO_3(s) \qquad (1)$$

This reaction proceeds first with the formation of pyramidal sulfite followed by the formation of oxygen bound sulfite. The following mechanism proposed by Low et al.[15] for the low temperature reaction agrees with the DR data. First, SO_2 immediately adsorbs and forms a coordinated complex I. At low surface coverage I rapidly converts to form pyramidal sulfite, II, in which an oxide ion is "plucked" from the CaO surface.

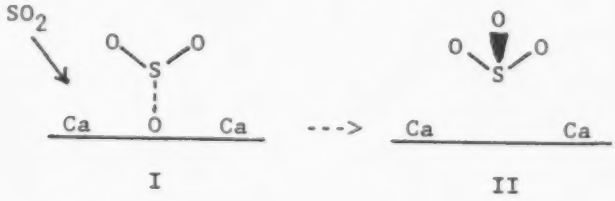

I II

This rapid conversion of I to II continues until sterically and energetically suitable sites for pyramidal sulfite formation are been diminished; At this point some of the type I complex forms and remains on the sample surface.[15]

2). From 500 to 630°C, the initial loss of $SO_3^=$ and production of $SO_4^=$

on the surface of the particles indicate that $CaSO_3$ is converted to $CaSO_4$. As shown in the post-exposure data, in the absence of O_2 this may occur through the following reaction:

$$2CaSO_3(s) + SO_2(g) \text{ ---> } 2CaSO_4(s) + 1/2S_2(g). \qquad (4)$$

This reaction indicates a 1:1 conversion of $SO_3^=$ to $SO_4^=$. However, the difference in the rate of $SO_3^=$ band intensity decrease *vs.* the rate of $SO_4^=$ band intensity increase suggests that either 1) reaction (1) is occurring at a much faster rate than reaction (4) or 2) that other reactions resulting in the formation of $SO_4^=$ without the consumption of $SO_3^=$ are occurring at these temperatures. The first suggestion is particularly plausible since additives such as NaCl (the sample diluent), KCl, NaOH and KOH have been reported to accelerate reaction (1).[10]

$Ca(OH)_2$

Calcination of $Ca(OH)_2$--

The spectra presented in Figure 26 were obtained for a 10% by weight sample of $Ca(OH)_2$ in NaCl heated under nitrogen to a temperature of 750°C at a rate of 5°C/min. A typical spectrum of $Ca(OH)_2$ shown in Trace A exhibits a sharp peak at 3641 cm^{-1} characteristic of the antisymmetrical OH^- stretching vibration of the hydroxide lattice.[51] As the sample is heated, the hydroxide peak and peaks at 3929 and 3867 cm^{-1} (vibrational combination bands of $Ca(OH)_2$) decrease in intensity. On the other hand, the lower frequency band at *ca.* 3300 cm^{-1} initially increases in intensity up to sample temperatures of *ca.* 300°C. This seemingly unexpected increase in intensity of the 3300 cm^{-1} band with temperature is, in fact, predictable; this band originates from an excited vibrational state that

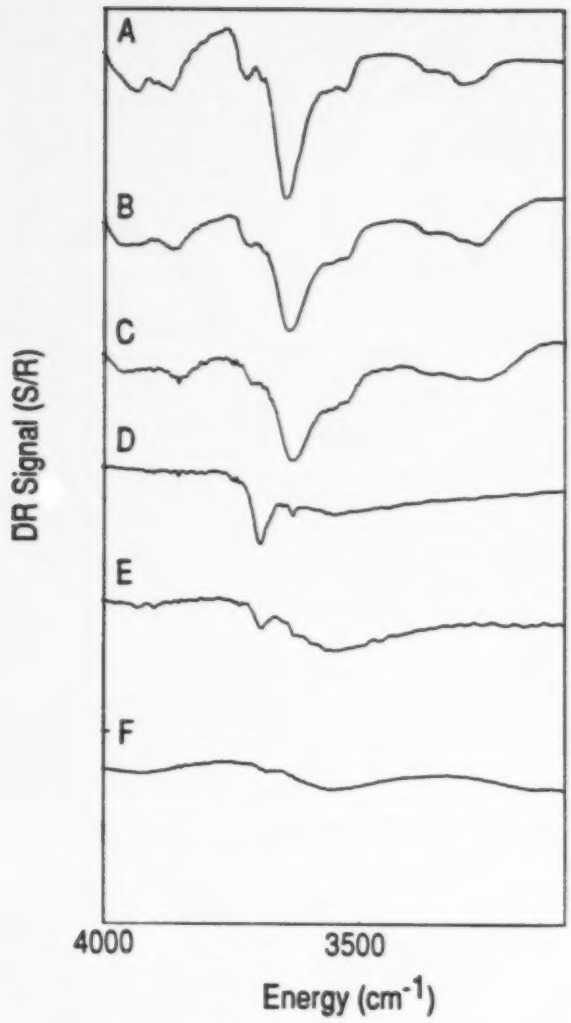

Figure 26. FTIR-DR spectra of a 10% by weight $Ca(OH)_2$ in NaCl sample as a function of temperature: (A) 25°C; (B) 200°C; (C) 500°C; (D) 512°C; (E) 600°C; (F) 750°C.

becomes populated with increases in the sample temperature and therefore results in the increased intensity.[52] This increase in intensity of the 3300 cm^{-1} band is reversed at sample temperatures just below 300°C.

Beginning at 512°C, further heating of the sample results in the loss of the 3641 cm^{-1} band and the appearance of peaks at 3690 and 3627 cm^{-1} (Traces C and D). This indicates that the bulk of OH^- from the lattice has been removed and only tightly bound water remains on the particle surface.[61] Finally at 750°C, nearly all characteristics of OH^- in the spectrum are gone, indicating that the sample is predominantly CaO.

Exposure of $Ca(OH)_2$ to SO_2 at 25, 200, 300 and 400°C--

The FTIR-DR spectra of 10% by weight samples of $Ca(OH)_2$ in NaCl exposed 1.5% SO_2 in N_2 (6 ml/min) at 25, 200, 300 and 400°C are depicted in Figures 27 and 28. Trace A for each of the figures represents the 10% by weight $Ca(OH)_2$ in NaCl sample at the designated temperature of exposure. Trace B represents the sample after its initial exposure (less than 30 s) to SO_2. After extensive exposure of the sample to SO_2 (30 min), the spectrum of each was again recorded and is shown in Trace C. Finally, the spectrum of the sample after being cooled and purged of excess gaseous SO_2, is shown Trace D.

Exposures of $Ca(OH)_2$ to SO_2 at each of these temperatures result in the immediate growth of a broad band at 940 cm^{-1} indicating the formation of pyramidal $SO_3^=$. For exposures at temperatures of 300 and 400°C, the weaker sulfite band at 632 cm^{-1} is also evident. In addition, these spectra also exhibit a band at 1014 cm^{-1} which is attributed to the ν_1 vibrational mode of oxygen coordinated $SO_3^=$. Finally, after extensive exposure of $Ca(OH)_2$ to SO_2 (30 min) at temperatures of 200, 300 and 400°C, the slight growth of a broad band at ca. 1200 cm^{-1} indicates the formation

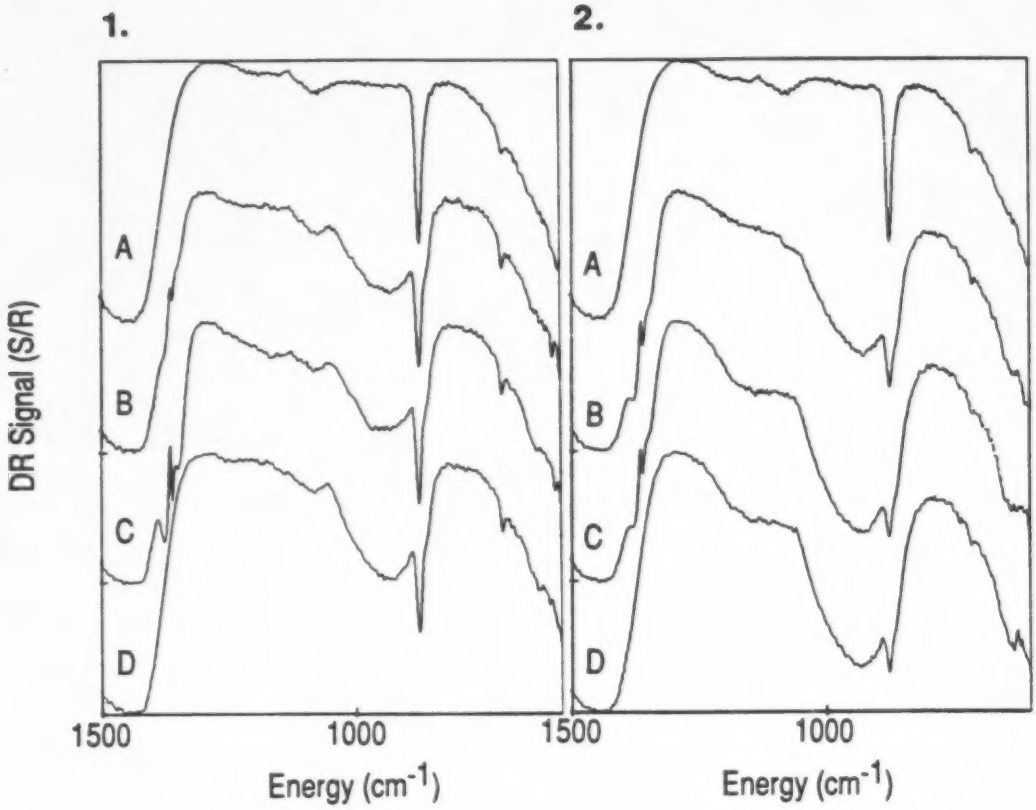

Figure 27. FTIR-DR spectra of a 10% by weight $Ca(OH)_2$ in NaCl sample at 25°C (1) and 200°C (2): (A); exposed to 1.5% SO_2 in N_2 for < 30 s (B); 30 min (C); and purged of excess SO_2 at 25°C (D).

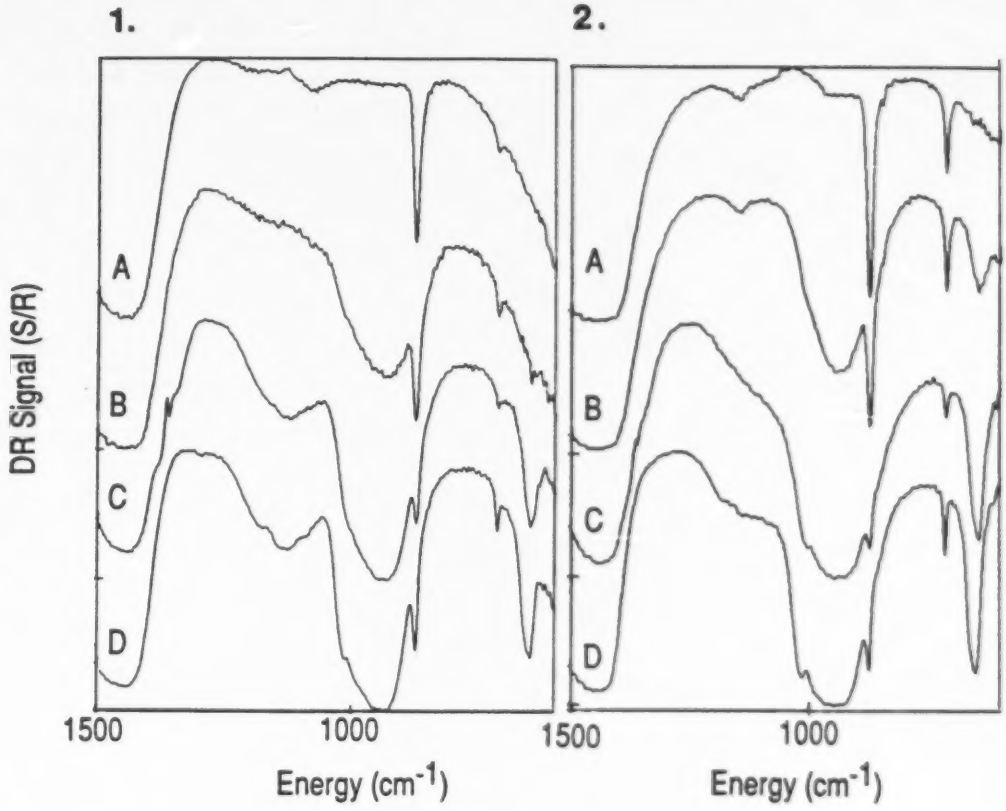

Figure 28. FTIR-DR spectra of a 10% by weight $Ca(OH)_2$ in NaCl sample at 300°C (1) and 400°C (2): (A); exposed to 1.5% SO_2 in N_2 for < 30 s (B); 30 min (C); and purged of excess SO_2 at 25°C (D).

of sulfate.[53]

The peak areas for the $SO_3^=$ and OH^- (not shown in the spectra) bands in K-M units as a function of time of exposure at temperatures of 25, 200, 300 and 400°C are shown in Figures 29, 30 and 31. Although, the plot of the $SO_3^=$ (A) peak area for the 25°C exposure of the 10% $Ca(OH)_2$ in NaCl sample to SO_2 clearly shows an increase in intensity of the sulfite peak over time (Figure 62, 1A), the OH^- peak (Figure 62, 1B) remains essentially constant. These data contradict post-exposure PA results indicating that the formation of sulfite was accompanied by a loss of OH^- from the $Ca(OH)_2$ sample surface. To test this observation further, the concentration of $Ca(OH)_2$ was increased to 100%, spectral band intensities for the $SO_3^=$ and OH^- peaks of this sample exposed to 1.5% SO_2 in N_2 at 25°C indicate that the formation of $SO_3^=$ is, in fact, accompanied by a loss of OH^- (Figure 29, 2A and 2B). Discrepancies between the 100 and 10% $Ca(OH)_2$ sample exposure data are perhaps due to the inability of this technique to detect the minute changes in the absorbance of the weak OH^- absorption. Furthermore, the loss of OH^- with the formation of $SO_3^=$ is observed for exposures of the 10% $Ca(OH)_2$ in NaCl samples at temperatures of 200 and 300°C (Figure 30, 1 and 2); these data and the data for the neat $Ca(OH)_2$ sample exposed to SO_2 support the hypothesis that the 10% $Ca(OH)_2$ in NaCl sample SO_2 exposed sample did in fact lose OH^- with the formation of $SO_3^=$.

Although, at elevated temperatures the loss of the OH^- may possibly be due to the calcination of the sample, the data presented in Figure 31 disprove this hypothesis. Figure 31 (1) depicts the mid-IR spectral region where water vapor bands are normally observed. Trace A represents the $Ca(OH)_2$ sample at 300°C before emission of SO_2 into the cell. The spectrum of the sample after ca. 200 s of exposure of the sample to SO_2 is shown in Trace B. And finally, Trace C was recorded after approximately 17 min of

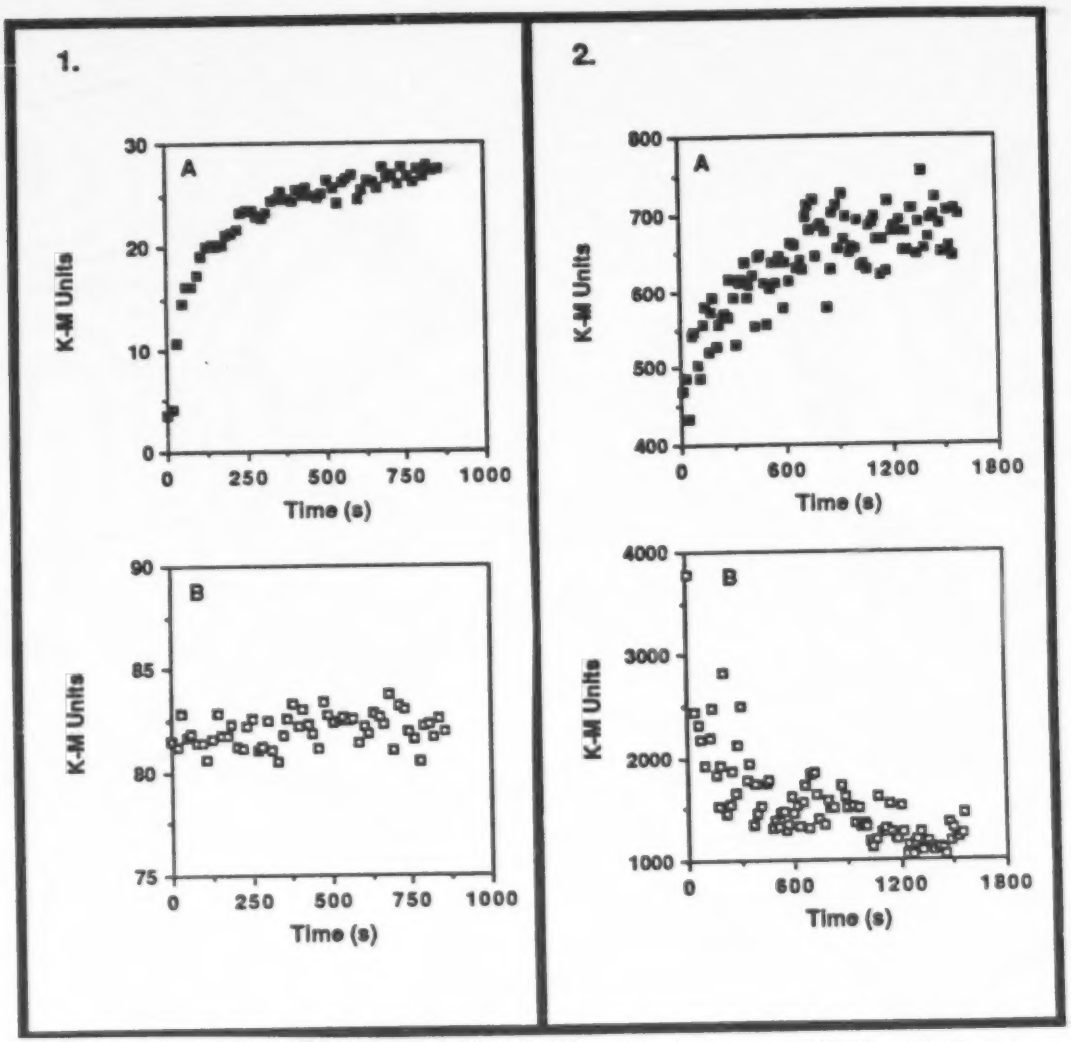

Figure 29. Plots of $SO_3^=$ (A) and OH^- (B) DR peak intensity (K-M units) as a function of time of exposure for a 10% by weight $Ca(OH)_2$ in NaCl sample (1) and a neat $Ca(OH)_2$ sample (2) to 1.5% SO_2 in N_2 at 25°C. (Each point of the plots correspond to the peak areas measured for a 16 scan spectrum that was acquired during the exposure of the sample to 1.5% SO_2 in N_2 at the selected temperature. Thus each spectrum depicted in the previous figures (27 and 28) produced a $SO_3^=$ and an OH^- point in the above plot.)

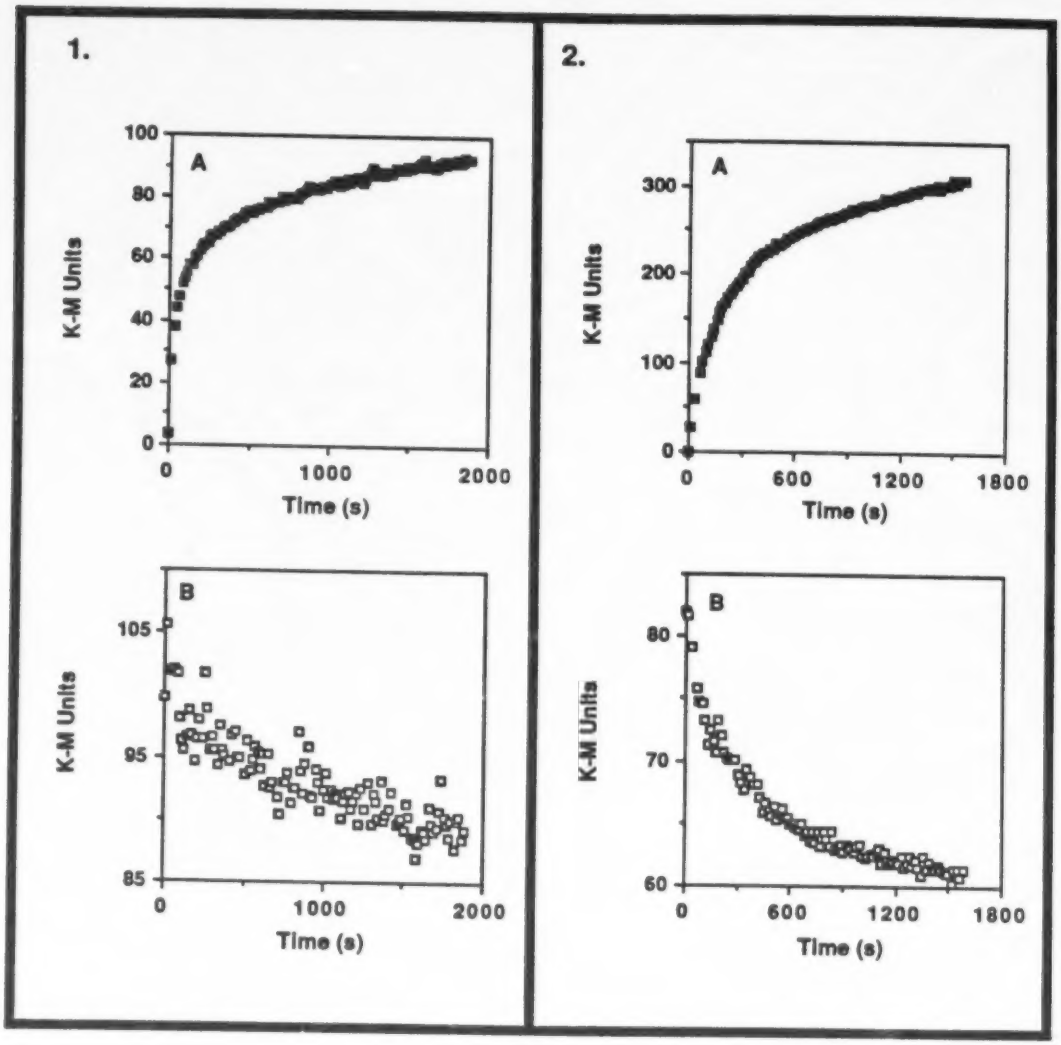

Figure 30. Plots of $SO_3^{=}$ (A) and OH^- (B) DR peak intensity (K-M units) as a function of time for the exposure of a 10% by weight $Ca(OH)_2$ in NaCl sample to 1.5% SO_2 in N_2 at 200°C (1) and 300°C (2).

exposure.

Before exposure of the sample to SO_2, no water vapor was present in the sample cell, as indicated by the lack of characteristic water vapor peaks at 1600 cm^{-1} in the sample spectrum.[57] However, immediately after the sample is exposed to SO_2, sharp peaks at ca. 1600 cm^{-1} appear in the sample spectrum. Simultaneously, a large loss of OH^- in the sample is indicated by the decreasing intensity of the 3641 cm^{-1} peak (Figure 31, 2B). Finally, after extensive exposure of the sample to SO_2, the production of $SO_3^=$ and loss of OH^- significantly decrease as indicated by the peak intensity data (Figure 31, 2C) and the disappearance of water vapor peaks from the sample spectrum (Figure 31, 1C).

Exposure of $Ca(OH)_2$ to SO_2 at 400°C results in the extensive formation of sulfite, as indicated by the large increase in spectral band intensity at 940 cm^{-1} (Figure 28). In this experiment, initially heating the sample to 400°C under N_2 resulted in calcining the $Ca(OH)_2$ sample such that only tightly bound water remained on the surface of the sample[25] as indicated by a peak at 3690 cm^{-1} (no peak indicative of lattice OH^- was observed). Upon the addition of SO_2 to the sample, the peak intensity for the remaining waters immediately decreased while the peak intensity for $SO_3^=$ increased. The formation of $SO_3^=$ continued to occur beyond the time required to remove all water and OH^- from the sample, indicating that the SO_2 must be reacting with nascent CaO formed during the calcination of the $Ca(OH)_2$.

Sulfite band intensities for the $\nu_1 + \nu_3$ band at 940 cm^{-1} (A), ν_2 band at 632 cm^{-1} (B) and overtone band for the $\nu_1 + \nu_3$ peak at 2100 cm^{-1} (C) for the sample exposed at 400°C are shown in Figure 32. The overtone and ν_2 bands are characteristically weak. The good correlation between these bands and the $\nu_1 + \nu_3$ band indicates that the $\nu_1 + \nu_3$ band is not

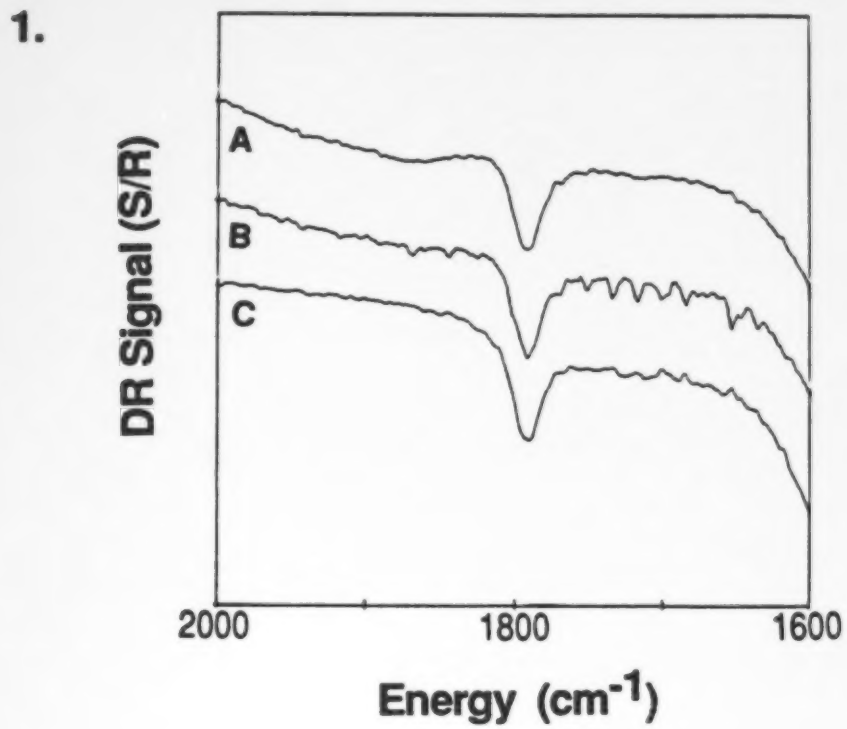

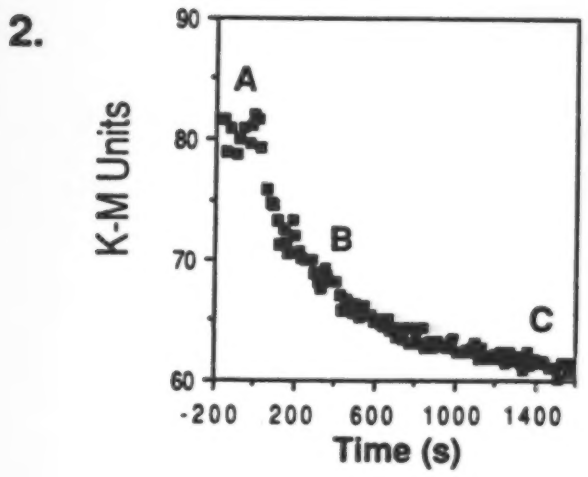

Figure 31. FTIR-DR spectra (1) of a 10% by weight $Ca(OH)_2$ in NaCl sample exposed to 1.5% SO_2 in N_2 at 300°C as a function of time: (A) before the reaction: (B) 200 s; (C) 17 min and (2) the corresponding OH^- peak areas for the sample during this exposure.

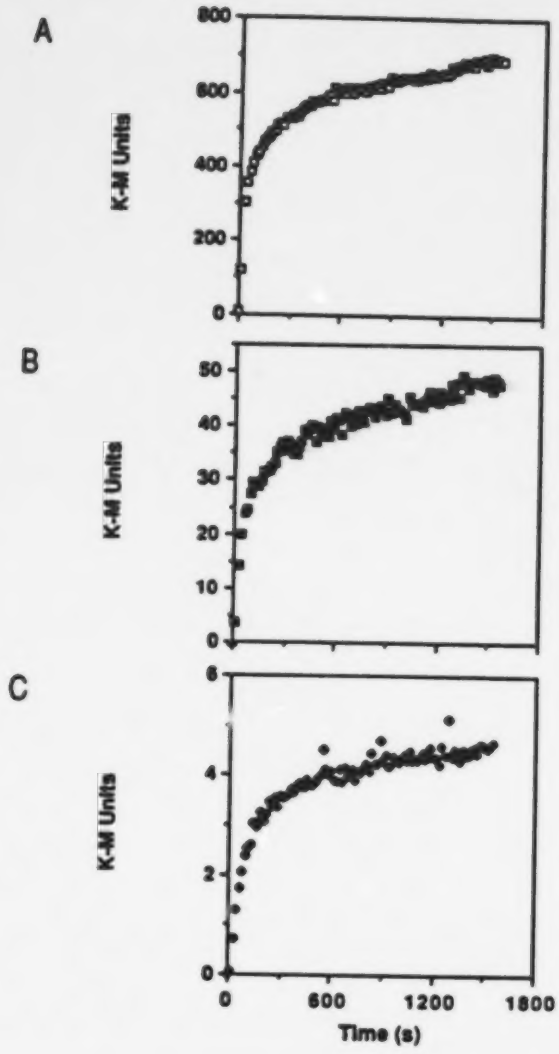

Figure 32. Plots of $SO_3^=$ peak intensity (K-M units) as a function of time for the exposure of a 10% by weight $Ca(OH)_2$ in NaCl sample to 1.5% SO_2 in N_2 at 400°C: (A) $\nu_1 + \nu_3$; (B) ν_4; (C) overtone band.

saturated.

The extent of SO_2 capture by the 10% by weight $Ca(OH)_2$ in NaCl samples at 25, 200, 300 and 400°C has been examined by comparing the intensities of the $\nu_1 + \nu_3$ $SO_3^=$ peaks at 940 cm^{-1} for each of the exposures to SO_2 (Figure 33). The data have been normalized for increases in sample temperature. (Peak areas for bands observed at elevated temperatures were divided by the band area increase caused by the increased temperature. This was determined as the ratio of the peak area of the final spectrum acquired at a selected elevated temperature to the corresponding peak area of the same sample at room temperature.) Based upon a calibration curve of IR peak intensity vs. % by weight $CaSO_3$, these data indicate that an estimated 26, 30, 44 and 69% of the $Ca(OH)_2$ sample was converted to $CaSO_3$ for exposures at 25, 200, 300 and 400°C, respectively.

Exposure of $Ca(OH)_2$ to SO_2 as a function of (steadily increasing) temperature--

Figures 34 and 35 depict data for the exposure of a 2% by weight $Ca(OH)_2$ in NaCl sample to 1.5% SO_2 in N_2 (3 ml/min flow rate) for increasing temperatures up to 700°C. Figure 34 is an overlay plot of spectra accumulated up to 468°C. Each spectrum represents 512 scans which were recorded over a 15°C range as the temperature of the sample was raised at a rate of 5°C/min.

The spectra of the exposed sample show the presence of three different sulfur-oxygen species which are identified in Table 6 (see below; Figure 34). Below 468°C, the spectra show the rapid growth of bands at 930 and 644 cm^{-1} indicating by the formation of $CaSO_3$. This is followed by the growth of a band at 1200 cm^{-1} and peaks on either side of the 632 cm^{-1} $SO_3^=$ peak which are characteristic of $CaSO_4$. Finally, the band observed at 1330

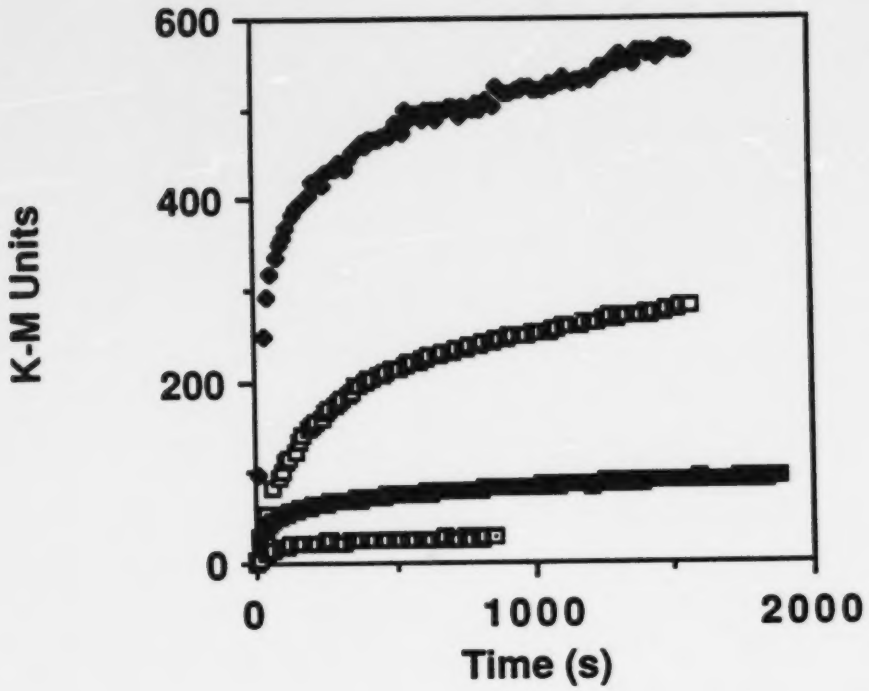

Figure 33. Plots of normalized $SO_3^=$ peak intensity for exposures of 10% by weight $Ca(OH)_2$ in NaCl samples to 1.5% SO_2 in N_2 at (◘) 25°C; (■) 200°C; (□) 300°C; and (◆) 400°C, as a function of time.

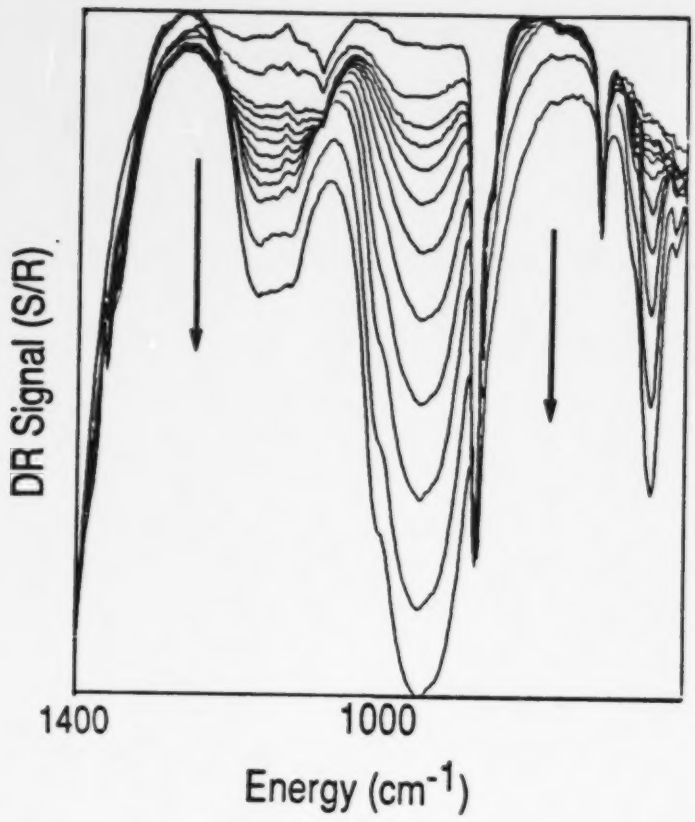

Figure 34. FTIR-DR spectra of a 2% by weight $Ca(OH)_2$ in NaCl exposed to 1.5% SO_2 in N_2 as a function of temperature up to 468°C.

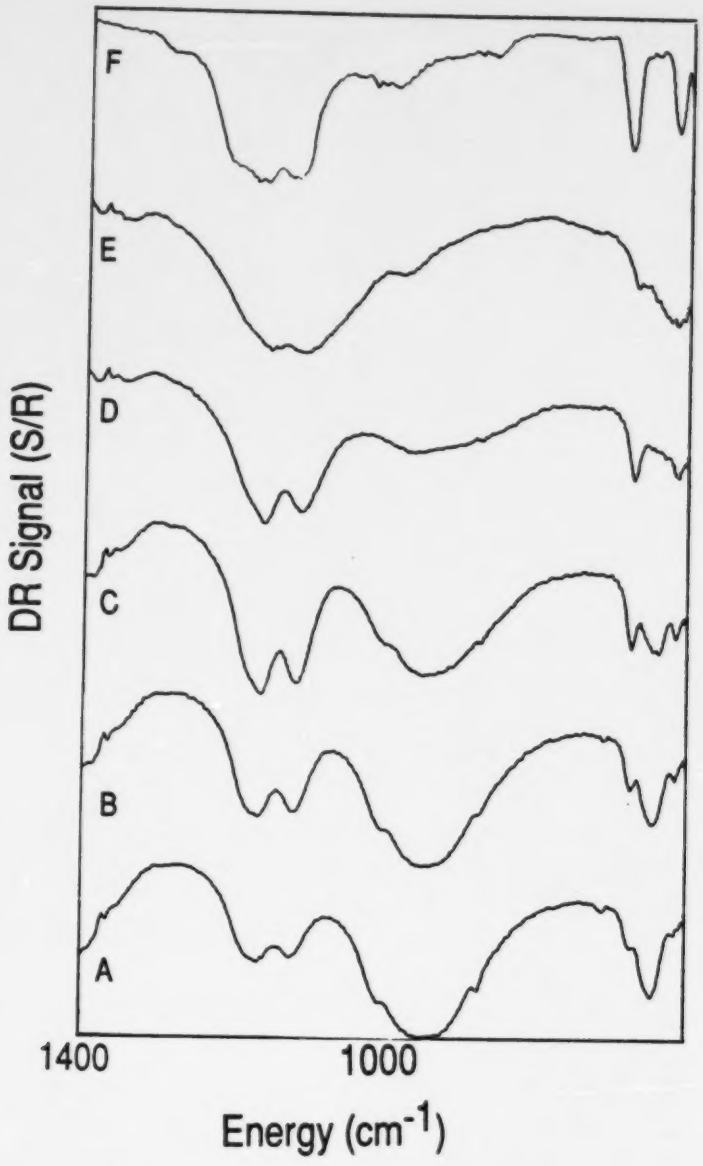

Figure 35. FTIR-DR spectra of a 2% by weight $Ca(OH)_2$ in NaCl sample exposed to 1.5% SO_2 in N_2 at temperatures of (A) 507°C; (B) 556°C; (C) 603°C; (D) 649°C; (E) 696°C; (F) cooled to 25°C under N_2.

Table 6.

Exposure of 2% by weight $Ca(OH)_2$ in NaCl sample to 1.5% SO_2 in N_2 up to Temperatures of 468°C

Absorption Band (cm^{-1})	Species	Assignment
1330	SO_2	ν_3
1163	$SO_4^=$	ν_3
1118		ν_3
671		ν_4
613		ν_4
1014	$SO_3^=$	ν_1
950		$\nu_1 + \nu_3$
644		ν_2

cm^{-1} is indicative of excess SO_2 in the cell.

Spectra of the sample exposed to SO_2 at temperatures above 468°C show increases in sulfate (1163, 1118, 671, 613 cm^{-1}) and decreases in sulfite (1014, 930, 644 cm^{-1}) species in the sample, as indicated by the increases and decreases in the respective band intensities (Traces A, B and C; Figure 35). At ca. 650°C (Trace D; Figure 35) only bands at 1163 and 1118 cm^{-1} are observed, indicating that only sulfate is present in the sample. As described earlier, the double sulfate band is indicative of the formation of the monodentate $SO_4^=$ species. At ca. 700°C (Trace E), this band becomes a single feature at 1200 cm^{-1} with a shoulder at 966 cm^{-1}. The appearance of these spectral bands suggests the formation of a $SO_4^=$ complex in which

the symmetry of the $SO_4^=$ is approximately tetrahedral.

Upon cooling the sample to room temperature under N_2 (Trace F, Figure 35), the broad peak at 1200 cm^{-1} shifts to higher frequencies and resolves into three components at 1199, 1163 and 1120 cm^{-1}. In addition, two peaks at 678 and 615 cm^{-1} are observed. Collectively, these peaks are assigned to the v_3 (1199, 1163, 1120 cm^{-1}) and v_4 (678 and 615 cm^{-1} (594 cm^{-1} not shown) vibrational modes of $CaSO_4$. The triply degenerate v_3 and v_4 vibrational modes are indicative of a bidentate $SO_4^=$ ion. Two types of bidentate complexes are possible; chelating and bridging. Typically, the v_3 vibrational frequencies of the chelating complex (1230, 1120, 1060 cm^{-1}) are higher than those of the bridging complex (1060, 1100, 1030 cm^{-1}).[53] The bands observed in Figure 35 occur at 1199, 1163 and 1120 cm^{-1}, indicating that a mixture of both chelating and bridging complexes is formed.

Although previous post-exposure PAS experiments showed the production of thiosulfate for the reaction of $Ca(OH)_2$ with SO_2 at temperatures of 550 and 750°C, no spectral bands indicative of $S_2O_3^=$ are observed in the DR spectra for exposures of the dilute sample to SO_2 at these temperatures. One significant experimental difference between these two exposures is that the $Ca(OH)_2$ is diluted in NaCl for the DR experiment and pure for the post-exposure PA experiment.

To test the effect of $Ca(OH)_2$ concentration upon the production of CaS_2O_3, a 50% by weight $Ca(OH)_2$ in NaCl sample was exposed to SO_2 at 700°C. Figure 36 depicts the DR spectrum of the sample that was exposed to SO_2 at 700°C and subsequently cooled to 25°C under N_2. This spectrum shows distinct bands at 1003, 984 and 656 cm^{-1} which are characteristic of thiosulfate. The additional peaks at 1200, 678 and 615 cm^{-1} are

characteristic of $CaSO_4$. There are no spectral peaks indicative of $CaSO_3$. These data suggest that the formation of thiosulfate occurs through the following reaction:

$$4CaSO_3(s) \text{ ---> } 2CaSO_4(s) + CaS_2O_3(s) + CaO(s) \qquad (5)$$

The differences between the DR spectra for exposures of 2% and 50% by weight samples of $Ca(OH)_2$ in NaCl to SO_2 suggest that the concentration of either the $Ca(OH)_2$ or NaCl diluent in the reactive sample is important to the formation of CaS_2O_3.

Halogenated additives, such as NaCl and KCl have been shown to accelerate the reaction between $CaSO_3$ and SO_2 described below:[10]

$$2CaSO_3(s) + SO_2(g) \text{ ---> } 2CaSO_4(s) + S(g) \qquad (4)$$

One possibility explaining the absence and presence of the $S_2O_3^=$ product for the above reactions is that the NaCl diluent in the 2% by weight $Ca(OH)_2$ sample accelerates the conversion of all the $CaSO_3$ to $CaSO_4$ via reaction (4). However, when the sample is more concentrated in $Ca(OH)_2$, the effects of the NaCl no longer dominate, and most of the $CaSO_3$ disproportionates via reaction (5).

Plots of the peak intensities for the sulfite and sulfate bands as a function of temperature for the exposure of the 2% by weight $Ca(OH)_2$ sample to 1.5% SO_2 in N_2 are depicted in Figure 37. The reaction of $Ca(OH)_2$ with SO_2 is very similar to the reaction of CaO with SO_2: 1) below 400°C the plots indicate extensive formation of $CaSO_3$ and no $CaSO_4$; 2) above 500°C the $SO_3^=$ band begins to decrease in intensity while the sulfate peak intensity increases; and 3) at 690°C, the intensity of the sulfite peak intensity has significantly decreased while the sulfate peak intensity

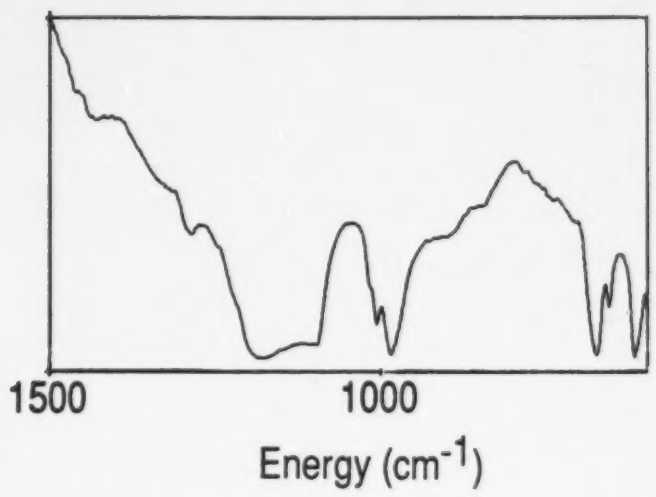

Figure 36. FTIR-DR spectra of a 50% by weight $Ca(OH)_2$ in NaCl sample after being exposed to 1.5% SO_2 in N_2 at 700°C and cooled to 25°C under N_2.

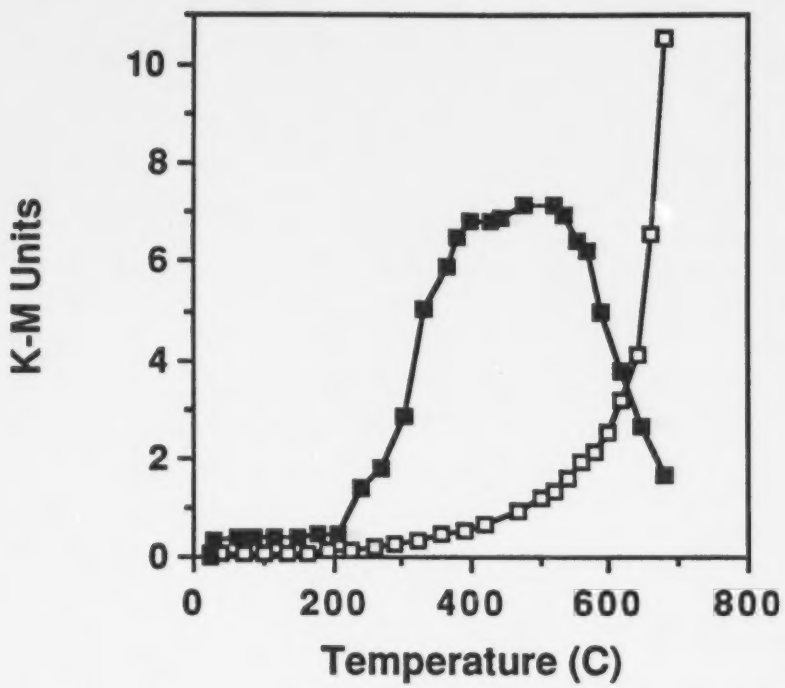

Figure 37. Plots of $SO_3^=$ (■) and $SO_4^=$ (□) peak intensity (K-M units) as a function of temperature for the exposure of a 2% by weight $Ca(OH)_2$ in NaCl sample to 1.5% SO_2 in N_2.

continues to increase. Collectively, the DR data for the reaction of $Ca(OH)_2$ with SO_2 indicate:

1). Below 500°C, the primary reaction is:

$$Ca(OH)_2 + SO_2(g) \text{ ---> } CaSO_3(s) + H_2O(g) \qquad (3)$$

For temperatures below 300°C this reaction forms only the pyramidal sulfite ion bound to the surface through the sulfur atom. At temperatures of 300°C and above a second type of sulfite is formed that is bound to the surface through an oxygen.

2). For temperatures of 500 to 690°C, all $CaSO_3$ formed on the surface of the particles is converted to $CaSO_4$. The initial $CaSO_4$ product is a monodentate species exhibiting C_{2v} symmetry. At 690°C the $SO_4^=$ species assumes a nearly T_d form. However, upon cooling the 690°C-exposed sample to 25°C, the sulfate reorganizes into the bidentate form.

3). NaCl was observed to be an important factor in preventing the conversion of $SO_3^=$ to $S_2O_3^=$.

$\underline{CaCO_3}$

Calcination of $CaCO_3$--

DR spectra plotted in Kubelka-Munk units (A) were obtained for a 10% by weight sample of $CaCO_3$ (calcite) in NaCl heated at a rate of 5°C/min under N_2 (Figure 38). Each spectrum was recorded over a period of 3 min and temperature range of 15°C. The prominent peak at 2360 cm^{-1} is characteristic of CO_2 gas.[25]

The K-M peak area of the CO_2 band plotted as a function of temperature is also shown in Figure 38. From this plot it is clear that the calcination of $CaCO_3$ under N_2 begins at ca. 525°C. This result correlates well with thermogravimetric studies of $CaCO_3$ in air which show initial

calcination processes occurring at temperatures of 530°C.[13]

Exposure of $CaCO_3$ to SO_2 at 400°C--

Although, DR spectra for the exposure of a 10% by weight sample of $CaCO_3$ in NaCl to 1.5% SO_2 in N_2 (6 ml/min) up to temperatures of 400°C indicated no reaction, at 400°C changes in the sample spectrum indicated the formation of sulfur-oxygen species (Figure 39). Trace A of Figure 39 depicts the spectrum of $CaCO_3$ at 400°C. After exposing this sample to 1.5% SO_2 in N_2 for 15 min at 400°C (Trace B) peaks at ca. 976, 940, 642, 609 cm^{-1} and a shoulder on the high frequency side of the 976 cm^{-1} band. These peaks are enhanced with further exposure to SO_2 (Trace C). Trace D is the spectrum of the sample cooled under N_2 to room temperature; in this spectrum the shoulder of the 976 cm^{-1} band is resolved into a peak at 1014 cm^{-1} and the 642 cm^{-1} peak has shifted to 676 cm^{-1}.

Although the peaks of the final product at 1014, 976, 940, 676 and 609 cm^{-1} differ considerably from those previously observed for the sulfite species, they are very similar to the sulfite peaks reported for $Tl_2[Cu(SO_3)_2]$ at 989, 902, 862, 673, and 602 cm^{-1}.[60] For the $Tl_2[Cu(SO_3)_2]$ compound, the bands at 989, 902 and 862 cm^{-1} represent the ν_1 (989 cm^{-1}) and doubly degenerate ν_3 (902, 862 cm^{-1}) vibrational frequencies of the sulfite ion.[60] The spectrum of the doubly degenerate ν_3 band for $Tl_2[Cu(SO_3)_2]$ splits slightly into two peaks ca. 40 cm^{-1} apart. This same behavior is also observed for the 976 and 940 cm^{-1} bands appearing in the spectrum of the sample of $CaCO_3$ exposed to SO_2. Furthermore, the ν_1 peak is nearly equal in intensity to the ν_3 peaks for the $Tl_2[Cu(SO_3)_2]$ compound and this also is the case for the $CaSO_3$ species shown in Figure 39.

Unlike most sulfite species, the $SO_3^=$ in $Tl_2[Cu(SO_3)_2]$ is unusual in that the $SO_3^=$ is coordinated to the metal through an oxygen. Based upon the

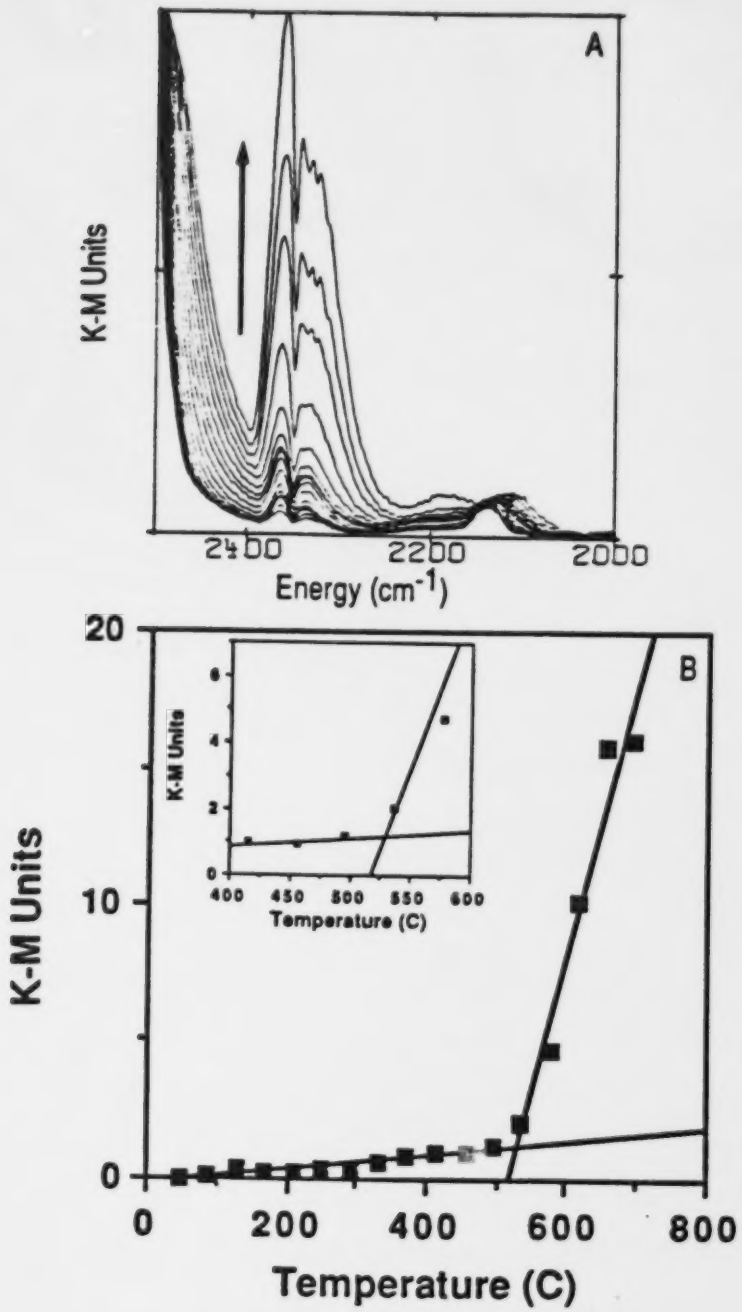

Figure 38. FTIR-DR spectra plotted in Kubelka-Munk units (A) and plots of CO_2 peak intensity (B) for a 10% by weight $CaCO_3$ in NaCl sample as a function of temperature. Reprinted with permission from Appl. Spectros., 42, 945 (1988). Copyright Kansas State University.

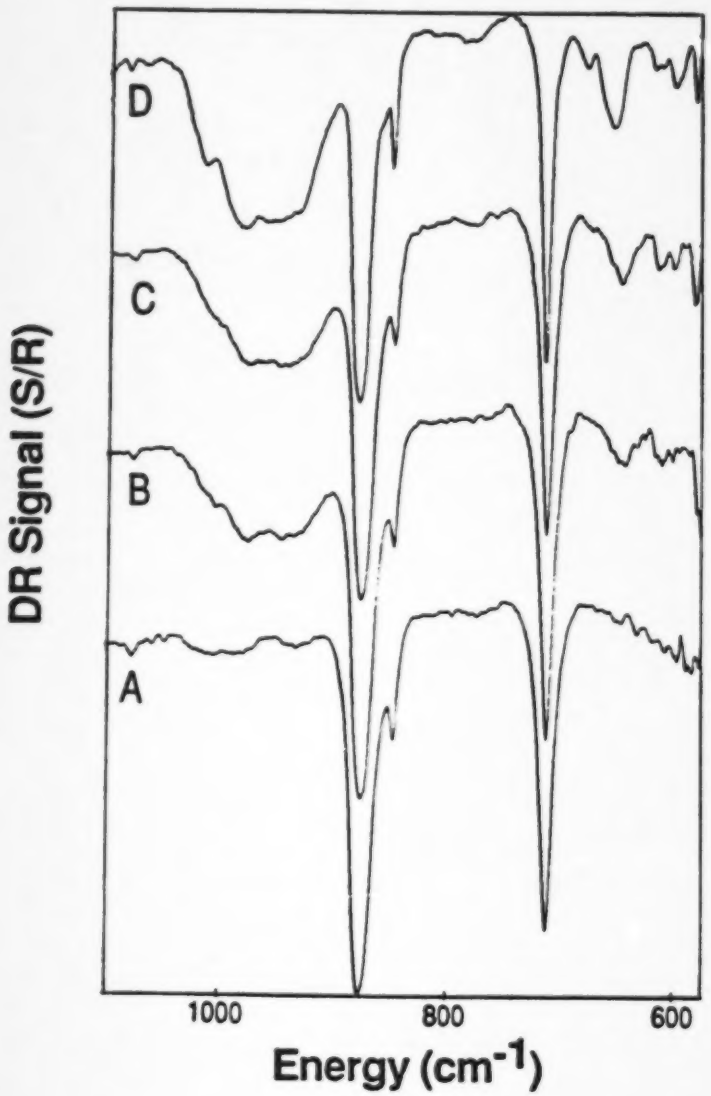

Figure 39. FTIR-DR spectra of a 10% $CaCO_3$ in NaCl sample at 400°C (A) exposed to 1.5% SO_2 in N_2 for 15 min (B); 26 min (C) and purged under N_2 at 25°C (D). Reprinted with permission from Appl. Spectros., 42, 945 (1988). Copyright Kansas State University.

similarities observed between the $Tl_2[Cu(SO_3)_2]$ spectrum and the sulfite spectrum resulting from the reaction of SO_2 with $CaCO_3$, this latter $SO_3^=$ must also be an oxygen coordinated species.

Other unusual characteristics for the reaction of SO_2 with $CaCO_3$ are realized by plotting the peak intensity of the $SO_3^=$ and $CO_3^=$ bands as a function of time of exposure (Figure 40). While the $SO_3^=$ band at 950 cm^{-1} exhibits an increase in intensity with exposure time, the carbonate peak intensity at 713 cm^{-1} shows no loss in intensity (Figure 40). Furthermore, no gaseous CO_2 is evident in the spectra (not shown). In addition, unlike the increases in $SO_3^=$ peak intensity *vs.* time of exposure for CaO and $Ca(OH)_2$, the $SO_3^=$ peak intensity for the carbonate sample increases linearly with time.

These data are interpreted to indicate:

1). The sulfite formed on the surface of $CaCO_3$ at 400°C is oxygen-coordinated to the Ca^{++} ions on the sample surface.

2). The inability to detect gaseous CO_2, as well as the slow and constant rate of the reaction, indicate that the initial sulfite formed on the $CaCO_3$ surface differs from that initially formed on the CaO and $Ca(OH)_2$ surface.

Exposure of $CaCO_3$ to SO_2 as a function of temperature--

Spectra for the exposure of a 2% by weight sample of $CaCO_3$ in NaCl to 1.5% SO_2 in N_2 (3 ml/min) as a function of temperature are depicted in Figure 41. Trace A of Figure 41 is a typical spectrum of $CaCO_3$ (calcite). The first bands to appear when $CaCO_3$ is exposed to SO_2 at 25°C, occur at 1350 and 1330 cm^{-1} (Figure 41, Trace B); these bands are characteristic of the ν_3 vibrational mode of SO_2 gas.

The reaction of SO_2 with $CaCO_3$ is first evident for exposures at

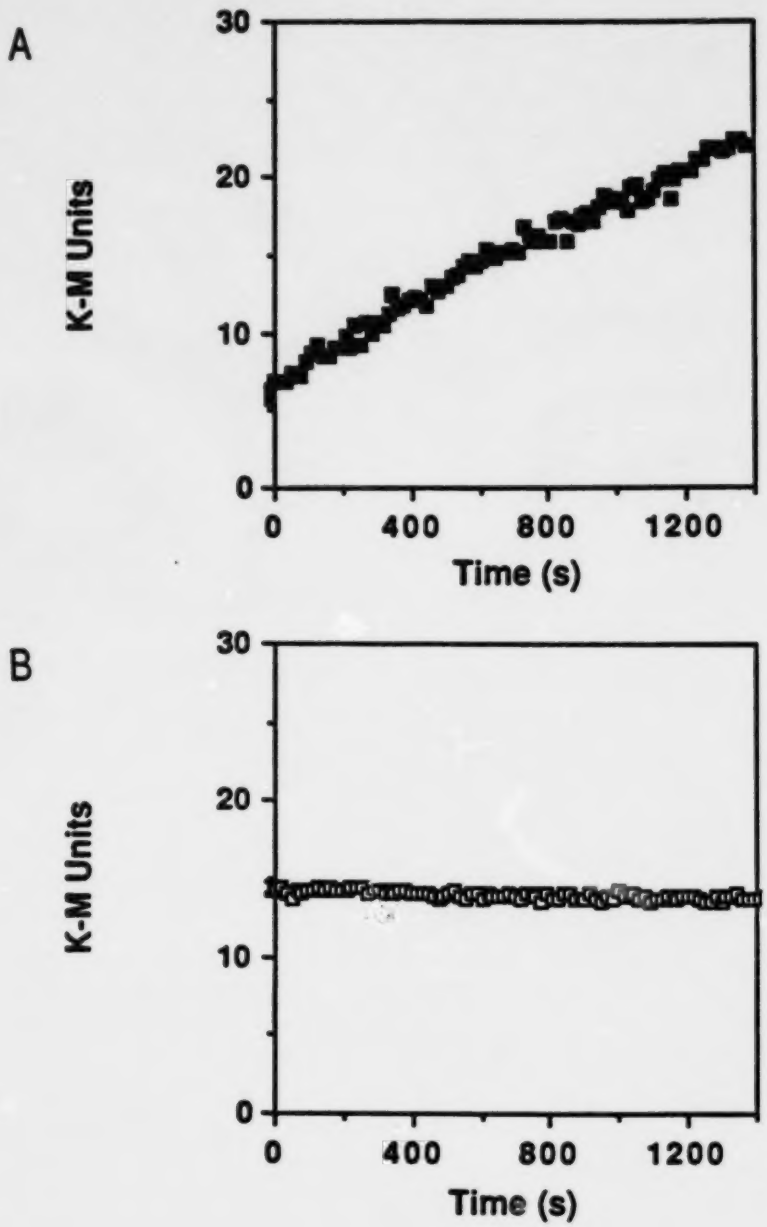

Figure 40. Plots of $SO_3^=$ (A) and $CO_3^=$ (B) peak intensity (K-M units) for the exposure of a 10% by weight $CaCO_3$ in NaCl sample to 1.5% SO_2 in N_2 at 400°C as a function of time. Reprinted with permission from Appl. Spectros., 42, 945 (1988). Copyright Kansas State University.

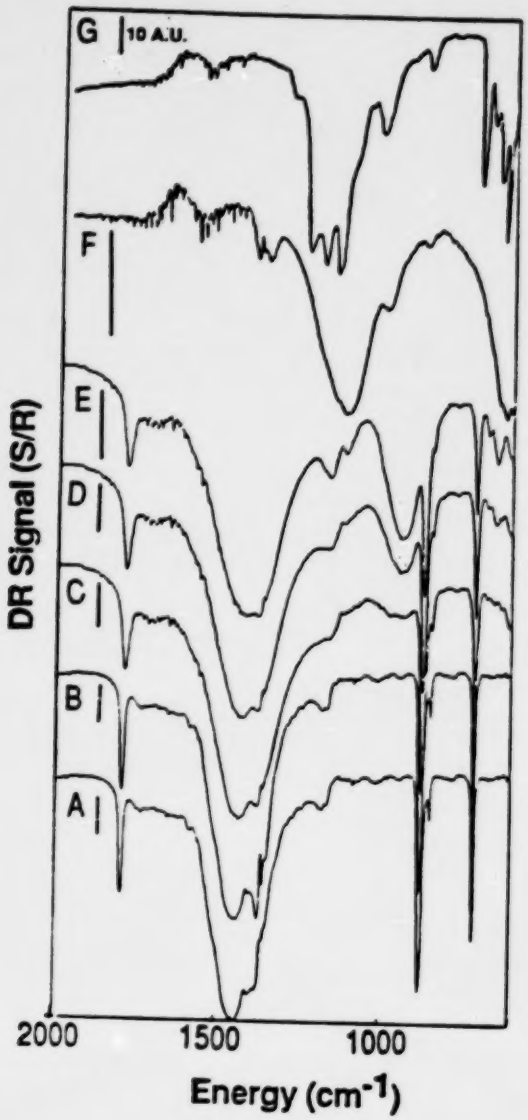

Figure 41. FTIR-DR spectra of a 2% by weight $CaCO_3$ in NaCl sample (A) exposed to 1.5% SO_2 in N_2 at (B) 25°C; (C) 400°C; (D) 440°C; (E) 500°C; (F) 640°C; (G) and then cooled and purged under N_2 at 25°C. Reprinted with permission from Appl. Spectros., 42, 946 (1988). Copyright Kansas State University.

400°C; a small split band at 950 cm^{-1} is again observed (Trace C), indicating the formation of the oxygen coordinated $SO_3^=$ on the surface of the particles. At ca. 440°C (Trace D) the two peaks at 976 and 940 cm^{-1} coalesce into one broad band and the peak at 1014 cm^{-1} is no longer observed. These peaks are characteristic of pyramidal sulfite. In addition, another double band at 1163 and 1118 cm^{-1} is observed. Spectra of the sample after increasing the time (to 100 min) and temperature (to 500°C) of the exposure show increases in band intensity at 950 and 640 cm^{-1}, as well as the appearance of new bands at 1163, 1118 and 676 cm^{-1} (Trace E). For higher temperatures of exposure, the 1163 and 1118 cm^{-1} bands increase in intensity while the 940 cm^{-1} peak decreases. Trace F depicts the spectrum of the sample exposed at 640°C. Once again the broad bands at 1100, 975 and 625 cm^{-1} are observed and indicate the formation of a nearly tetrahedral $SO_4^=$ species. These bands are observed in the DR spectra up to temperatures of 690°C. However, upon subsequent cooling of the 690°C-exposed sample, the bands at 1100 and 625 cm^{-1} resolve into peaks at 1205, 1155, 1114, 997, 675, 613 and 594 cm^{-1}, which are characteristic of the bidentate form of sulfate.[53] Furthermore, the position of the ν_3 peaks (1205, 1155, 1114 cm^{-1}) suggests the formation of the chelating complex.

Plots of $SO_3^=$ and $SO_4^=$ peak intensity vs. the temperature of exposure indicate that no reaction occurs on the $CaCO_3$ surface until 400°C (Figure 42). At 400°C there is a simultaneous increase in both $SO_3^=$ and $SO_4^=$ band intensity up to 500°C. Above this temperature, the $SO_3^=$ peak intensity decreases while $SO_4^=$ peak intensity continues to increase.

These data for the exposure of $CaCO_3$ to SO_2 indicate:

1). The reaction of $CaCO_3$ with SO_2 occurs only for temperatures greater than or equal to 400°C. At this temperature the reaction results

in the formation of an oxygen coordinated $SO_3^=$ species. Increasing the temperature and time of exposure results in the production of pyramidal $SO_3^=$.

2). Above temperatures of 500°C the $CaSO_3$ is converted to $CaSO_4$, as in the reactions of CaO and $Ca(OH)_2$ with SO_2.

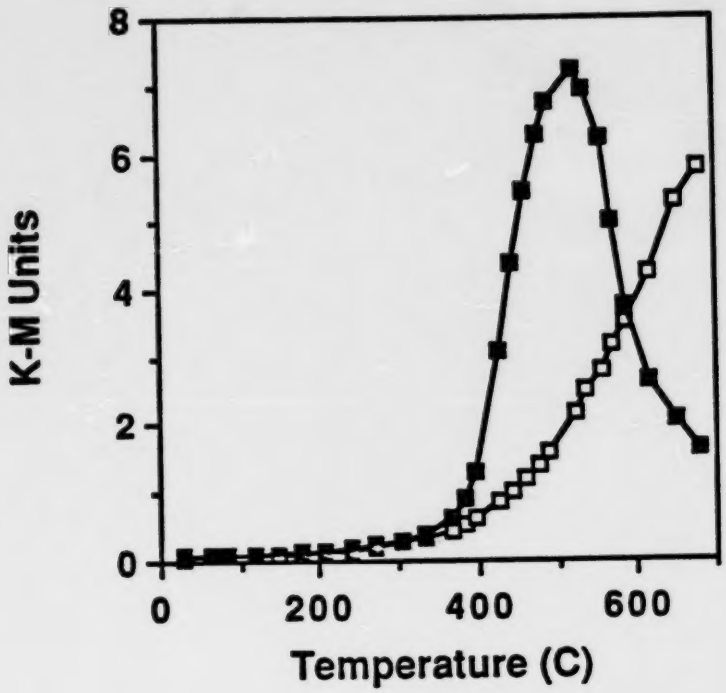

Figure 42. Plots of $SO_3^=$ (□) and $SO_4^=$ (■) peak intensity as a function of temperature of the exposure of a 2% by weight $CaCO_3$ in NaCl sample to 1.5% SO_2 in N_2. Reprinted with permission from Appl. Spectros., 42, 946 (1988). Copyright Kansas State University.

IN SITU PHOTOACOUSTIC SPECTROSCOPY

The ease of sample preparation and ability to detect both solid and gas phase signals simultaneously affords photoacoustic spectroscopy many advantages for studying solid-gas reactions. In order to evaluate the effectiveness of this technique for studying the basic chemical steps involved in the capture of SO_2 by powdered samples of alkali and alkaline earth compounds, experiments involving *in situ* FTIR-PA monitoring of the reaction of SO_2 with Na_2CO_3, $Ca(OH)_2$ and $CaCO_3$ were conducted. These experiments were carried out using the high temperature PAS cell described in the Experimental section.

Characteristics of the gas phase photoacoustic signal--

One of the applications for which photoacoustic spectroscopy has been claimed to be particularly appropriate is the characterization of surface species and the monitoring of reactions at solid surfaces.[63,64] However, most PA investigations have avoided studies in which components of the coupling gas as well as the solid exhibit absorption bands in the spectral region investigated since the gas phase PA signal tends to dominate the spectrum. (One recent exception is an investigation by Royce et al.[48] of the adsorption of gas phase CO_2, H_2O and methanol on -alumina.) As an example of this effect, the spectrum of powdered Na_2CO_3 under N_2 and exposed to 1.5% SO_2 in N_2 is shown in Traces A and B, respectively, of Figure 43. The spectrum exhibited in Trace A is dominated by the gas phase SO_2 signal at 1350 cm^{-1}, while the spectrum of the sample purged of excess SO_2 gas with N_2 (Trace B) clearly exhibits the features of the powder. The spectra are scaled to the value of maximum absorbance of each spectrum.

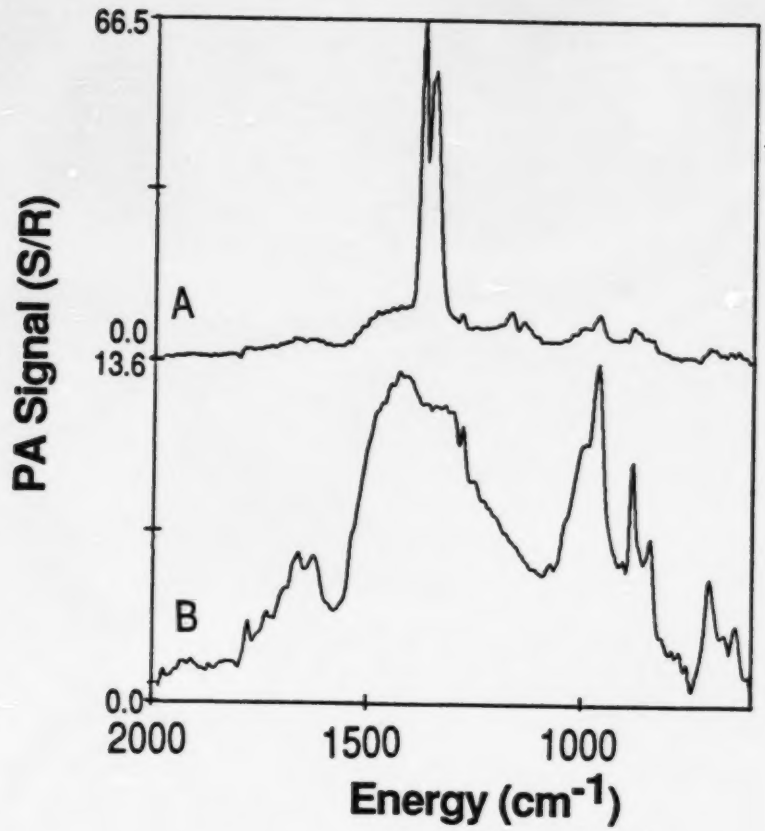

Figure 43. In situ FTIR-PA spectra of Na_2CO_3 (A) exposed to 1.5% SO_2 in N_2; and (B) purged of the excess SO_2 gas.

$\underline{Na_2CO_3}$

Exposure of Na_2CO_3 to SO_2 at 25°C--

HT-PA <u>in situ</u> spectral measurements of the reaction of 1.5% SO_2 in N_2 with a single sample of Na_2CO_3 (40 mg) are illustrated in Figure 44. The reaction was conducted at 25°C with a gas flow of 2 ml/min. Trace A is a spectrum of the as-received "Na_2CO_3" sample. (All spectra are scaled equally.) The spectrum exhibits peaks at 1450, 870 and 690 cm^{-1} which are characteristic of the ν_4, ν_2 and ν_3 vibrational modes of carbonate, respectively.[64] In addition, a broad peak from 3600 to 2600 cm^{-1} is observed. This peak is characteristic of H_2O, indicating that the Na_2CO_3 is hydrated.[63]

There are three known sodium carbonate hydrates: mono-, hepta- and deca-.[65] The intensities and positions of the bands at 906, 870 and 686 cm^{-1} correspond to the spectral characteristics of $Na_2CO_3.H_2O$. In addition to these peaks, the spectrum also exhibits a small band at 1700 cm^{-1} which is characteristic of both the hepta- and decahydrate species. In fact, sodium carbonate hepta- and decahydrate exhibit identical spectra, which differ from the sodium carbonate monohydrate spectrum only by the presence of a band at 1660 cm^{-1} and the lower intensity of the bands at 868 and 686 cm^{-1} bands relative to those of the hepta- and decahydrate.[65] Therefore, the spectrum of the "Na_2CO_3" sample (Trace A) indicates that the sample is predominantly composed of $Na_2CO_3.H_2O$ with traces of $Na_2CO_3.7H_2O$ and/or $Na_2CO_3.10H_2O$.

Shortly after exposure of the $Na_2CO_3.H_2O$ sample to SO_2, peaks at 2350, 960, 667 and 629 cm^{-1} are observed (Trace B). The peaks at 2350 and 667 cm^{-1} are characteristic of the ν_3 and ν_2 vibrational stretching and bending modes of CO_2, respectively,[25] while the bands at 960 and 629 cm^{-1}

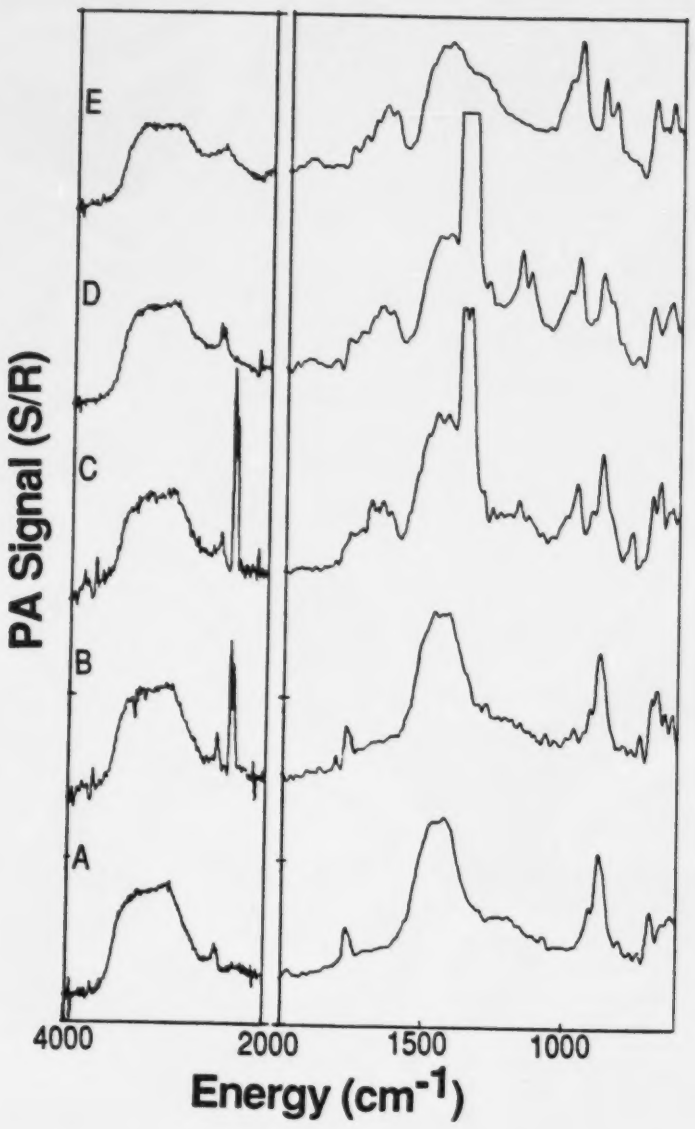

Figure 44. In situ FTIR-PA spectra of $Na_2CO_3.H_2O$ (A) exposed to 1.5% SO_2 in N_2 at 25°C as a function of time: (B) 2.5 min; (C) 5 min; (D) 30 min; (E) sample purged.

represent the $v_1 + v_3$ symmetric and asymmetric S-O stretching modes and the v_2 symmetric bending mode of the sulfite ion, respectively.[25] Continued exposure of the sample to SO_2 results in increased intensity of the CO_2 and $SO_3^=$ bands, as well as the appearance of additional bands at 2511, 1350, 1650, 1150 and 840 cm^{-1} (Trace C). The peaks at 1350, 2511 and 1150 cm^{-1} (Trace C) are characteristic of SO_2.[25] (The intensity of the gas phase peaks remains constant during the reaction because the gas is constantly flowing through the cell.) The absorption peaks observed at 1650 and 840 cm^{-1} are similar to bands at 1630-1660, 1295 and 838 cm^{-1} reported by Miller and Wilkins for $NaHCO_3$.[66] For this experiment, the third $NaHCO_3$ band at 1295 cm^{-1} is apparently masked by the intense SO_2 gas peak. After approximately 30 min of exposure the peaks at 2350 and 667 cm^{-1} are no longer observed (Trace D), indicating the absence of CO_2 from the sample chamber.

The sample was then purged overnight with pure N_2 (Trace E). The spectrum of the purged sample exhibits a loss in intensity for the hydrate band from 3600 to 2600 cm^{-1}. The dehydration of $Na_2CO_3.H_2O$ normally occurs at a temperature of 100°C[64] which is 70°C in excess of the sample temperature. However, the $Na_2CO_3.7H_2O$ and/or $Na_2CO_3.10H_2O$ species are reported to lose water at temperatures of <u>ca.</u> 30°C, consequently, the decrease in the H_2O band is attributed to their dehydration.

These data are interpreted to indicate that the first reaction occurring on the surface of the Na_2CO_3 particles is:

$$Na_2CO_3(s) + SO_2(g) \quad ---> \quad Na_2SO_3(s) + CO_2(g) \qquad (8)$$

With continued exposure of the sample to SO_2, the spectra (Traces C, D and E) indicate increasing Na_2SO_3 production in addition to the formation of $NaHCO_3$. These data then indicate that a second reaction is occurring on the

surface of the particles:

$$2Na_2CO_3.H_2O(s) + SO_2(g) \quad ---> \quad 2NaHCO_3.H_2O(s) + Na_2SO_3(s) \qquad (9)$$

It is reasonable to expect that the bicarbonate would then react with the SO_2:

$$2NaHCO_3.2H_2O(s) + SO_2(g) \quad ---> \quad Na_2SO_3(s) + 3H_2O(g) + 2CO_2(g) \qquad (10)$$

However, no vapor phase H_2O is observed in the spectra, and only after the exposed sample is purged under N_2 overnight did the sample exhibit a loss of water. Therefore, this last reaction does not appear to be an important mechanism in the formation of Na_2SO_3. After 30 min of exposure of the $Na_2CO_3.H_2O$ sample to SO_2, the formation of sulfite and release of CO_2 cease, as indicated by the constant intensity of the $SO_3^=$ peaks and absence of the CO_2 peak in the spectrum. Based on the interpretation of previous results, this can be interpreted as indicating the formation of an impervious product layer on the surface of the particles.

Heating of the exposed Na_2CO_3 sample under N_2 to 100°C--

In order to further characterize the reaction between $Na_2CO_3.H_2O$ and SO_2, the product from the above reaction was heated under a constant flow of N_2 (2 ml/min) to 100°C (Figure 45). In the figure, the spectral region from 1700 to 600 cm^{-1} shown in Box 1 is expanded in Box 2; all spectra are scale expanded. Trace A depicts the spectrum of the Na_2CO_3 sample that had been exposed to SO_2 at room temperature. Upon heating the sample from 30 to 50°C (Trace B), sharp peaks at 3600 and 1600 cm^{-1} are observed; these peaks are characteristic of water vapor. At temperatures greater than 50°C the vapor phase spectrum for H_2O increases in intensity and bands at 2350 and 667 cm^{-1} which are characteristic of CO_2 are observed (Traces C and D).

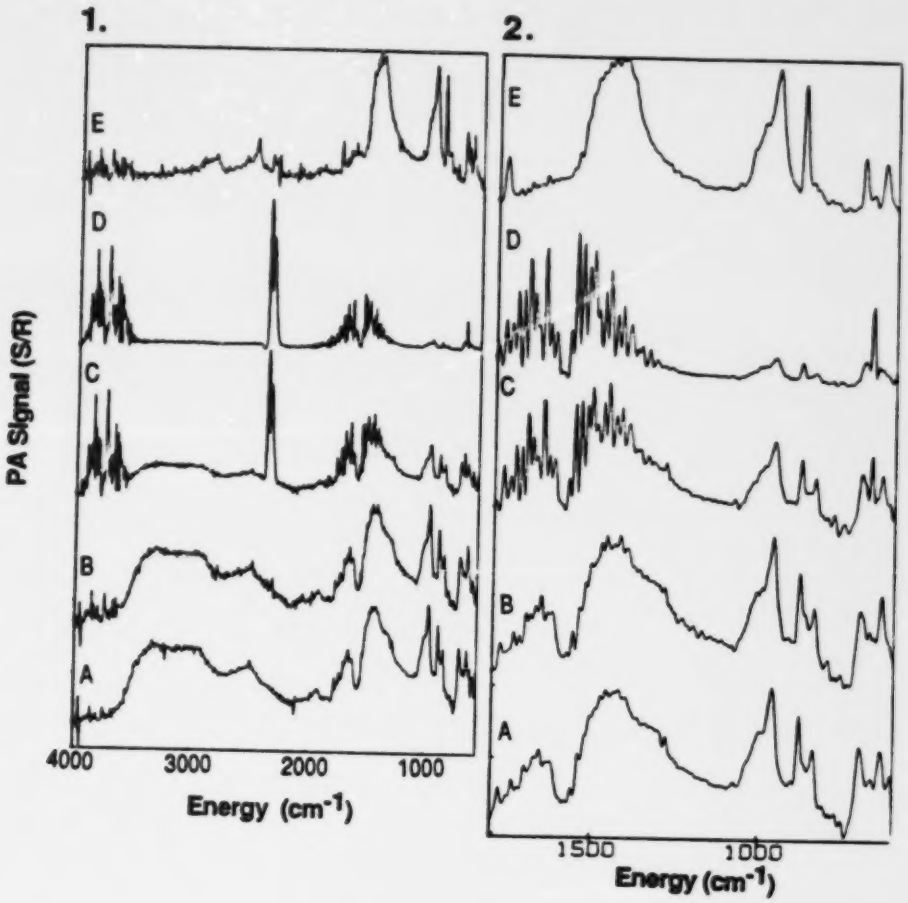

Figure 45. In situ FTIR-PA spectra of the sample of $Na_2CO_3.H_2O$ after exposure to 1.5% SO_2 in N_2 as a function of temperature: (A) 25-30°C; (B) 30-50°C; (C) 50-72°C; (D) 72-97°C; (E) 100°C (1) Full spectral range; (2) Expansion of the lower energy region.

The intensity of both the H_2O and CO_2 vapor phase peaks continues to increase for sample temperatures up to 100°C. At 100°C (Trace E), only bands at 2700, 2500, 1450, 960, 876, 668 and 622 cm^{-1} are observed. These peaks are characteristic of Na_2CO_3 and Na_2SO_3 only.

These data are interpreted to indicate that the release of H_2O and CO_2 from the sample must occur through the dehydration of the sodium carbonate mono-, hepta- and decahydrates as well as the decomposition of the $NaHCO_3.H_2O$. Sodium carbonate hepta- and decahydrates have been reported to lose water readily at ca. 35°C in the presence of air to form the monohydrate species, which is converted to the anhydrous form upon heating to 100°C.[67] The decomposition of $NaHCO_3.H_2O$ can then be described by the following reaction:

$$2NaHCO_3.H_2O(s) \text{ ---> } Na_2CO_3(s) + 2CO_2(g) + 2H_2O(g) \qquad (11)$$

In summary, the final reaction product is composed only of Na_2CO_3 and Na_2SO_3.

Exposure of $Na_2CO_3.H_2O$ to SO_2 at elevated temperatures--

In situ HT-PA spectral measurements acquired during the exposure of $Na_2CO_3.H_2O$ (40 mg) to 1.5% SO_2 in N_2 (2 ml/min) for 30 min at selected temperatures from 25 to 300°C are depicted in Figure 46. For these experiments, the excess SO_2 was purged from the sample after each exposure and before each spectrum was acquired. The typical ambient temperature spectrum of $Na_2CO_3.H_2O$ is shown in Trace A of Figure 46. As shown in the experiments above, after the initial exposure of the sample to SO_2 at 25°C, a band centered at ca. 960 cm^{-1} is observed (Trace B). Continued exposure of the sample to SO_2 results in increased intensity of the 960 cm^{-1} band and the appearance of bands at 1650, 1330, 840 and 629 cm^{-1} (Trace C). The

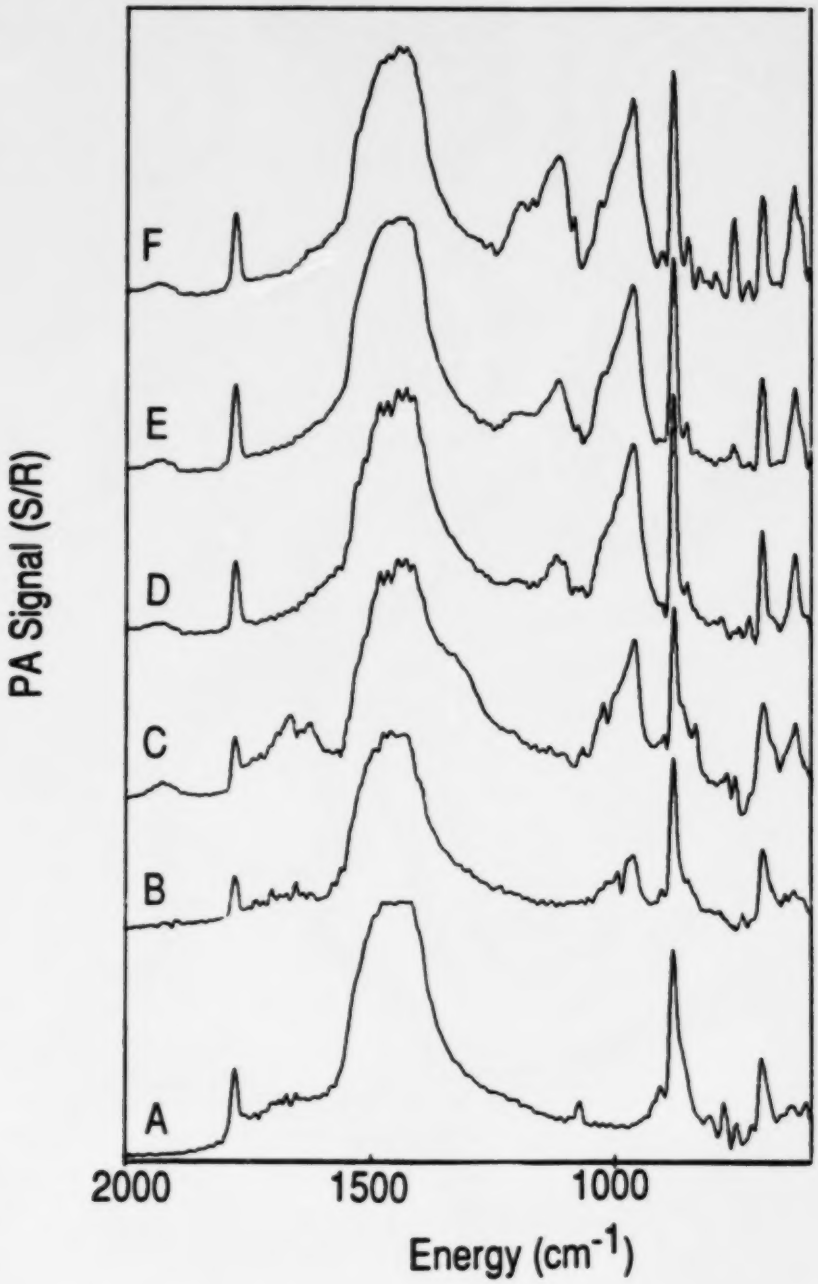

Figure 46. In situ FTIR-PA spectra of (A) $Na_2CO_3.H_2O$ and $Na_2CO_3.H_2O$ exposed to 1.5% SO_2 in N_2 as a function of temperature: (B) 25°C; (C) 75°C; (D) 100°C; (E) 200°C; and (F) 300°C.

Reprinted with permission from Anal. Chem., 60, 1027 (1988). Copyright American Chemical Society.

bands at 960 and 629 cm^{-1} are characteristic of those reported for Na_2SO_3[56], while the bands observed at 1650, 1330 and 840 cm^{-1} are characteristic of $NaHCO_3$.[66] The $NaHCO_3$ peaks are no longer present in the spectrum acquired at 100°C due to the decomposition of the $NaHCO_3$ to Na_2CO_3, H_2O and CO_2 (Trace D). On the other hand, as the sample is exposed to increasing amounts of SO_2 at elevated temperatures the absorption bands centered at 960 and 629 cm^{-1} continue to increase in intensity (Traces D, E and F).

The spectrum for the exposure of the sample to SO_2 at 100°C exhibits small bands at 1140 and 617 cm^{-1} (Trace D). These bands, which increase in intensity with the temperature of exposure (Traces D, E and F), are characteristic of Na_2SO_4.[57] Finally, the presence of other bands at 1080, 1030 and 752 cm^{-1} in the spectrum recorded at 300°C are indicative of the formation of other $S_xO_y^{-n}$ species on the surface of the Na_2CO_3 particles.

$\underline{Ca(OH)_2}$

Exposure of $Ca(OH)_2$ to SO_2 at 25°C--

The spectral data obtained for a single sample of $Ca(OH)_2$ exposed to 1.5% SO_2 in N_2 (1 ml/min) at 25°C are shown in Figure 47. Spectra consisting of 128 accumulated scans were collected every 2.5 min. The spectrum of unexposed $Ca(OH)_2$ exhibits only a single sharp peak at 872 cm^{-1} (for the spectral range shown) indicative of an aragonite carbonate[64] impurity in the sample.

Exposure of the sample to SO_2 results in the appearance of a broad band at ca. 960 cm^{-1} indicative of the formation of $CaSO_3$. Spectra of this sample obtained after 40 min of exposure show increases in intensity of this band up to ca. 20 min of exposure. The increases in sulfite peak area with time are depicted in Figure 48. Also shown in Figure 48 is the peak

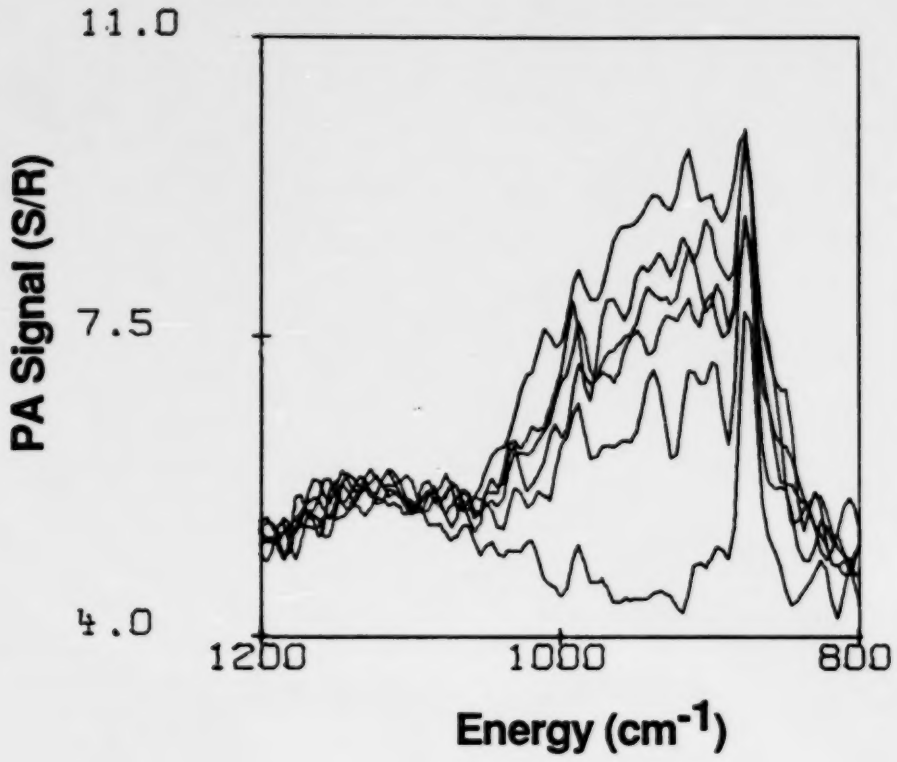

Figure 47. In situ FTIR-PA spectra of $Ca(OH)_2$ exposed to 1.5% SO_2 in N_2 at 25°C.

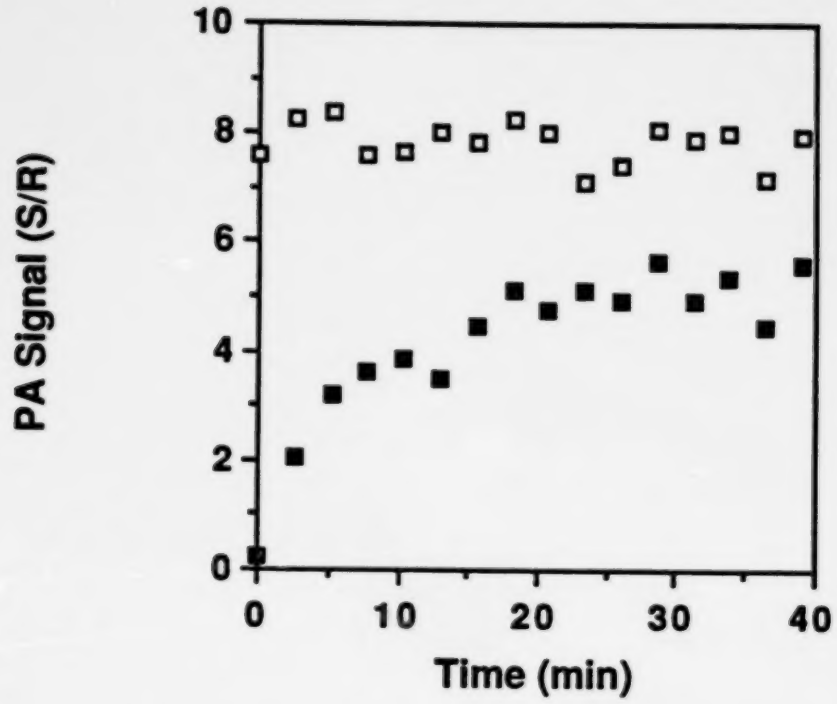

Figure 48. Peak areas for $SO_3^=$ (950 cm^{-1}) (■) and OH^- (3641 cm^{-1}) (□) as a function of reaction time for $Ca(OH)_2$ exposed to 1.5% SO_2 in N_2 at 25°C.

area of the hydroxyl band (not shown in the spectrum) as a function of exposure time. The plot clearly illustrates the simultaneous increase and decrease of the $SO_3^=$ and OH^- peak areas, respectively, as a function of reaction time. This observation is in agreement with previous in situ DRS and post-exposure PAS experiments, indicating that the reaction occurring on the surface of the particles is:

$$Ca(OH)_2(s) + SO_2(g) \text{ ---> } CaSO_3(s) + H_2O(g). \qquad (3)$$

Exposure of $Ca(OH)_2$ to SO_2 at elevated temperatures

The spectral data recorded for the exposure of $Ca(OH)_2$ to 1.5% SO_2 in N_2 (2 ml/min) as a function of increasing temperature are depicted in Figure 49. (Each spectrum represents 128 scans and is scaled equally.) A typical spectrum of $Ca(OH)_2$ is shown in Trace A of Figure 49. Carbonate (aragonite) impurities in the sample are indicated by the peaks at 1450 and 872 cm^{-1}. After the initial exposure of the sample to SO_2 at 25°C, bands centered at ca. 1330 and 960 cm^{-1} are observed (Trace B). Continued exposure of the sample to SO_2 (26-48°C, Trace C) results in increases in intensity of both these bands and the appearance of an additional band at 1150 cm^{-1}. The bands at 1330 and 1150 cm^{-1} are characteristic of gaseous SO_2, while the broad band at 960 cm^{-1} represents $SO_3^=$.

Increasing the temperature of exposure from 48 to 250°C (Traces D, E, F and G) results in decreases in intensity for all spectral bands due to the effects of the temperature upon the PA signals. This effect severely limits the ability to interpret elevated temperature PA spectra. However, when the sample is exposed to increasing amounts of SO_2 at elevated temperatures an absorption band at 633 cm^{-1} is observed. This band is characteristic of the $SO_3^=$ ν_2 bending vibrational mode and therefore the appearance of this band indicates that increasing amounts of $CaSO_3$ are

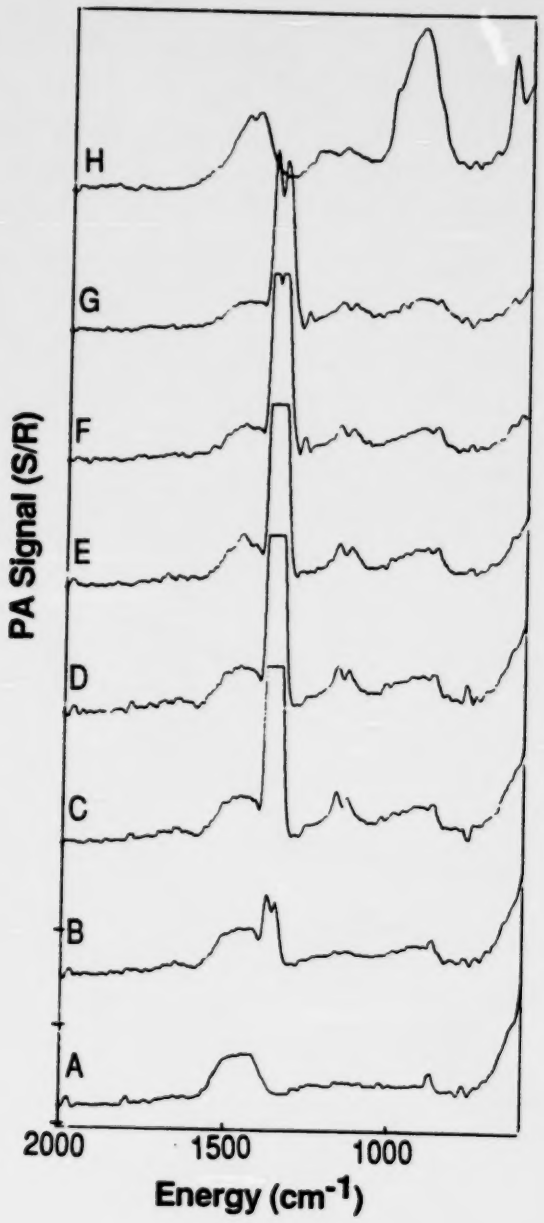

Figure 49. In situ FTIR-PA spectra of $Ca(OH)_2$ (A) exposed to 1.5% SO_2 in N_2 as a function of temperature: (B) 25°C; (C) 25-48°C; (D) 48-73°C; (E) 98-122°C; (F) 170-195°C; (G) 226-250°C; (H) exposed to 400°C, cooled to 25°C and purged under N_2.

being formed on the sample surface even though the intensity of the 960 cm^{-1} band decreases (due to the temperature effect). Above 260°C, the PA signal for this sample was undetectable.

Although spectra could not be measured for this particular sample <u>in situ</u> at temperatures above 260°C, the sample was exposed to SO_2 up to 400°C. After the sample was cooled and purged under N_2 in the HT-PA cell a post-exposure PA spectrum was collected (Trace H). The resulting sample spectrum exhibits prominent bands at 1450 characteristic of carbonate and at 960 and 633 cm^{-1} characteristic of pyramidal sulfite. In addition to these bands, peaks at 1014 and 1200 cm^{-1} appear. The peak at 1014 cm^{-1} is indicative of the extensive $SO_3^=$ production which results in the formation of oxygen coordinated $SO_3^=$, while the 1200 cm^{-1} peak is indicative of $SO_4^=$ formation.

The above experiment was repeated by exposing a single sample of $Ca(OH)_2$ to 1.5% SO_2 in N_2 at temperatures of 25, 100, 200, 300 and 400°C (Figure 50). After exposure of the sample to SO_2 at the designated temperature for 30 min, it was cooled to 25°C and purged of the excess SO_2 gas. Using this procedure, the experiment is very similar to the post-exposure PAS studies described in Section III. B. except that in this case all spectra are of the same sample, undisturbed between exposures and spectral measurements, as opposed to those of replicate samples changed between exposures and measurements. Traces of residual SO_2 in the cell are evident in each spectrum at 1330 cm^{-1}.

The spectra in Figure 50 illustrate peaks identical to those observed in the <u>in situ</u> PA exposure spectra. The initial exposure results in the growth of peaks at 950 and 633 cm^{-1}, which are indicative of $SO_3^=$ (Trace B, Figure 50). Continued exposure of the sample to SO_2 with increasing temperature results in increased intensity of the 966 and 633 cm^{-1} bands

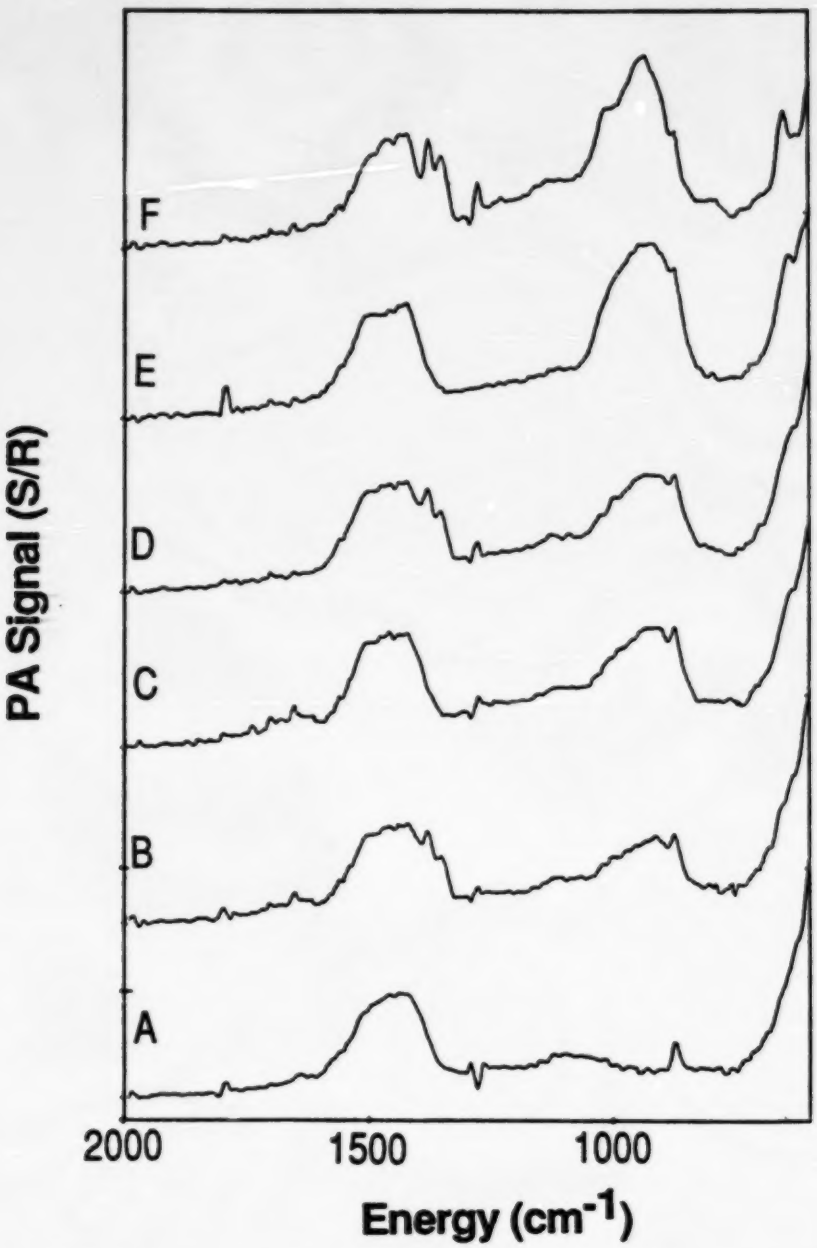

Figure 50. FTIR-PA spectra of a single sample of $Ca(OH)_2$ (A) exposed to 1.5% SO_2 in N_2 at (B) 25°C; (C) 100°C; (D) 200°C; (E) 300°C; (F) 400°C. The sample has been cooled to 25°C and purged under N_2 for each spectrum.

and the appearance of a peak at 1014 cm^{-1} (Traces C, D, E and F). The peak at 1014 cm^{-1} is characteristic of oxygen bound $SO_3^=$ on the $Ca(OH)_2$ surface. (Trace F). In addition, the spectrum for this exposure shows a slight increase in the intensity at the 1200 cm^{-1}, which is indicative of the formation of $CaSO_4$.

$\underline{CaCO_3}$

Exposure of $CaCO_3$ to SO_2 at 25°C--

Spectra recorded during the exposure of $CaCO_3$ to 1.5% SO_2 in N_2 (2 ml/min) at 25°C from 0 to 34 min are shown in Figure 51. Trace A of Figure 51 is a typical spectrum of $CaCO_3$ (calcite) exhibiting carbonate peaks at 1450, 876 and 713 cm^{-1}. Exposure of the sample to SO_2 at 25°C results only in the growth of gaseous SO_2 peaks at 1330 and 1150 cm^{-1}. These data confirm previous post-exposure PAS and <u>in situ</u> DRS results which indicated that no reaction occurs between $CaCO_3$ and SO_2 at this temperature.

Exposure of $CaCO_3$ to SO_2 at elevated temperatures--

Spectra acquired during the exposure of $CaCO_3$ to 1.5% SO_2 in N_2 (2 ml/min) up to temperatures of 360°C are depicted in Figure 52. Spectra of the sample exposed to SO_2 below temperatures of 300°C show only the presence of unreacted $CaCO_3$ and SO_2. However, at a temperature of 360°C, new bands at 1276, 1022 and 813 cm^{-1} are observed; upon cooling the sample under N_2 to room temperature, these bands disappear from the spectrum (Trace G). Low et al.[15] reported the appearance of a small peak between 1250 and 1100 cm^{-1} after the exposure of CaO to SO_2 at 25°C, which he attributed to a group of several absorptions some of which were masked by the intense $SO_3^=$ peak (1000-800 cm^{-1}). The peak observed by Low, between

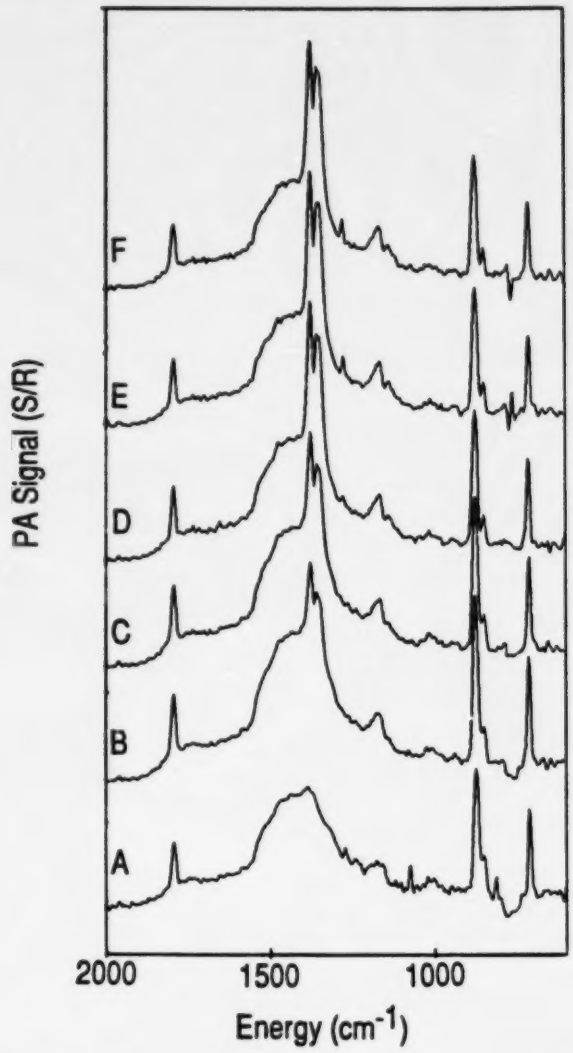

Figure 51. In situ FTIR-PA spectra of $CaCO_3$ (A) exposed to 1.5% SO_2 in N_2 at 25°C as a function of time: (B) 2.5 min; (C) 5.2 min; (D) 13 min; (E) 23 min; (F) 34 min.

1250 and 1100 cm^{-1}, correlates well with the absorption observed at 1276 cm^{-1} in this study. Low assigned the 1250-1100 cm^{-1} band to a structure consisting of an SO_2 molecule physically coordinated to a surface oxide. Such a species might be expected to have some gas like properties, and therefore result in a relatively intense photoacoustic signal. It is not unreasonable then to assign the 1276 cm^{-1} peak and the intense peaks at 1022 and 813 cm^{-1} to such a physisorbed SO_2 species. These molecules, as they become more tightly bound to the surface oxide, would become chemisorbed $SO_3^=$ coordinated to the Ca^{++} of the $CaCO_3$ surface through an oxygen. Trace G of Figure 52 supports these assignments in that 1) the peaks at 1276, 1022 and 813 cm^{-1} are no longer observed, indicating that this species is an unstable intermediate; and 2) the peaks at 970 and 940 cm^{-1}, characteristic of the $SO_3^=$ species coordinated to a metal through an oxygen (a chemisorbed species), are observed for the cooled and purged sample.

Figure 52. In situ FTIR-PA spectra of $CaCO_3$ (A) exposed to 1.5% SO_2 in N_2 as a function of temperature: (B) 28-31°C; (C) 77-100°C; (D) 198-222°C; (E) 295-319°C; (F) 344-369°C; (G) cooled to 25°C. Reprinted with permission from Appl. Spectros., 42, 946 (1988). Copyright Kansas State University.

SECTION 6

REFERENCES

1. E. S. Rubin, M. A. Cushey, R. J. Marinicio, C. N. Bloyd, J. F. Skea, Environ. Sci. Technol. 20, 960 (1986).

2. R. H. Borgwardt, R. D. Harvey, Environ. Sci. Technol. 6, 350 (1972).

3. G. Van Houte, B. Delmon, J. Chem. Soc., Faraday Trans. I 75, 1593 (1979).

4. D. L. Dorsey, B. Buecker, Research and Development 28, 93 (1986).

5. R. Snyder, W. I. Wilson, I. Johnson, Thermochim. Acta 26, 257 (1978).

6. R. K. Chan, K. S. Murthi, D. Harrison, Can. J. of Chem. 48, 2979 (1970).

7. G. Van Houte, B. Delmon, Bull. Soc. Chim. Belg. 87, 241 (1978).

8. G. Van Houte, B. Delmon, Chem. Eng. Tech. 48, 863 (1976).

9. G. Van Houte, B. Delmon, Bull. Soc. Chim. France 11-12, 413 (1978).

10. G. Van Houte, B. Delmon, Bull Soc. Chim. Belg. 88, 205, (1979).

11. G. Van Houte, L. Rodrique, B. Delmon, Environ. Sci. Technol. 15, 327 (1981).

12. S. K. Bhatia, D. D. Perlmutter, AIChE J. 27, 226 (1981).

13. S. M. Hawkins, K. Ramanathan, D. Lentzen, C. E. Howard, R. Truesdale, private communication.

14. F. Foerster, K. Kubel, Z. Anorg. Allg. Chem. 139, 261 (1924).

15. M. J. D. Low, A. J. Goodsel, N. Takezawa, Environ. Sci. Technol. 5, 1191 (1971).

16. J. S. Burton Developments In Applied Spectroscopy E. L. Grove and A. J. Perkins, Eds. (Plenum Press, New York, 1971) 9, p. 143.

17. L. C. Feldman, J. W. Mayer Fundamentals of Surface and Thin Film Analysis (North-Holland, New York, 1986).

18. S. Brunauer, P. Emmett, F. Teller, J. Am. Chem. Soc. 60, 309 (1938).

19. R. P. Eischens, W. A. Plisken, Advances in Catalysis 10, 1 (1958).

20. M. L. Hair Infrared Spectroscopy in Surface Chemistry (Marcel Dekker, Inc., New York, 1967) p. 71.

21. G. D. Blyholder, G. W. Cagle, Environ. Sci. Technol. 5, 158 (1971).

22. J. P. Blitz, R. S. Shreedhara Murthy, D. E. Leyden, Appl. Spectrosc. 40, 829 (1986).

23. G. Herzberg Infrared and Raman Spectra of Polyatomic Molecules (Van Nostrand, Princeton, New Jersey, 1945).

24. E. B. Wilson, Jr., J. C. Decius, P. C. Cross Molecular Vibrations (McGraw-Hill, New York, 1955).

25. K. Nakamoto Infrared Spectra of Inorganic and Coordination Compounds, (Wiley-Interscience, New York, 1963).

26. K. Nakamoto, Infrared and Raman Spectra of Inorganic and Coordination Compounds, 4th ed., (Wiley-Interscience, New York, 1986).

27. A. Rosencwaig Photoacoustics and Photoacoustic Spectroscopy (Wiley-Interscience, New York, 1980) p. 141.

28. M. Born, E. Wolf Principles of Optics, 2nd ed. (Pergamon Press, Oxford, 1964).

29. P. Kubelka, F. Munk, Z. Tech. Phys. 12, 593 (1931).

30. G. Kortum Reflectance Spectroscopy (Springer-Verlag, New York, 1969).

31. P. R. Griffiths, J. A. de Haseth Fourier Transform Infrared Spectroscopy (Wiley-Interscience, New York, 1986) p. 544.

32. N. J. Harrick Diffuse Reflection (Harrick Scientific Corporation, Ossining, New York, 1984).

33. M. A. Martin, J. W. Childers, and R. A. Palmer, Appl. Spectros. 41, 120 (1987).

34. M. A. Martin Thompson, Ph.D. Dissertation, Duke University, 1988; Diss. Abs., Int. B, 49, 3154 (1989).

35. M. A. Martin, J. W. Childers, R. A. Palmer, Appl. Spec. 39, 668 (1985).

36. D. Beruto, L. Barco, A. Searcy, G. Spinolo, J. Am. Ceram. Soc. 63, 439 (1980).

37. D. Beruto, L. Barco, A. Searcy, J. Am. Ceram. Soc. 66, 893 (1983).

38. J. Ewing, D. Beruto, A. Searcy, J. Am. Ceram. Soc. 62, 580 (1979).

39. H. R. Chandrasekhar, L. Genzel, J. Kuhl, Opt. Commun. 17, 106 (1976).

40. L. Genzel, J. Kuhl, Infrared Phys. 18, 113 (1978).

41. L. Genzel, J. Kuhl, Appl. Opt. 17, 334 (1978).

42. F. J. Harris, Proceedings of the IEEE 66, 51 (1978).

43. D. J. Gerson, J. S. Wong, J. M. Casper, Am. Lab. 16 (11), 63 (1984).

44. J. W. Childers Ph. D. Dissertation, Duke University, 1985.

45. M. P. Fuller, P. R. Griffiths, Anal. Chem. 50, 1906 (1978).

46. P. S. Bechthold, J. of Photoacoustics 1, 87 (1982).

47. B. S. H. Royce, J. B. Benziger, Am. Lab. 17 (3), 16 (1985).

48. S. J. McGovern, B. S. H. Royce, J. B. Benziger, Applications of Surface Science 18, 401 (1984).

49. S. McGovern, B. S. H. Royce, J. Benziger, Appl. Opt. 24, 1512 (1985).

50. A. P. Malvino Electronic Principles 3rd ed. (McGraw-Hill Book Co., New York, 1983) p. 663.

51. J. Bertolacini, J. E. Barney II, Anal. Chem. 29, 281 (1957).

52. W. R. Busing, J. Chem. Phys. 23, 933 (1955).

53. E. Steger, W. Schmidt, Ber. Bunsen-Ges. Phys. Chem. 68, 102 (1964).

54. D. E. Leydon, R. S. Shreedhara Murthy, Spectroscopy 2 (2), 28 (1987).

55. I. Hamadeh, D. King, P. Griffiths, J. of Catalysis 88, 264 (1984).

56. J. C. Evans, H. J. Bernstein, Can. J. Chem. 33, 1270 (1955).

57. C. Ricchioccioli, Compt. Rend. 244, 2704 (1957).

58. B. Nyberg, R. Larsson, Acta Chem. Scand. 27, 63 (1973).

59. K. Nakamoto, J. Fujita, S. Tanaka, M. Kobayashi, J. Am. Chem. Soc. 79, 4904 (1957).

60. G. Newman, D. B. Powell, Spectrochim. Acta 19, 213 (1963).

61. M. J. D. Low, N. Takezawa, A. J. Goodsel, J. of Colloid and Interface Science 37, 422 (1971).

62. S. R. Lowry, D. G. Mead, D. W. Vidrine, Anal. Chem. 54, 546 (1982).

63. M. G. Rockley, J. P. Devlin, Appl. Spectrosc. 34, 407 (1982).

64. S. Bhagavantam, T. Venkatarayudu, Proc. Indian Acad. Sci. 9A, 224 (1939).

65. K. Buijs, C. J. H. Schutte, Spectrochim. Acta 17, 917 (1963).

66. F. Miller, C. Wilkins, Anal. Chem. 24, 1253 (1952).

67. Mellor's Comprehensive Treatise on Inorganic and Theoretical Chemistry, 11 (John Wiley and Sons, New York, 1961).